TRW Tech. Report No. 23499-6027-UT-00

NASA CR-166814

PLASMA WAVE EXPERIMENT FOR THE ISEE-3 MISSION

Semi-Annual Report
(Period Covered: August 20, 1981 - February 19, 1982)

by

F. L. Scarf
Principal Investigator

Contract No. NAS5-20682

Prepared for
NASA Goddard Space Flight Center
Greenbelt, Maryland 20771

March 4, 1982

Bldg R-1, Rm 1176
Applied Technology Division
TRW Space and Technology Group
One Space Park
Redondo Beach, California 90278
(213) 536-2015

(NASA-CR-166814) PLASMA WAVE EXPERIMENT FOR THE ISEE-3 MISSION Semiannual Report, 20 Aug. 1981 - 19 Feb. 1981 (TRW, Inc., Redondo Beach, Calif.) 94 p HC A05/MF A01 CSCL 03B

N82-27209

Unclas
G3/92 22772

PREFACE

1. OBJECTIVE

The purpose of this report is to summarize the performance of work for the period 20 August 1981 through 19 February 1982, in compliance with Modification 19 to Article XXI of Contract NAS5-20682, entitled, "Plasma Wave Experiment for ISEE-C (Heliocentric) Mission," dated 20 November 1974.

The objective of this contract is to provide analysis of data from a scientific instrument designed to study solar wind and plasma wave phenomena on the ISEE-3 Mission.

2. SCOPE OF WORK

Project activities during this past six months have included successful return of data from the instrument, continuing analysis of all data, publication of results, and deposit in National Space Science Data Center of the data.

3. CONCLUSIONS

Not applicable.

4. SUMMARY OF RECOMMENDATIONS

Not applicable.

1.0 INTRODUCTION

The purpose of this report is to summarize the various activities and tasks accomplished on the data analysis phase of the contract during the 27th and 28th quarters of work.

2.0 WORK ACTIVITIES FOR THE SIX-MONTH PERIOD

2.1 Research

During this interval, there was much research activity involving the ISEE-3 Plasma Wave Investigation and the (unfunded) counterparts on ISEE-1 and -2. The paper, "Non-Local Plasma Turbulence Associated with Interplanetary Shocks," appeared in Journal of Geophysical Research, 87, 17, 1982; and the paper, "Energetic Electrons and Plasma Waves Associated with a Solar Type III Radio Burst," appeared in Astrophysical Journal, 251, 336, 1981.

Two new papers were completed and submitted to journals, and these are attached to this report as Appendices A and B. The paper by Greenstadt, et al., has been revised and accepted for publication in Geophysical Research Letters. The paper by Coroniti, et al., is now being revised and will be accepted by the Journal of Geophysical Research.

During this period, F. L. Scarf and E. W. Greenstadt attended the ISEE Science Working Team Meeting, the Type II Shock Workshop, and the CDAW at Goddard Space Flight Center.

Dr. Scarf has been asked to provide a report on the ISEE-3 Mission to the Geomagnetic Tail, and a draft of this report is attached hereto as Appendix C.

2.2 Other Activities

During this period, we submitted a fourth data set to the National Space Science Data Center (2/12/82), we circulated ISEE-3 data to participants of the ISEE Workshop, and we continued to support the NOAA Real Time Data Link.

TRW Tech. Report No. 23499-6026-UT-00

PLASMA WAVE LEVELS AND IMF ORIENTATIONS PRECEDING OBSERVATIONS OF INTERPLANETARY SHOCKS BY ISEE-3

by

E. W. Greenstadt[1], F. L. Scarf[1], C. F. Kennel[2],
E. J. Smith[3], and R. W. Fredricks[1]

[1]Applied Technology Division, TRW Defense & Space Systems Group,
Redondo Beach, California 90278

[2]Department of Physics and Institute of Geophysics and Planetary Physics,
University of California, Los Angeles, California 90024

[3]Jet Propulsion Laboratory, California Institute of Technology,
Pasadena, California 91109

November 1981

Space Sciences Department
Bldg R-1, Rm 1176
TRW Defense & Space Systems Group
One Space Park
Redondo Beach, California 90278

APPENDIX A

ABSTRACT

Some interplanetary shocks detected at ISEE-3 are preceded by many hours of strongly-enhanced plasma wave noise, while others have essentially no wave precursors above background. It has been shown that these extremes correspond to quasi-parallel and quasi-perpendicular shocks, respectively, based on the instantaneous orientation angle θ_{Bn} of the interplanetary magnetic field (IMF) to the shock normal at the time the shocks cross the spacecraft. Moderate precursor activity corresponds to cases of intermediate shock-normal geometries. Since the IMF direction is widely variable, however, it may be asked whether one θ_{Bn} at the shock crossing can explain the presence or absence of noise for several hours. We show that precursor wave noise level is correlated with field orientation and an extrapolated θ_{Bn} throughout the preshock observation interval for two contrasting active and quiet cases, and that intermediate, variable noise levels correspond to intermediate, variable IMF orientations. We infer that quasi-parallel, interplanetary shocks are preceded by foreshocks whose presence is not obviously attributable to scattering out of ion beams generated at quasi-perpendicular zones of these interplanetary shocks.

INTRODUCTION

The solar wind is subject to almost continual variation in many of its constituents. The composition of the wind plasma, the velocity distributions of its elements, the variations of the interplanetary magnetic field (IMF), and the rise and fall of passing waves over a broad range of frequencies are among the many variable phenomena of interest. Indeed, the observational study of the solar wind consists essentially of attempts to organize diverse variations into repeatable patterns.

In recent years, comprehensive investigation of the macrostructure of the Earth's bow shock has provided a context in which to organize one class of solar wind events; namely, the enhancement of kilohertz-range plasma wave electrical signals upstream (ahead) of quasi-parallel, but not quasi-perpendicular, interplanetary (IP) shocks (Kennel et al., 1982). We perceive these events not only as interplanetary counterparts of analogous extended bow shock structures, but as a potential tool for illuminating an unsettled question in bow shock phenomenology. We aim in this report to sharpen both the analogy and the tool.

SELECTED CASES

Figure 1 displays four of the examples of Kennel et al. (1982) spanning the range of preshock conditions, from noise-free (25 December) to almost continuously noisy (12 November), with two intermediate cases of fluctuating noise levels, one occasionally above background (8 November) and one consistently above background (27 August). The average electric field in the 3 kHz channel is a representative diagnostic for plasma waves in the 1-10 kHz frequency range. The number at the upper left in each panel gives the angle θ_{Bn} between the local shock normal and the IMF at the time each interplanetary shock crossed the spacecraft. The correspondence of small θ_{Bn} with enhanced upstream <E> suggests that the presence or absence of plasma wave noise was related to the quasi-parallel or quasi-perpendicular structure of the approaching shock, implying the existence of interplanetary foreshocks similar to the foreshock outside the Earth's curved, non-uniform bow shock (Greenstadt and Fredricks, 1980).

One important caveat must be attached to the apparent correspondence of θ_{Bn} and preshock noise. The distinctions among plasma wave activity levels visible in Figure 1 depended on the presence or absence of noise for hours preceding shock encounter, while the lone θ_{Bn} calculated for each shock was based on the instantaneous IMF immediately before shock encounter. Since the IMF is seldom constant in direction over time intervals longer than ten to thirty minutes, how do we explain enhanced noise, say, three hours before shock arrival, in terms of extended quasi-parallel structure? Also, how do we exclude the possibility that noise so far ahead of the interplanetary shocks wasn't simply a manifestation of the Earth's foreshock? We attempt, here, to add confidence to the structural explanation by filling in the pattern of preshock field behavior.

METHOD OF ANALYSIS

Technique. We have used the ISEE-3 data pool tapes, together with computational graphic techniques, to illustrate the approximate relationships of spacecraft, IMF, wave noise, IP shocks, and bow shock. The data pool supplies plasma wave fields, IMF vectors, and solar wind velocity, among other measurements, averaged every 128 seconds. In a given 128-second interval, we take the average IMF $\Delta \mathbf{B}$ to be the field vector that prevailed during that interval, and we wish to represent it as a small vector $\Delta \mathbf{R}$ in metric space whose length is proportional to $\Delta \mathbf{B}$. Then, the vector's x-component is given by 128 V_{sw}, where V_{sw} is the solar wind speed during the interval. The solar wind is assumed to flow in the minus-x direction in the usual solar ecliptic coordinate system. The vector's direction is taken as the direction of $\mathbf{B}$, and its origin is located in the SEC frame so as to attach to the field line segments in adjacent intervals, derived in the same manner. For a sequence of intervals, the result, when represented in a three-dimensional graph, is a constructed section of an IMF field line.

An example of the above technique is shown in Figure 2(a). The field line through the ISEE-3 position at the origin is represented as a set of connected line segments; each segment is also connected by vertical lines to its projection on the ecliptic, to locate the field in the illustrated frame. The shock is drawn as two plane sections: The observed (solid) shock plane at one end of the field line locates the shock at the moment it crossed the spacecraft; the phantom (dotted) plane locates the shock earlier, at the moment the time series began (that is, at the time associated with the other end of the preshock field line at far right). Thus, the sequence of field segments was passing the spacecraft toward the right in the unshocked solar wind as the shock was traversing the space between the two planes. The intersection of the observed shock with the ecliptic is drawn inside its rectangle, and a line connecting the intersection to the top line of the rectangle is drawn as a visual clue to the tipping of the shock with respect to the ecliptic. The plasma wave noise is drawn as a graph on the x-y plane; the line is actually made up of a sequence of segments each of which corresponds to a contemporaneous segment of $\underset{\sim}{B}$.

Limitations. The hazards of the foregoing technique can be severe under certain circumstances and must be considered in making any interpretation. The hazards are invited by the four major assumptions underlying the technique:

1. The general orientation of the constructed field line corresponding to the preshock plasma noise can also be used as an approximation of θ_{Bn} where it intersects the oncoming shock. This is a crucial assumption! The spacecraft never records the IMF directly in front of the shock except just before the shock crosses the observation point, because the shock, necessarily traveling faster than the solar wind, has overtaken all the relevant portions of the IMF by the time it reaches the spacecraft. All the IMF segments recorded after the shock's passage have been modified by the shock; all the IMF segments recorded before the shock's passage, even the last one, have not yet been seen by the shock. Thus, the stream of preshock plasma wave noise, if it relates to shock structure, can be tied only to points on the oncoming shock whose exact orientation to the IMF cannot be measured by a single spacecraft.

2. The normal of an IP shock remains invariant as it travels toward the observation point. However, at a typical shock speed of, say, 700 km/sec, this would imply, for five hours of preshock observation, a constant shock orientation over a distance of about 18 solar radii. The longer the interval over which we try to construct a field line, the more problematical this assumption.

3. The IMF has a uniform direction over the dimensions of time and space defined by a given construction. However, the magnetometer actually measures segments of many field lines as the solar wind convects them past the spacecraft, so that each off-axis segment of a constructed field line is really a translation from a measurement made on the x-axis, and assumed to be connected to the segment next to it, similarly translated. Once again, long observation intervals, or grossly wandering field lines, weaken the assumption.

4. Each interplanetary shock is locally a plane with a single normal over an area extending from the x-axis to wherever it touches the constructed field line. However, we note that the locally planar nature of interplanetary shocks has never been established on a small scale, while on a heliospheric scale these shocks are believed to have radii of curvature on the order of a few tenths of an astronomical unit. If the constructed IMF were to connect to the approaching shock many solar radii off the x-axis, the assumption that the normal at that point was the same as the one estimated at the spacecraft

would be tenuous.

In the following examples, we apply the above technique to selected cases which, we believe, minimize these limitations.

EXAMPLES

High Noise: 11-12 November 1978. The first case is our outstanding example of high plasma wave noise that preceded an interplanetary shock for a long time. Figure 2(a) shows that the IMF was steadily out of the ecliptic but projected essentially at a solar-radial, rather than stream-angle, orientation, and that the IP shock was moving in a slightly northeasterly direction. The figure covers about 4½ hours of data, and the average 3 kHz plasma wave noise was always above the nominal background of 10^{-8} V/m/Hz$^{1/2}$ and steadily above 10^{-7} V/m/Hz$^{1/2}$ during the final approach of the shock.

The distance between the beginning and ending shock positions was large because the shock speed of 700 km/s was the highest of these examples; this is why the phantom shock section is so far to the left. This means that extrapolation of the recorded IMF into the region ahead of the unseen approaching shock may be particularly questionable for the first half of the interval. During the last 3 million km of solar wind before the shock, however, when the noise was steadily high, and rising, the IMF turned almost directly into the shock. This can best be appreciated in the graphs of Figure 2(b), where the upper panel is a plot of the 3 kHz noise, and the lower panel is a plot of θ_{Bn}, the angle formed by each segment of B and the shock normal as if the shock had been at ISEE-3 [the plots run right-to-left in time, with the shock coming from the left, just as in Figure 2(a)]. During the "closing interval," θ_{Bn} was never greater than 30°, and often less than 20°.

Finally, we note that in Figure 2(a), the out-of-ecliptic orientation of the field line means that, despite its nearly radial projection, the IMF missed contact with Earth's bow shock by a wide margin, passing far to the north.

The three other examples of Figure 1 are depicted in Figure 3.

Low Noise: 25 December 1978. One of the quietest preshock cases recorded is shown in Figure 3(a). The IMF was close to the nominal stream angle, thereby pointing far to the east of the bow shock, and remained almost parallel to the IP shock, which was traveling diagonally westward. The IP shock was slow (400 km/s) and so did not move far during the illustrated interval. Angle θ_{Bn} was close to 90° almost throughout the interval, and the electric field noise remained at the 10^{-8} background level. A comparatively short interval is portrayed because the IMF underwent a radical reorientation just before its displayed construction; the orientation before the discontinuity was also unfavorable to preshock noise, but could not reasonably be part of any extrapolation to the arriving IP shock and was difficult to represent clearly in the diagram.

Medium, or Variable, Noise: 7-8 November 1978 and 27 August 1978. The IP shock of 8 November was preceded by wave noise generally at or near background, but with occasional enhancements to amplitudes between 10^{-8} and 10^{-7} V/m/Hz$^{1/2}$. The geometry of the field appears in Figure 3(b). The angle θ_{Bn} ran generally from a little above 60° to a little below 50°, and we see in Figure 3(b) that the IMF crossed the ecliptic at a large angle and missed the bow shock completely. If we recall that in the bow shock system the transition to quasi-parallel structure takes place when $\theta_{Bn} \lesssim 50°$ (Greenstadt and Fredricks, 1979), we may interpret the sporadic, moderate wave noise as indicative of a similar transition in the IP shock, subject to extrapolation of the IMF into the unknown region in the same range of θ_{Bn}.

In contrast, the preshock wave noise of 26-27 August was almost always above background, near 10^{-7} V/m/Hz$^{1/2}$, and often variable. The field was close to the ecliptic, Figure 3(c), and followed a slightly acute stream angle, but passed to the east of the bow shock, possibly touching the latter on the far evening flank under locally perpendicular conditions unlikely to project foreshock phenomena back to ISEE-3.

Angle θ_{Bn} varied between 10° and 65° during the whole preshock interval, but was between 30° and 65° as the shock neared, with an average around 40°. Extrapolation of the trend in θ_{Bn} would put this angle in the 40° to 60° range in the unknown region ahead of the shock sunward of its arrival at ISEE-3. We would thus expect a geometry marginally favorable to enhanced noise associated with a quasi-parallel foreshock, and this seems to have been what the plasma wave detector recorded.

DISCUSSION

Summary. Figure 4 combines the critical data of the four cases elaborated upon above. The upper panel depicts the plasma wave noise for about the last 100 R_E before shock arrival (time from right to left, as before). The small digits refer to the dates of the selected examples. The lower panel gives the angle θ_{Bn} for the same cases. There appears to have been a progressive correspondence from high noise/low angle to low noise/high angle. We interpret the data to sustain the following conclusions:

1. The anticorrelation of preshock plasma wave noise level with θ_{Bn} based on general orientation of the IMF for extended intervals preceding the shocks was consistent with the IMF directions immediately preceding the interplanetary shock encounters at ISEE-3 (Kennel et al., 1982).

2. Under the assumptions, and subject to the limitations, enumerated earlier, preshock (upstream) plasma wave noise in the solar wind correlated with interplanetary shock field geometry in the same way as it does with the field geometry of the Earth's bow shock. That is, high noise levels correspond to quasi-parallel shocks, low noise levels to quasi-perpendicular shocks, and intermediate, or variable, levels to transitional shocks; the division between quasi-parallel and quasi-perpendicular preshock signal conditions appeared to occur for $60° \gtrsim \theta_{Bn} \gtrsim 40°$, just as it does for the bow shock.

3. Little or none of the upstream plasma wave activity was attributable to connection of the observation point to the bow shock by the IMF.

4. The unambiguous way in which preshock wave activity seemed to reflect q-parallel/q-perpendicular geometry suggests that the data representations of this report should be useful generally for working with the IMF and IP shocks, and that their limitations are not prohibitive, at least for moderate intervals preceding shock arrival.

Implications. The correlation of high <E> with low θ_{Bn} suggests that the waves were one constituent of what might have been interplanetary foreshocks accompanying locally quasi-parallel IP shocks. This idea has been explored already by Kennel et al. (1982), who pointed out that the vastly larger scale of IP shocks compared to the bow shock could serve to differentiate properties inherent in collisionless shocks from properties peculiar to curved, non-uniform, planetary shocks.

One outstanding question concerning the Earth's bow shock is the origin of the foreshock; specifically, the region occupied by ULF waves and diffuse ion energy distributions outside the quasi-parallel part of the shock. Is this foreshock an intrinsic part of quasi-parallel structure, or does it arise from an interaction between the solar wind and beams of reflected ion streaming into the wind from the quasi-perpendicular side of the shock (Bame et al., 1980)? In the latter situation, a uniform, plane, quasi-parallel shock, having no source of quasi-perpendicular beams, would have no foreshock.

The evidence of this report encourages belief that q-parallel, IP shocks have foreshocks. It is, of course, conceivable that a given IP shock might be a large-scale version of the bow shock, with appropriate curvature and non-uniform structure producing a foreshock by a secondary beam-interaction. It seems probable, however, that a group of IP shocks such as those pictured here would have had a diverse assortment of travel directions and radii of curvature. It would, therefore, be unlikely that together they would have formed a pool of data imitating a composite shock with the q-perpendicular/q-parallel transition at about the same local θ_{Bn} as in the bow shock. We note, further, that when wave noise was continuously present before IP shocks, the wave amplitude tended to rise toward the shock as if the shock were the source (Figure 10 of Kennel et al., 1982). We therefore interpret these results as supporting the notion that the foreshock is a natural part of each quasi-parallel, collisionless shock structure.

The obvious next step in studying IP shock precursors is to examine high-resolution particle and field data in the detail necessary to determine whether enhanced plasma wave noise is, indeed, accompanied by the low-frequency magnetic waves and ion distributions familiar in the Earth's foreshock.

ACKNOWLEDGMENTS

Preparation of this report was funded by Independent Research and Development Project 81004307, and NASA Contracts NASW-3449, NASW-3427, and NAS5-20093. The assistance of H. Schurr and R. Tsugawa was essential to the analysis.

REFERENCES

Bame, S. J., J. R. Asbridge, W. C. Feldman, J. T. Gosling, G. Paschmann, and N. Sckopke, Deceleration of the Solar Wind Upstream from the Earth's Bow Shock and the Origin of Diffuse Upstream Ions, J. Geophys. Res., 85, 2981, 1980.

Greenstadt, E. W., and R. W. Fredricks, Shock Systems in Collisionless Space Plasmas, in Solar System Plasma Physics, Vol. III (L. Lanzerotti, C. Kennel, and E. Parker, eds.), p. 4, North-Holland Publ. Co., 1979.

Kennel, C. F., F. L. Scarf, and F. V. Coroniti, Non-Local Plasma Turbulence Associated with Interplanetary Shocks, J. Geophys. Res., in press, 1982.

FIGURE CAPTIONS

Figure 1. Four cases of plasma wave electrical signals preceding the arrival of interplanetary shocks.

Figure 2. Field geometry accompanying the preshock noise of 11-12 November 1978. (a) Three-dimensional computer sketch; the sun's direction is to the left, the solar wind and the shock travel to the right; the distance between adjacent tics is 10^6 km. See text for full explanation. (b) Plots of 3 kHz signal level (upper panel) and imaginary angle θ_{Bn} between B and shock normal as if interplanetary shock were static at ISEE-3 (lower panel); time increases to the left with plots starting at 11 November 20:00:07, ending at 12 November 00:26:41; 10^6 km between tics.

Figure 3. Field geometry accompanying the preshock noise of (top to bottom) 25 December, 8 November, and 27 August 1978, symbolized as in Figure 2(a).

Figure 4. Superposed segments of plasma wave signals (upper panel) and IMF-shock normal angles (lower panel) for the four cases described in this report; the segments represent the last intervals of data before shock arrival, equivalent to a distance of about 100 R_E in front of each shock; time runs to the left; tics separated by 10^6 km.

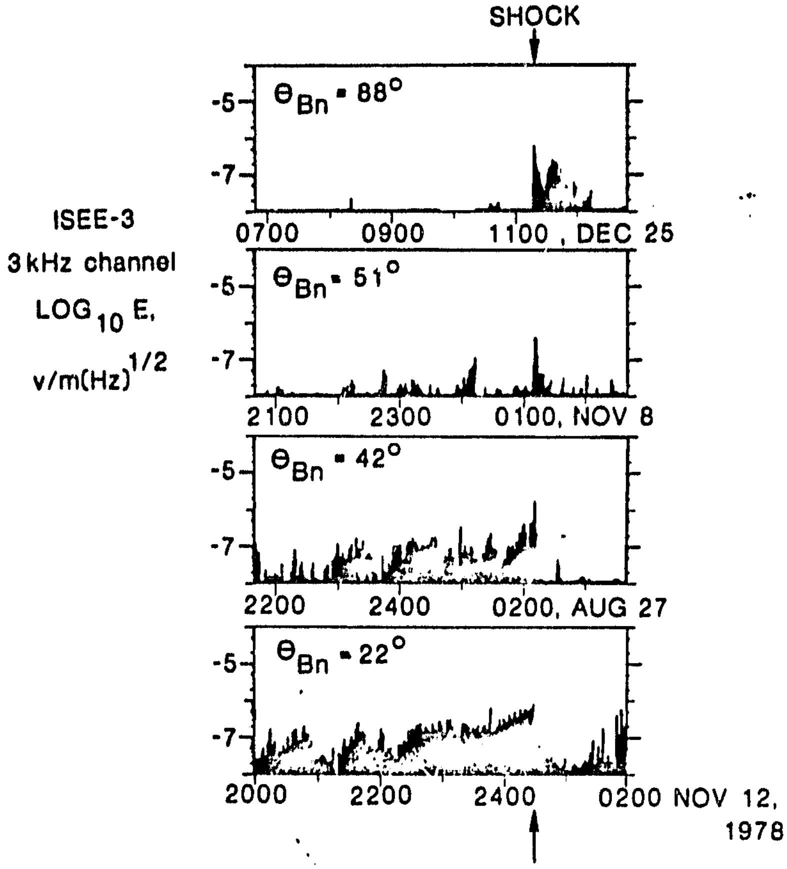

Figure 1. Four cases of plasma wave electrical signals preceding the arrival of interplanetary shocks.

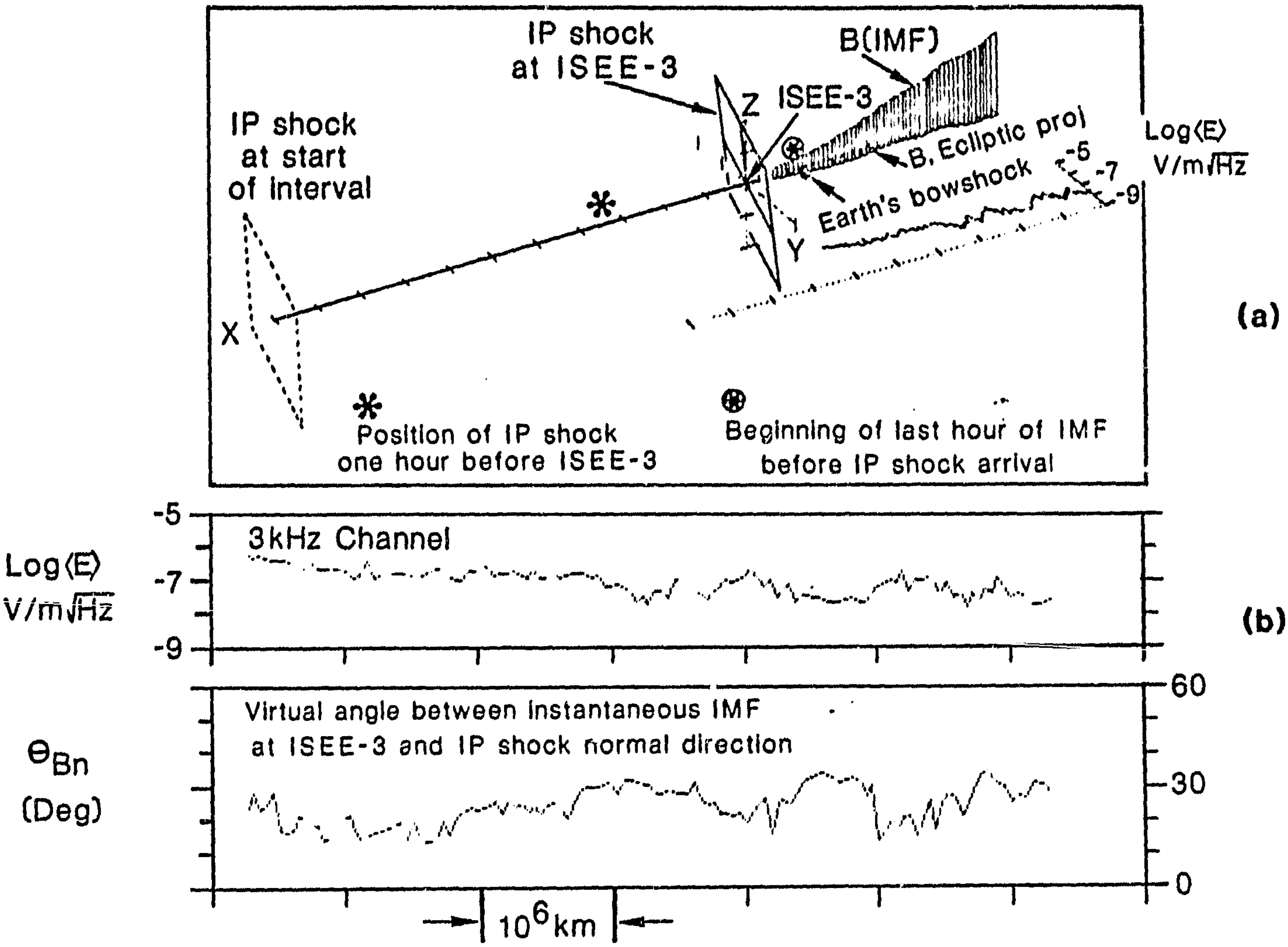

Figure 2. Field geometry accompanying the preshock noise of 11-12 November 1978. (a) Three-dimensional computer sketch; the sun's direction is to the left, the solar wind and the shock travel to the right; the distance between adjacent tics is 10^6 km. See text for full explanation. (b) Plots of 3 kHz signal level (upper panel) and imaginary angle θ_{Bn} between B and shock normal as if interplanetary shock were static at ISEE-3 (lower panel); time increases to the left with plots starting at 11 November 20:00:07, ending at 12 November 00:26:41; 10^6 km between tics.

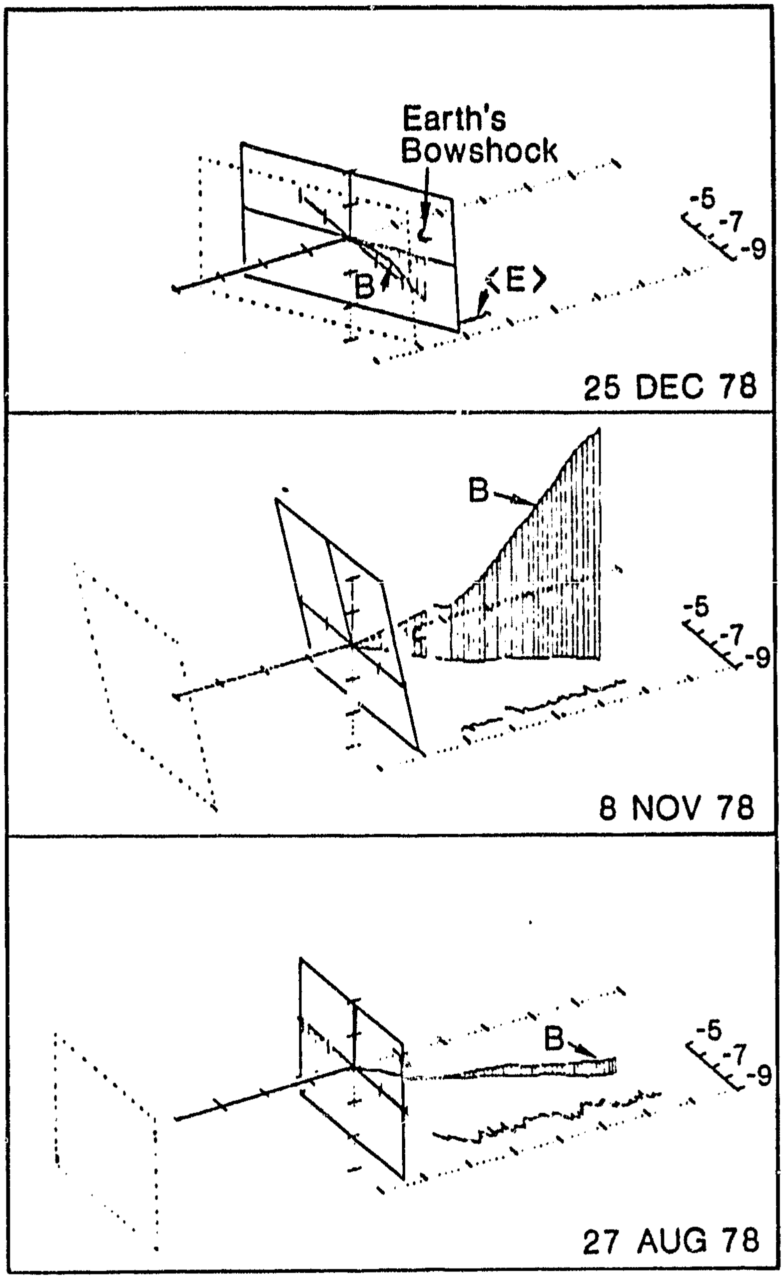

Figure 3. Field geometry accompanying the preshock noise of (top to bottom) 25 December, 8 November, and 27 August 1978, symbolized as in Figure 2(a).

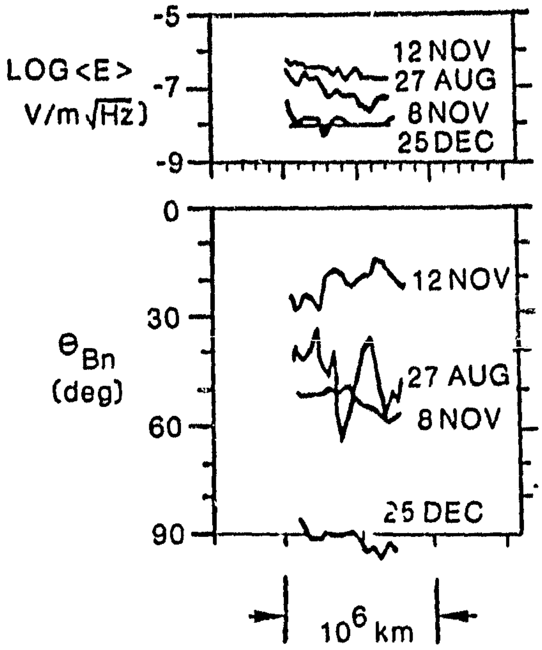

Figure 4. Superposed segments of plasma wave signals (upper panel) and IMF-shock normal angles (lower panel) for the four cases described in this report; the segments represent the last intervals of data before shock arrival, equivalent to a distance of about 100 R_E in front of each shock; time runs to the left; tics separated by 10^6 km.

TRW Tech. Report No. 23499-6025-UT-00

WHISTLER MODE TURBULENCE IN THE DISTURBED SOLAR WIND

F. V. Coroniti[1], C. F. Kennel[2], and F. L. Scarf

Applied Technology Division
TRW Defense and Space Systems Group
Redondo Beach, California 90278

E. J. Smith

Jet Propulsion Laboratory
California Institute of Technology
Pasadena, California 91109

November 1981

[1]Also at: Department of Physics and Department of Astronomy, University of California at Los Angeles

[2]Also at: Department of Physics and Institute of Geophysics and Planetary Physics, University of California at Los Angeles

Bldg R-1, Rm 1176
TRW Defense and Space Systems Group
One Space Park
Redondo Beach, California 90278
(213) 536-2015

APPENDIX B

ABSTRACT

Magnetic field fluctuations with frequencies f between the ion (f_{ci}) and electron (f_{ce}) cyclotron frequencies are enhanced downstream of interplanetary shocks and in fast streams. In both cases, the noise persists for hours and usually remains detectable until the solar wind re-achieves a quiescent state. These $f > f_{ci}$ fluctuations are related to those below f_{ci} which also accompany solar wind activity. The spectra over the range $10^{-2} f_{ci} \leq f \leq f_{ce}$ synthesized from ISEE-3 magnetometer and plasma wave instrument data are different behind shocks and in fast streams. The spectrum can generally be described by one power law below $f \approx 1$ Hz $\approx f_{ci}$ and a different one above. However, behind shocks, the spectral index above f_{ci} is about twice that below f_{ci}, whereas no clear relationship is apparent in the weaker fast stream events. Behind one shock, the interference in the low-frequency electric field channels of the ISEE-3 plasma wave instrument was small enough to permit a statistical study of the B/E ratios or, equivalently, the indices of refraction, of the $f_{ci} \leq f \leq f_{ce}$ waves. This confirmed that the waves are whistler mode emissions, as their frequency range already suggested. Various indirect lines of evidence indicate that these whistler waves are generated propagating at large angles to the local interplanetary field, a fact which helps identify possible free energy sources for their growth.

1. INTRODUCTION

High-sensitivity search coil magnetometers on Helios detected a weak background of low-frequency (4.7 - 220 Hz) magnetic field noise that is nearly always present in the solar wind (Neubauer et al., 1977a). Its spectrum, typically a power law, falls with increasing frequency, and its amplitude diminishes with increasing distance from the sun. Extrapolation of the Helios trend, deduced from observations between 0.31 and 0.86 AU, suggests that this natural background is near the sensitivity threshold of the ISEE-3 plasma wave instrument at 1 AU, $3\times10^{-4}\gamma/\sqrt{Hz}$ at 17.8 Hz. Such a background is often present in the ISEE-3 data, but it is difficult to study because it is near threshold. The Helios team also found that $f_{ci} \leq f \leq f_{ce}$ noise was strongly enhanced by a quasi-perpendicular (Neubauer et al., 1977a) and a quasi-parallel (Neubauer et al., 1977b) interplanetary shock. Neubauer et al. (1977a,b) and Gurnett et al. (1979) did not discuss how far downstream the noise initiated by the shocks extended. However, $f_{ci} \leq f \leq f_{ce}$ electric field fluctuations remained enhanced many hours downstream of three interplanetary shocks observed by Voyagers 1 and 2 (Burlaga et al., 1980). Although the Voyager 1 and 2 plasma wave instrument had no wave magnetic field sensor, it probably detected the same kind of waves as did Neubauer et al. (1977a,b). Our previous ISEE-3 study (Kennel et al., 1982) found that nearly all interplanetary shocks initiate strong (> 17.8 Hz) magnetic field noise that extends downstream through the region of the shock driver. Broadband electromagnetic noise with $f > f_{ci}$ is also a ubiquitous feature of the magnetosheath downstream of the earth's bow shock (Smith et al., 1967; Smith et al., 1969; Olson et al., 1969; Smith and Tsurutani, 1976; Anderson et al., 1982). The $f > f_{ci}$ magnetic spectra downstream of interplanetary shocks and of the bow shock are similar in amplitude level and frequency dependence (Kennel et al., 1982). Measured in units scaled to the ion cyclotron frequency, these spectra are also similar to that found downstream of the shock in a high Mach number, high β laboratory simulation of the magnetosphere (Podgorny et al., 1979).

Beinroth and Neubauer (1981) showed that $f_{ci} \leq f \leq f_{ce}$ magnetic noise is intensified in the high-density leading edges of fast stream events and generally remains detectable throughout the stream encounters. Our ISEE-3 data confirms their conclusions. $f_{ci} < f \leq f_{ce}$ magnetic noise enhancements are also associated with small-scale structures in the solar wind. Neubauer et al. (1977a,b) found increases associated with directional and tangential discontinuities, as well as reversible dips, in the interplanetary field. Although we will not repeat the above studies, we will document our belief that $f_{ci} < f \leq f_{ce}$ magnetic noise is enhanced whenever the interplanetary field direction is variable.

The evidence cited above indicates that magnetic field noise between the electron and ion cyclotron frequencies is nearly always present in the solar wind and that it intensifies when the solar wind is disturbed. Its ubiquitousness is enough to suggest that its role in determining solar wind transport processes needs to be evaluated. More experimental information is needed before this can be done. This paper addresses two questions: First, what is the relationship between the magnetic noise below and above the ion cyclotron frequency, and how does this relationship depend on solar wind conditions? Secondly, for the noise above f_{ci}, can the plasma mode be identified well enough to suggest possible free-energy sources for its growth?

In Chapter 2, we characterize the events to be studied in this paper. There we present interplanetary field, density, flow velocity, and plasma wave data for 24 hours surrounding the passage over ISEE-3 of two interplanetary shocks (April 5 and June 6, 1979), two fast streams (January 1-2 and May 22-23, 1979), and a possible weak shock or tangential discontinuity (February 5-6, 1979).

In Chapter 3, we study the relationship between the portions of the magnetic field spectrum above and below the ion cyclotron frequency in the disturbed solar wind. Since the ISEE-3 magnetometer and plasma wave instrument provide spectral analysis that overlaps at 3 Hz, the full magnetic spectrum can be determined essentially up to the electron cyclotron frequency. Above 10 Hz, the spectral density has an $f^{-\alpha}$ power law frequency dependence, with $1 \leq \alpha \leq 2$ in both the magnetosheath (Smith et al., 1967; Olson et al., 1969) and solar wind (Neubauer et al., 1977a,b; Gurnett, 1978; Kennel et al., 1982). Below 1 Hz, both magnetosheath and solar wind spectra can be characterized by another power law with a smaller spectral index. The two spectra meet, with a break in the frequency dependence, between 1-10 Hz. However, because both the low and high-frequency ends of the interplanetary spectrum vary with the level and type of solar wind disturbance, only individual case studies can determine how its two parts are physically related. We will present examples of magnetic spectra at different positions behind interplanetary shocks and in fast streams and document tantalizing evidence that even though the high and low-frequency spectral indices are variable, they are locked in a 2:1 ratio behind shocks, but not in fast streams. To our knowledge, there has been no corresponding study of the dependence of the magnetosheath magnetic spectrum upon upstream solar wind parameters.

It is reasonable to assume that electromagnetic waves with frequencies between the ion and electron cyclotron frequencies are in the whistler mode. Chapter 4 begins our considerations of what particles the $f_{ci} \leq f \leq f_{ce}$ waves observed on ISEE-3 might resonate with, by assuming the waves are indeed whistlers. The region downstream of the April 5, 1979, interplanetary shock permits an interesting test of the whistler hypothesis, because the magnetic energy per particle, $B^2/8\pi N$, which scales all resonant particle energies, varied by several orders of magnitude. Using common data pool solar wind parameters, we calculate the parallel energy necessary for electrons to cyclotron resonate with whistlers of the observed frequencies, assuming parallel wave propagation. Although the cyclotron resonance energy varied by four orders of magnitude during the event, the observed magnetic noise amplitudes remained relatively constant. Clearly, one would have expected a striking response if cyclotron resonance interaction had destabilized or damped parallel whistlers. This puzzling result motivates questions to be taken up in Chapter 5. Given that other electromagnetic modes with $f_{ci} < f < f_{ce}$ are theoretically conceivable in a high β plasma (Kennel and Scarf, 1969), are the observed waves really whistlers? If they are whistlers, at what angle to the interplanetary field do they propagate? Do they refract as they propagate through the turbulent solar wind from their source to the spacecraft? At what angle to the magnetic field do they propagate when they are generated?

Sections 5.1 and 5.2 take up the first of the above questions: Are the observed waves really whistlers? We compare the measured ratios of wave magnetic (B) to electric (E) field amplitudes with the theoretical parallel whistler index of refraction, $n_{\parallel}$, calculated using common data pool solar wind parameters, for the event of June 6, 1979, when a low interference level permitted good electric field measurements. Given the limited time resolution of common pool data, and the fact that ISEE-3 had single non-orthogonal electric and magnetic antennas, no single comparison can be conclusive. We therefore resorted to a statistical study whose overall conclusion is clear. The measured values of $B/En_{\parallel}$ fall in the range 0.5-4 with few exceptions, confirming the waves are whistlers, as had first been suggested by Neubauer et al. (1977a,b).

Section 5.3 addresses the final question mentioned above: At what angle to the magnetic field do the whistlers propagate when they are generated? The normal frequency spectrum, which is a smooth power law, probably results from a volume average of whistlers which propagate to the spacecraft from distant sources. However, ISEE-3 occasionally detects intense bursts of whistler noise whose frequency spectrum is peaked. Although these bursts have frequencies similar to those of "lion roars" observed in the magnetosheath (Smith and Tsurutani, 1976), they have longer duration than lion roars and, unlike lion roars, are not associated with localized magnetic field depressions. If we assume that these bursts occur when a source passes near or over ISEE-3, the measured B/E ratios yield an estimate of the angle of propagation at which whistlers are generated. We find that the whistler bursts have a consistently larger B/E ratio than those typically encountered and larger than the parallel whistler index of refraction calculated using common data pool solar wind parameters. This suggests that whistler bursts propagate at large oblique angles to the interplanetary field.

The experimental uncertainties associated with each of our conclusions are discussed in detail in Chapters 3-5. In Chapter 6, we summarize these conclusions and present a picture of the way in which solar wind whistlers affect solar wind electron transport.

2. EVENT SYNOPSIS

2.1 Shock Event of April 4-5, 1979

Figure 1 shows 24 hours of 311 Hz - 3.11 kHz electric field, 17.8 - 178 Hz magnetic field, and interplanetary field data surrounding the passage of an interplanetary shock over ISEE-3 at 0120 UT on April 5, 1979. The impulsive 1 - 3 kHz ion acoustic noise upstream suggests the shock was quasi-parallel, and shock-normal analysis reveals it propagated at 44° to the upstream magnetic field (Kennel et al., 1982). The Rankine-Hugoniot relations imply that the downstream β, the ratio of plasma to magnetic pressure, exceeded unity, given the estimated upstream β of 0.2 and the fast Mach number of 2.9.

The interplanetary field components B_x, B_y, B_z indicate that the post-shock flow can be divided into two different regions. Between the shock at 0120 UT and an interface at 0950 UT, the interplanetary field direction was highly variable, whereas after 0950 UT, and especially after 1100 UT, the direction varied more smoothly. After 1100 UT, the field went through one large rotation before achieving a quiet state at 1800 UT. The interplanetary field magnitude B_T time profile indicates there was a third, still different period between 0720 and 0950 UT, during which B_T was depressed and β was large. The solar wind number density (Figure 9) increased from 12 cm^{-3} at 0720 UT to a broad maximum of about 90 cm^{-3} during the magnetic field minimum between 0840 UT and 0900 UT. The density decreased from 90 to 50 cm^{-3} at the B_T increase at 0900 UT and decreased again from 50 to 5 cm^{-3} at the second jump in B_T at 0950 UT. If pressure balance was maintained across these two magnetic interfaces, the sum of the electron and ion temperatures was about 60 eV ahead of each, and β was about 20 ahead of the 0900 UT interface.

The above evidence suggests that the driver of the April 5, 1979, shock was associated with a low β magnetic loop, similar to the one studied by Bame et al. (1981), that was preceded by a slug of dense hot plasma.

The 17.8 - 178 Hz magnetic fields behaved differently in the three regions identified above. Their spectral densities are plotted on a logarithmic scale in Figure 1, whereas the interplanetary field is on a linear scale. The spectral densities averaged over 128 seconds are solid, whereas dots indicate the peaks detected during the same 128-second interval. Relatively brief increases in spectral density were associated with dips in the interplanetary field at 0540 and 0650 UT; the one near 0650 UT is similar to the event documented in Figure 3 of Neubauer et al. (1977a). A broader enhancement between 1140 and 1230 UT appears to be a weaker version of that between 0720 and 0950 UT. In general, the wave amplitudes are stronger during the period of disorderly field direction preceding 0950 UT than in the low β interplanetary field rotation that follows. They were strongest in the dense high β region between 0720 and 0950 UT; during this period, the amplitudes, though elevated, were remarkably constant, despite the extreme variations in plasma parameters that took place (Figure 9).

2.2 Shock and Fast Stream Event of June 6-7, 1979

The June 6, 1979, shock at 1845 UT led a fast stream that passed over ISEE-3 at 2145 UT. Figure 2 shows 24 hours of interplanetary field and wave electric and magnetic field data for this event. The magnetic field magnitude B_T jumped from 13 to 27γ at the shock and remained nearly constant until it dipped suddenly to 10γ at 1920 UT. It then gradually increased to a maximum of 55γ at 2100 UT. This region of strong magnetic field terminated in a decrease at 2145 UT. It was followed by a period of gradual but structured decline that brought B_T back to its undisturbed state through a final small sudden decrease near 0500 UT on June 7 that may have been a developing reverse shock (Kennel et al., 1982). The solar wind density (Figure 11), which increased from 27 cm^{-3} to 112 cm^{-3} at the shock, decreased to 75 cm^{-3} ten minutes downstream. The density dropped from 78 cm^{-3} to 25 cm^{-3} at the 1920 UT magnetic field dip. Thereafter, while the field magnitude recovered and increased, the density commenced a further decline, reaching 1.2 cm^{-3} between 2115 UT and 2145 UT. The solar wind speed (Figure 11) increased from 450 km/sec at 1930 UT to above 900 km/sec just before the interface at 2145 UT. On crossing the interface, B_T decreased, the density returned to 25 - 30 cm^{-3}, and the solar wind speed diminished to 550 km/sec, about 100 km/sec faster than upstream of the shock.

The bottom inset of Figure 2 shows 3.2 - 178 Hz magnetic field data for this event. Data from the 3.2 and 8.8 Hz channels of the plasma wave instrument were processed using the ISEE-3 magnetometer electronics. The format is the same as in Figure 1. A period of weakly disturbed 3.2 - 56.2 Hz magnetic field noise commenced about 1220 UT, six hours upstream of the shock. The amplitudes in all channels up to 178 Hz increased sharply at the shock and remained enhanced throughout the following period of disorderly interplanetary field direction. They returned to threshold at the 0500 UT developing reverse shock.

The top inset in Figure 2 shows 31.1 Hz - 100 kHz wave electric field data for this event. The behavior above 1 kHz has been documented in Kennel et al. (1982). 1 kHz noise is enhanced between the 1845 UT shock and the 0500 UT possible reverse shock. Note the 31.6 kHz electron plasma wave bursts downstream of the developing reverse shock at 0500 UT. The smooth components at 31.6, 56.2, and 100 kHz are a combination of a shock-associated electron plasma wave continuum (Hoang et al., 1980) and type III bursts. The 31.6 - 100 Hz electric field measurements are the most significant new feature of the data for our purposes. The strong interference upstream disappears at the shock and is replaced by a variable, apparently natural, signal that is particularly strong in the low-density region near 2100 UT. This is one of the rare occasions when the ISEE-3 plasma wave instrument can determine B/E ratios, and therefore indices of refraction, for the low-frequency magnetic fluctuations. This will be taken up in Chapter 5.

2.3 Fast Stream Event of January 1-2, 1979

Figure 3 shows 24 hours of solar wind magnetic field, density, and flow speed data, drawn from the ISEE-3 common data pool, together with 17.8 Hz magnetic and 1.78 kHz electric field spectral densities, surrounding the passage of a gentle fast stream over ISEE-3 at 1730 UT on January 1, 1979. Unlike the June 6-7, 1979, event, this fast stream was not so strong that the compressional magnetohydrodynamic wave ahead of it could steepen into a shock before reaching 1 AU. Although a period of directional disorder in the interplanetary field began near 0500 UT, there was no jump in the field magnitude B_T that could be associated with a finite amplitude shock. Rather, B_T commenced a broad gradual increase that continued until 1130 UT. The magnetic field was depressed and more irregular between 1130 and 2130 UT, at which point it recovered its smooth character. The field depression was most pronounced between 1730 and 1930 UT, when the density was highest. The density, which had increased from ~ 2.5 to 7.5 cm^{-3} between 0900 and 1000 UT, rose sharply beginning at 1720 UT to a plateau of about 12.5 cm^{-3}, which suddenly terminated at 1930 UT. The solar wind speed, which had been around 460 km/sec, began to increase to 560 km/sec when the density increased at 1720 UT. A rarefaction zone followed the density peak in which the density decreased irregularly to a minimum below 1 cm^{-3} at 2300 UT, during which time the solar wind speed held roughly constant at ~ 560 km/sec. The sequence of events described above is compatible with the typical phenomenology of fast streams (Gosling <u>et al.</u>, 1978).

Bursts of 1.78 kHz electric field noise commenced after 0400 UT. Their increasing intensity raised the peak amplitudes, and their increasing repetition rate raised the average amplitude, until an overall activity maximum was reached near 0500 UT, at which time the interplanetary field direction became variable. The 1.78 kHz electric fields dropped precipitously near 0700 UT, but activity remained detectable throughout the event. These waves are similar in frequency range and burstiness to the solar wind ion acoustic waves discussed by Gurnett and Anderson (1977), and Gurnett and Frank (1978). The most intense ion acoustic waves occurred in the leading edge of the January 1-2 fast stream, when the solar wind density was low and just beginning to increase.

The 17.8 Hz magnetic field amplitudes were lower during the shock-free fast stream of January 1-2, 1979, than after the shocks of April 4-5, 1979, and June 6-7, 1979. The first noticeable burst of 17.8 Hz noise occurred near 0620 UT during a small local maximum in density and a local minimum in ion acoustic wave activity. 17.8 Hz noise remained consistently above threshold after the density increase between 0900 and 1000 UT until the end of the day. A broad gentle amplitude maximum was associated with the high-density region between 1720 and 2000 UT.

2.4 Fast Stream Event of May 22-23, 1979

Figure 4 presents 24 hours of solar wind magnetic field, density, and velocity data, as well as 17.8 Hz magnetic and 1.78 kHz spectral density, during the passage of a fast stream over ISEE-3 on May 22-23, 1979.

Inspection of plasma wave data, not shown, shows that weak ion acoustic wave activity terminated, and weak 17.8 - 178 Hz electric field activity began, near 1210 UT on May 21, 1979. This may be evidence of a weak shock at 1210 UT. By the time Figure 4 begins, 0230 UT on May 22, the interplanetary field magnitude was in the midst of a broad gentle increase, and the field direction was highly variable. The solar wind speed increased irregularly but continually throughout the day from 350 km/sec at 0230 UT on May 22 to 600 km/sec at 0230 UT on May 23. The solar wind density had two peaks; it rose smoothly to a local maximum at 0800 UT, dropped sharply into a broad depression between 0800 and 1330 UT, and then rose equally sharply to a peak of 23 cm^{-3} at 1400 UT. The density then declined until the final rarefaction zone began at 2100 UT. The density drop at 2100 UT could be a developing fast shock. Thus, the May 22-23, 1979, fast stream was stronger and of longer duration than the one on January 1-2, 1979. The density maximum associated with the leading edge of this fast stream took 19 hours, from 0200 UT to 2100 UT, to pass over ISEE-3 on May 22.

Impulsive 1.78 kHz ion acoustic noise was present throughout the event, although the 1.78 kHz average amplitude never reached the level it did at 0500 UT on January 1, 1979. The ion acoustic wave activity was more intense before the second density maximum at 1400 UT than after. It suddenly decreased to threshold at 2230 UT in the rarefaction zone. Bursts of 17.8 Hz magnetic noise were detectable between 0230 and 0430 UT on May 22, though the averages were at threshold. Peaks and averages were both above threshold from 0430 UT on May 22 until 0100 UT, well into the rarefaction zone. After 0100 UT, both 1.78 kHz ion acoustic waves and 17.8 Hz magnetic fluctuations remained near threshold until a data gap at 0400 on May 23.

2.5 Discontinuity of February 5-6, 1979

Figure 5 shows 24 hours of solar wind magnetic field, velocity, and density data, together with 17.8 Hz magnetic and 5.62 kHz electric fields surrounding the passage of a discontinuity over ISEE-3 near 2155 UT on February 5, 1979.

The discontinuity is most apparent in the Y-component of the interplanetary field, which changes sharply from a period of relative constancy to one of great variability at 2155 UT. Accompanying this change is a slight increase in the field magnitude and a jump of ~ 50 km/sec in the solar wind speed. The absence of a sharp density jump, on the 5-minute time resolution of the common data pool density, weakens the interpretation of this event as a weak shock. The 5.62 kHz electric field noise is found upstream of the 2155 UT discontinuity, and the 17.8 Hz magnetic noise is downstream, reminiscent of shock-associated plasma waves (Kennel et al., 1982). In any case, Figure 5 illustrates our contention that low-frequency magnetic noise accompanies a disorderly interplanetary field direction.

3. DISTURBED INTERPLANETARY ELECTROMAGNETIC SPECTRA

In this chapter, we examine the detailed relationship between the high-frequency spectra and the corresponding spectra of the disturbed interplanetary magnetic field. In Figure 6, we show magnetic amplitude spectra obtained behind four interplanetary shocks and in two fast stream interaction regions. Overview 24-hour plots of the November 12, 1978, and April 24, 1979, shocks can be found in Kennel et al. (1982). The low-frequency IMF spectra were measured by the JPL DC magnetometer. The plotted spectra are for the B_z-component of the IMF over the frequency range $0.04 < f < 3$ Hz and thus represent the high-frequency end of the total IMF spectrum. The B_z-component was chosen in order to minimize the effects of spin modulation. The spectral densities at 3.2 and 8.8 Hz (crosses) were measured by the TRW search coil, whose digital data was read-out through the DC magnetometer electronics. The spectra from 17.8 Hz to 310 Hz were obtained from 128-second averages of the search coil digital out-put. As is evident from Figure 6, the 3 Hz spectral amplitude from the DC magnetometer does not exactly match that obtained by the search coil at 3.2 Hz; however, given the different measurement and spectral processing techniques, the disagreement between the DC magnetometer and search coil data is minimal. No attempt was made to "normalize" the low and high-frequency spectra by forcing the two to match, since the spectral break is expected to lie in the frequency range 1-10 Hz where the different measurement techniques merge. Straight lines (eyeball fit) have been drawn through the DC magnetometer and $f \geq 8.8$ Hz search coil spectral measurements; power law spectral indices were estimated from these straight line "fits".

The four post-shock spectra are similar in amplitude and spectral shape. Table I lists the UT of the shock and the estimated spectral indices for the low and high-frequency "straight line" portions of the spectra. Even though the spectra were taken at very different times in the post-shock flows, the spectral indices are all comparable, indicating the general uniformity of the downstream electromagnetic spectra. In addition, for all four shocks the spectral indices in the high-frequency range are about twice the indices of the corresponding low-frequency IMF spectrum.

The left-hand side of Figure 6 shows two spectra taken during the January 2 and May 22, 1979, fast stream encounters. Their IMF and $f > 3.2$ Hz spectra have lower amplitudes and steeper spectral slopes than in the downstream shock flows. Because the spectral amplitudes above 56 Hz are near the threshold of the search coil, the data do not indicate a flattening of the spectra. From Table I, the spectral index at higher frequencies is about 2.5 times that of the IMF.

Although the post-shock IMF and high-frequency spectral indices have "typical" values, the approximate doubling of the high to low-frequency spectral slopes is somewhat unexpected considering the large-scale disorder generally observed throughout the downstream shock flow. In order to examine this point further, Figure 7 plots the IMF vs high-frequency spectral index for four separate spectral determinations downstream of each of the four shocks in Figure 6; the individual spectra were separated by one or more hours in time. Although the data is clearly of limited statistical significance, the points in Figure 7 cluster about their average value (denoted by "A") of a 2 to 1 ratio of high to low-frequency spectral indices; the average value of the high-frequency (IMF) spectral index is $\alpha = 1.6$ ($\alpha = 0.8$). For comparison, we also include two separate spectra from each of the three non-shock fast stream events (shown in Figures 3, 4, and 5). The non-shock high-frequency spectra are significantly steeper than the post-shock spectra, and the IMF spectral index is somewhat more variable.

Although the above evidence is only suggestive, the possibility of a close coupling between the $f > f_{ci}$ and IMF spectral indices is further strengthened by an event which occurred downstream of the June 6, 1979, shock. Returning to Figure 2, the f > 3.2 Hz amplitudes behind the shock remained enhanced until about 2030 UT, when a significant decrease began which reached a minimum at 2100 UT. The intensity gradually recovered, so that by 2200 UT, the amplitudes had regained their immediate post-shock level. During the amplitude minimum, the IMF magnitude reached a peak of 55 gamma, and the B_z-component (as well as B_x and B_y, not shown) was fairly steady. Figure 8 shows the magnetic amplitude spectra taken at the f > 3.2 Hz amplitude minimum (2100 UT) and about one hour on either side. The IMF spectrum at 2100 UT is very flat ($\alpha = 0.4$), and the low-frequency (f < 0.1 Hz) amplitude is about a factor 10 below the "typical" shock spectra of Figure 6. The 2100 UT f > 3.2 Hz spectrum is very steep ($\alpha = 2.7$) and reaches the search coil background at f = 56 Hz. The spectrum taken before (2010 UT) the f > 3.2 Hz amplitude minimum has a low-(high) frequency spectral index of $\alpha = 0.85$ ($\alpha = 1.75$), for a ratio of nearly 2 to 1. After the minimum (2200 UT), the nearly 2 to 1 ratio is re-established with an IMF high-frequency spectral index of $\alpha = 1.02$ ($\alpha = 2.0$).

The magnetically quiet interval around 2100 UT separated two disordered regions of the post-shock flow. The distinctive nature of this interval is also demonstrated by the common data pool data from the LANL/MPI plasma probe. The solar wind density decreased from 20 cm^{-3} at 2000 UT to about 2 cm^{-3} near

2100 UT (see Figure 11), and then recovered to above 20 cm^{-3} after 2200 UT. Hence, the re-establishment of the approximate 2 to 1 ratio of high to low-frequency spectral indices after the quiet interval suggests that the spectral slopes in the two frequency ranges may be dynamically coupled. In addition, the persistence of the 2 to 1 spectral relationship for many hours downstream of the shock indicates that the dynamical coupling may be a general feature of the post-shock flow that is probably maintained on a quasi-local spatial scale. On the other hand, the IMF and f > 3 Hz spectra in fast streams do not show the 2 to 1 relationship of spectral indices, at least on the basis of the limited number of events examined here. Clearly, only a more extensive investigation can establish the generality of, and the plasma conditions under which, the 2 to 1 spectral relationship occurs.

4. RESPONSE TO CHANGING PLASMA CONDITIONS

Plasma waves often depend quite sensitively on local plasma conditions for both their propagation characteristics and their excitation and damping interactions with particles. For example, the whistler mode index of refraction (n') in the quasi-transverse approximation is given by (Stix, 1962),

$$n'^2 = \frac{k^2c^2}{\omega'^2} = \frac{\omega_p^2}{\omega'(\Omega\cos\theta-\omega')} \quad (1)$$

where $\omega_p = (4\pi Ne^2/m)^{\frac{1}{2}}$ is the electron plasma frequency, $\Omega = eB/mc = 2\pi f_{ce}$ is the electron cyclotron frequency, and ω' is the wave frequency in the plasma rest frame. The angle $\theta = \cos^{-1}(\hat{k}\cdot\hat{B})$ where $\underline{k}$ is the wave vector and $\underline{B}$ is the local direction of the magnetic field; $\hat{k}$ and $\hat{B}$ are the corresponding unit vectors. For the low frequencies of interest here ($\omega' << \Omega$), the index of refraction is proportional to the ratio of plasma density (N) to magnetic field strength (B). Low-frequency ($\omega' << \Omega$) whistlers have first order cyclotron resonant interactions with electrons of characteristic parallel energy (Kennel and Petschek, 1966),

$$E_c = \frac{B^2}{8\pi N}\frac{1}{\bar{k}^2\cos^2\theta} \quad (2)$$

where $\bar{k} = kc/\omega_p$. Oblique whistlers ($\theta \neq 0$) also interact at Landau resonance with electrons of parallel energy (Kennel, 1966),

$$E_L = \frac{B^2}{8\pi N}\frac{\bar{k}^2}{(1+\bar{k}^2)^2}\ . \quad (3)$$

Finally, whistlers have a forward (or anomalous) cyclotron resonant interaction with ions of energy $(m_i/m)E_L$. Hence, the characteristic energy $B^2/8\pi N$ determines whether the whistler will have strong or weak resonant interactions with various parts of the plasma distribution.

To determine the resonant energies, we must estimate the wave number $\overline{k}$ which corresponds to the frequency ω observed in the spacecraft frame. From the Doppler relation, we have $\omega = |\omega' + \underline{k}\cdot\underline{v}| = |\omega' + kv\cos\phi|$ where v is the solar wind speed, ϕ is the angle between $\underline{k}$ and $\underline{v}$, and the absolute value implies that the observed frequency ω is interpreted as positive for $\omega' > 0$. For low-frequency whistlers ($\omega' << \Omega_e\cos\theta$ and $\overline{k} << 1$), the possible wave numbers for an observed ω is given by

$$\overline{k} = \pm \frac{V|\cos\phi|}{2C_a|\cos\theta|} + \left[\frac{V^2\cos^2\phi}{4C^2_a\cos^2\theta} + \frac{\omega}{\Omega_e|\cos\theta|}\right]^{\frac{1}{2}} \tag{4}$$

where $C_a = B/(4\pi nm)^{\frac{1}{2}}$ is the electron Alfvén speed. For $|\cos\phi| = 1$, the maximum (minimum) value of $\overline{k}$ corresponds to a rest frame frequency ω' which has been red-shifted (blue-shifted) to the observed frequency ω by the solar wind flow. If $\overline{k} > 1$, the whistler propagates near the resonance cone $\omega' \simeq \Omega\cos\theta$, and the estimate of $\overline{k}$ from the observed wave frequency (ω) becomes uncertain. In this case, the cyclotron and Landau energies depend sensitively on θ, and the wave has a strong electrostatic field.

An interesting interval in which to examine the effects of changing solar wind conditions on the $f > f_{ci}$ electromagnetic waves occurred several hours after the April 5, 1979, shock. Figure 2 shows that between 0800 and 1000 UT, the magnetic field decreased from about 40γ to 10γ and then suddenly increased; the high-frequency waves were enhanced from about 0730 UT to 1000 UT. Figure 9 displays the interval 0700 UT to 1000 UT in greater detail. The plasma density, flow speed, and magnetic field are from the common data pool. The top panel shows that the solar wind velocity gradually increased from about 600 km/sec at 0700 UT to about 700 km/sec by 0820. From 0700 to 0750 UT, the magnetic field gradually decreased from 38γ to 34γ. After a sharp drop at 0750 UT, the field strength underwent an erratic decline to 8.6γ at 0857 UT and then increased to above 30γ by 09C1 UT. A second decrease and rapid increase in the field strength occurred between 0930 UT and 0950 UT. The solar wind plasma density (dashed curve) gradually increased from 30 cm^{-3} to 50 cm^{-3} during the interval 0700 to 0830 UT. A sharp increase to 95 cm^{-3} between 0830 and 0840 UT was followed by a rapid density decrease to 55 cm^{-3} at 0902 UT. The density then remained roughly constant until 0945 UT, whereafter it declined to 5 cm^{-3} at 1000 UT. Clearly, the characteristic whistler energy $B^2/8\pi N$ underwent extremely large variations during this three-hour period. At 0700, $B^2/8\pi N$ was 120 eV, which probably corresponds to $\beta < 1$(_ = $8\pi NT/B^2$) solar wind conditions (the plasma temperature is not available on the common data pool tape, but is typically 20-60 eV). After the large reduction in B and increase in N, $B^2/8\pi N$ had fallen to 2 eV near 0850 UT. The sharp rise in B and decrease in N near 0900 meant that $B^2/8\pi N$ increased to 66 eV at 0905 UT.

The third panel in Figure 9 shows 128-second averages of the 17 Hz high-frequency wave spectral amplitude, which increased by about an order of magnitude between 0720 and 0800 UT and then remained constant to within a factor of 2 until 0950 UT. Figure 10 displays eight high-frequency wave spectra (peaks and 128-second averages) taken at various times during the 0700-1000 UT interval. After the 0720-0750 UT amplitude increase, the spectral amplitudes and overall shapes remained essentially similar. In particular, the two spectra at 0845 and 0856, for the period of maximum N and minimum B, differed a little from the spectra at 0902, during the rapid rise in B and fall in N, and at 0910, after B and N became constant. Hence, the spectra were relatively unaffected by the large density and magnetic field variations.

Returning to Figure 9, in the fourth panel we have plotted the minimum electron energy (E_c) which would be in cyclotron resonance with a parallel propagating ($\theta = 0$), 17 Hz whistler. The blue and red shift curves correspond to the two possible values of the wave number from (4) assuming $\overline{k} < 1$; $\cos\phi$ was calculated assuming that the solar wind velocity was radial. The bottom panel shows the electron Landau resonant energy (E_L) using the same values of $\overline{k}$ obtained by assuming $\theta = 0$; recall, however, that whistlers interact at Landau resonance only for oblique propagation. From 0700 to 0800 UT, the cyclotron resonant energies were in the range 1-10 keV, so that only the high-energy tail of the solar wind electron distribution could have interacted with 17 Hz whistlers. Near the magnetic field minimum and density maximum (0850 UT), E_c decreased to 10 to 40 eV. Since the solar wind electron temperature is typically 10 to 40 eV, strong cyclotron interactions would be expected if the high-frequency waves are parallel propagating whistlers; strong growth (damping) would occur if the thermal electrons had a perpendicular (parallel or zero) anisotropy. The 17 Hz amplitudes and the entire high-frequency spectrum exhibited neither strong growth nor damping between 0840 and 0900 UT. Since it is unlikely that the anisotropy could adjust to precise marginal stability at all frequencies, we conclude that either the high-frequency waves were not whistlers, or that they were whistlers which propagate at large angles ($\cos\theta << 1$) to the magnetic field. The cyclotron resonant energy for very oblique whistlers could be much higher than the minimum value shown in Figure 9, thereby reducing the strength of the cyclotron resonant (damping or growth) interaction.

The electron Landau energies are $\lesssim$ 3 eV for the entire interval 0700-

1000 UT and vary considerably less than the cyclotron energies; from (3), decreases in $B^2/8\pi N$ are partially compensated by the increase in $\overline{k}^2$ due to increasing ω'/Ω. Since the Landau energy is less than the typical solar wind electron thermal energy, slightly oblique whistlers ($\cos\theta < 1$) would have reasonably strong Landau resonant interactions with thermal electrons. However, if $\cos\theta << 1$, the whistler Landau energy would exceed the values shown in Figure 9, and the Landau resonance could lie in the energy range of the superthermal or halo electrons (Feldman, 1979).

In conclusion, the absence of any significant change in the high-frequency spectra during large variations in $B^2/8\pi N$ casts doubt on the hypothesis that these waves are parallel propagating whistlers, at least during the 0700-1000 UT interval. Of course, the estimates of the whistler resonant energies E_c and E_L are quite uncertain; large-scale magnetic field fluctuations and local variations in solar wind density and velocity probably introduce considerable error in $B^2/8\pi N$, the propagation angle (θ), and the Doppler shift ($v\cos\phi$). Nevertheless, the factor of 10^4 change in E_c should have produced some observable variation in the high-frequency spectra if these waves were parallel whistlers. However, oblique whistlers should be less sensitive to $B^2/8\pi N$ variations.

5. HIGH-FREQUENCY WAVE INDEX OF REFRACTION

A definitive method to identify a plasma wave mode is to measure the electric and magnetic field polarizations and, for an electromagnetic wave, to demonstrate that the measured magnetic to electric field ratio is consistent with the index of refraction. The ISEE-3 wave instrument has a single-axis electric antenna and one search-coil magnetometer; the electric and magnetic sensors do not measure orthogonal components of the respective fields. Hence, accurate electromagnetic polarization measurements are not possible. Another instrumental difficulty is that the electric field channels at frequencies below 100 Hz often suffer from spacecraft interference. However, occasionally the interference levels are greatly reduced, permitting accurate wave electric field measurements.

A further uncertainty in determining the index of refraction is introduced by the Doppler shift. The relation between a wave magnetic field ($\underline{B}$) and the wave electric field ($\underline{E}$) measured in the spacecraft frame is given by,

$$\underline{B} = \frac{\underline{n}' \times \underline{E}}{1 + \underline{n}' \cdot \underline{v}/c} \tag{5}$$

where $\underline{n}' = \underline{k}\, c/\omega'$. If the wave polarization is predominantly electromagnetic, $|\underline{n}' \times \underline{E}| \sim n'E$, so that the ratio of the wave fields becomes

$$\frac{B}{E} \approx \frac{kc}{\omega' + \underline{k} \cdot \underline{v}} = \frac{kc}{\omega} = n \, . \tag{6}$$

Hence, the measured B/E ratio provides an estimate of the index of refraction in the spacecraft frame, or, for a fixed ω, an estimate of the wave number k.

From Figure 2 for the June 6, 1979, shock, the interference levels in the f $\gtrsim$ 31 Hz electric field channels decreased by about an order of magnitude behind the shock and remained depressed for many hours. In this section, we attempt to evaluate the index of refraction of the $f > f_{ci}$ magnetic waves by three different techniques. Given the limitations of the wave detector and the uncertainties due to the Doppler shift, none of these methods is definitive. However, taken together, the B/E estimates of the index of refraction support the conclusion that the high-frequency modes are whistlers.

5.1 Average Refractive Indices

Figure 11 summarizes the plasma and wave conditions behind the June 6, 1979, shock. The top panel shows the solar wind plasma density and flow velocity from the common data pool listings provided by the LANL/MPI plasma instrument. At the shock, the density jumps to over 100 protons/cm^{-3}; after about 1920 UT, the density drops from about 80 cm^{-3} to 20-15 cm^{-3}, and then decreases slowly to the minimum of ~1-2 cm^{-3} at 2100 UT. Behind the shock, the flow velocity gradually increases from ~400 km/sec to above 800 km/sec at 2100 UT, suggesting that the June 6 shock was driven by a fast solar wind stream. After 2200 UT, the density and velocity are roughly constant at 20-30 cm^{-3} and 500-600 km/sec, respectively. The second panel shows the common data pool magnetic field strength from the JPL magnetometer. After the termination of the high density region, the field strength slowly increased from 40 to 55 gammas until 2100 UT and then gradually declined until about 2330 UT, when a sharp decrease occurred. From Figure 1, the B_Z component was highly variable behind the shock, except for a quiescent interval around 2100 UT during the density minimum.

The bottom two panels of Figure 11 show the 178-second average (shaded) and peaks (line) of the 56 Hz electric and magnetic field spectral amplitudes. Ahead of the shock, the 56 Hz E-field signals were dominated by spacecraft interference which is characterized by relatively steady levels in both the peaks and averages. After the shock, the interference level dropped, and the variability of E-field signals above the new interference level indicates that wave amplitudes were accurately measured. The E-field amplitudes increase to a maximum near 2100 UT, the density minimum, and then decline slowly to the interference background near 2330 UT. The 56 Hz magnetic amplitude rises sharply at the shock and remains enhanced except for the deep minimum near 2100 UT.

In the middle panel, we show the results of estimating the 56 Hz index of refraction by taking the ratio of the measured 128-second average magnetic and electric field amplitudes. The average wave amplitudes are used rather than the peak values since the E-field measurements are read-out every 0.5 seconds, whereas each channel of the search coil is sampled only four times (in successive 0.5-second intervals) every 16 seconds; thus, the electric and magnetic field peaks do not necessarily correspond to the same time. In addition, the average values may, to some uncertain extent, compensate for the non-orthogonal alignment of the electric and magnetic sensors. For ease of interpretation, we have normalized the measured ratio $n = B/E$ to the local parallel ($\theta = 0$) 56 Hz whistler index of refraction ($n_{||}$) calculated from the common data pool density and magnetic field. Doppler broadening introduces a ± 5-12% uncertainty in $n_{||}$ and has not been included in the figure. We have only plotted $B/En_{||}$ for the time interval 1900-2340 UT when the E-field amplitudes are clearly above threshold.

From 1900 to about 2045 UT and after 2200 UT, the estimated index of refraction typically lies between 0.5 and 1.0 of the parallel whistler index, with two notable exceptions. At 2002 UT, a large E-field burst occurs which is not accompanied by a corresponding increase in the B-field signal. Here the ratio $B/En_{||}$ decreases to less than 0.1, suggesting that the emission is electrostatically polarized. Also, from 2222-2230 UT, a strong intensification of the B-field amplitude coupled with a modest E-field increase results in $B/En_{||}$ exceeding 3. During the interval surrounding 2100 UT, $B/En_{||}$

becomes quite small (< 0.3) despite the decrease in $n_{\|}$ due to the reduced plasma density. The enhanced E-field and diminished B-field amplitudes, which produce the low $B/En_{\|}$ values, suggest that the 56 Hz emissions were predominantly electrostatic during the density minimum.

In the quasi-transverse approximation, the smallest whistler index of refraction occurs for parallel propagation. Since the error introduced in using average B-field and E-field amplitudes from non-orthogonal sensors is unknown, we cannot conclude that the typical values of the estimated index in the range $0.5 < B/En_{\|} < 1.0$ are necessarily inconsistent with a whistler mode identification for the high frequency magnetic waves. However, the low values of $B/En_{\|}$ obtained at 2002 UT and near 2100 UT are difficult to reconcile with a whistler interpretation and probably indicate that these E-field signals are nearly electrostatic. The presence of electrostatic waves at these times raises the possibility that, during the entire post-shock flow, some fraction of the E-field amplitudes are due to electrostatic emissions. Hence, a possible explanation for the persistent estimate of $0.5 < B/En_{\|} < 1$ may be that only part of the E-field amplitude is due to whistlers, with the residual E-field signals being due to either an electrostatic emission or spacecraft interference, possibly from the solar array (Anderson et al., 1982).

5.2 Instantaneous Refractive Indices

A different technique for estimating the index of refraction of the high frequency waves is to compute a B-to-E ratio using the simultaneously measured, 0.5-second (instantaneous) digital electric and magnetic field amplitudes. During a 16-second instrument cycle, each of the eight B-field frequency channels is sampled for four sequential 0.5-second measurements. Each of the 16 E-field frequency channels is sampled every 0.5 second, so that four B-to-E ratios at a given frequency can be obtained every 16 seconds. Since the 17 Hz E-field signals are dominated by interference, and the 310 Hz B-field amplitudes are nearly always close to the instrument threshold, we are only able to determine B-to-E ratios for the four frequencies 31.6, 56, 100, and 178 Hz.

We have applied the above technique for the post-shock interval 2010 to 2030 UT during which 292 simultaneous E and B measurements were made at each of the four frequencies. This interval was chosen because the solar wind density, flow velocity, and magnetic field strength were relatively constant, thus minimizing the variations in the normalizing whistler index $n_{||}$. The common data pool tape lists the plasma density about every five minutes. These five-minute density measurements were linearly extrapolated between adjacent points, and a new normalizing whistler $n_{||}$ was computed every minute, the time resolution of the common data pool magnetic field measurements. The calculated $n_{||}$ was used to normalize the B-to-E ratios for the following minute.

Figure 12 shows a histogram of the number of times during the 20-minute interval that a given $B/En_{||}$ ratio was measured versus $B/En_{||}$ for each of the four frequencies. The size of each bin in $B/En_{||}$ was chosen as 0.1, which is roughly the uncertainty in $n_{||}$ due to the Doppler shift. At each frequency, the histograms peak at values of $B/En_{||} < 1$, with a general tendency for the peak to occur at smaller $B/En_{||}$ at the higher frequencies. Thus, the histogram distribution determined from the simultaneously measured electric and magnetic fields is consistent with $B/En_{||}$ values obtained from the 128-second averages (Figure 11). Although the majority of the ratios lie below unity, the 31.6 and 56 Hz histograms have a significant tail extending out to $B/En_{||} \geq 2$.

As before, it is difficult to make a definitive mode identification from the simultaneous $B/En_{||}$ histograms. However, what may be significant is that a substantial fraction of the estimated refractive indices B/E fall within a factor of 2 to 3 of the parallel whistler index of refraction. If the high-frequency magnetic emissions were not predominantly whistler mode waves, the observed rough (factor 2 to 3) equality of most of the measured B/E's and calculated $n_{||}$'s (whistler) would certainly be unexpected. The occurrence of low $B/En_{||}$ values, especially at 100 Hz and 178 Hz, again suggests the presence of an electrostatic emission in addition to whistlers. Short wave length electrostatic modes would probably suffer a highly variable Doppler shift, thereby blending the electrostatic component of the E-field amplitudes into different frequency channels, and thus introducing a further uncertainty into the B/E ratios. Finally, the occurrence of $B/En_{||} \gtrsim 1$ is consistent with a whistler interpretation since oblique whistlers ($\cos\theta < 1$) do have indices of refraction exceeding those of parallel whistlers.

5.3 Magnetic Bursts

In the solar wind, the whistler group velocity typically exceeds the wind velocity by a factor 5 to 10. Hence, a satellite wave instrument locally samples whistlers which could have been generated at a large distance from the spacecraft and/or propagated over a large volume. The monotonic power law frequency spectrum, which is observed in the average magnetic amplitudes, may simply represent a large-scale spatial average of the wave energy density; the relatively constant average magnetic amplitudes which are observed downstream of shocks are also consistent with this view.

As is evident in Figure 11 for June 6, 1979, there are occasional short-duration magnetic wave bursts in which the amplitude increases substantially above the average downstream value. A possible interpretation is that the wave bursts are regions of local wave generation in which the conditions for instability are achieved. If this possibility is correct, an analysis of the index of refraction during the bursts might provide additional insight not only in the mode identification, but also on the unstable generation process. In this section, we examine the amplitude spectra and the $B/En_{||}$ ratios for two bursts which occurred between 1941:28-1944:30 UT and 2222:46-2226:21 UT.

In Figure 13, the top two panels show the peak and 16-second average amplitude spectra for the wave electric and magnetic fields during the 1941 UT burst. The four spectra are taken at approximately one-minute intervals during the burst. At 1941:28 UT, the magnetic spectra exhibit the monotonic amplitude decrease with increasing frequency which is typical of the power law behavior of the average downstream spectrum. As the burst develops, the magnetic spectrum evolves first into a broad plateau between 17.8 and 56 Hz (1942:38 UT) and then exhibits a definite peak at 31.6 Hz (1943:24). Between 1941:28 and

1944:30 UT, all the individual 16-second magnetic spectra (not shown) exhibit a peak or plateau at 31.6 and/or 56 Hz. Both the peak and average electric field spectrum have a small "bump" near 56 Hz; the 17.8 Hz E-field channel is dominated by interference. As the burst decays (1944:30 UT), the magnetic spectrum returns to the monotonic, decreasing power law shape. The E-field spectrum shows a broad peak above 100 Hz which is not present in the magnetic spectrum, thus suggesting the presence of an electrostatic mode in addition to the high-frequency magnetic waves.

The bottom panel in Figure 13 presents the $B/En_{||}$ (solid circles) estimate of the index of refraction, which is calculated from the 16-second average E and B amplitudes, and the normalized wave number $\overline{k}$ (dotted circles) which is calculated from the relation $\overline{k} = \omega B/\omega_p E$ (equation 6). As before, only the frequencies 31.6, 56, 100, and 178 Hz are included, and the Doppler shift has been neglected in calculating $n_{||}$. At 1941:28 UT, the ratio $B/En_{||}$ is slightly above unity at 56 and 100 Hz, and below unity at 31.6 and 178 Hz. Using the common data pool plasma density and magnetic field strength, a parallel propagating 56 Hz whistler should have a (calculated) wave number $\overline{k}_{||} = 0.2$ (from equation 1); the estimate of $\overline{k}$ determined from the B/E ratio is 0.29 at 56 Hz, in reasonable agreement with the parallel whistler value. At the peak of the burst (1943:24 UT), the estimated index at 56 Hz reaches a value $B/En_{||} = 2.9$ with a corresponding wave number of $\overline{k} = 0.6$; at 31.6 Hz, $B/En_{||} = 2.1$ and $\overline{k} = 0.3$. After the burst decays (1944:30 UT), $B/En_{||}$ is significantly less than unity at all frequencies, and $\overline{k}$ has decreased to near $\overline{k} \sim 0.1$.

Figure 14a,b shows the amplitude spectra and $B/En_{||}$ results for the strong magnetic wave burst at 2222:46-2226:21 UT. The burst starts (2222:46 UT) with a slight enhancement of the magnetic amplitude at 56 and 100 Hz; the estimated index of refraction ratio is close to unity at these frequencies.

By 2223:52 UT, a broad plateau between 17.8 and 100 Hz has developed in the magnetic spectrum, and the average E-field spectrum exhibits a peak at 100 Hz. The plateau continues until 2225:31 UT, and then decays toward the monotonic decreasing spectrum, with the 31.6 Hz magnetic amplitude still enhanced at 2226:21 UT. During the peak of the burst (2223:19 to 2224:42), the index of refraction at 100 Hz is in the range $3.6 \leq B/En_{||} < 4.6$, and the corresponding wave number is $1.13 \leq \overline{k} \leq 1.36$. The other frequency components in the plateau have $2 < B/En_{||} < 3$, $0.3 \leq \overline{k} \leq 0.4$ for 31.6 Hz, and $3.3 \leq B/En_{||} \leq 4.0$, $0.78 \leq \overline{k} \leq 0.88$ for 56 Hz. For comparison, a parallel whistler should have a wave number $\overline{k}_{||} = 0.17$ at 31.6 Hz, $\overline{k}_{||} = 0.27$ at 56 Hz, $\overline{k}_{||} = 0.3$ at 100 Hz, and $\overline{k}_{||} = 0.4$ at 178 Hz. As the burst decays (2226:21 UT), the $B/En_{||}$ ratios decrease to about one or less, except at 31.6 Hz ($B/En_{||} = 1.75$) which remains enhanced.

The above two wave bursts exhibit spectral amplitude peaks or plateaus which contrast strongly with the monotonic power law spectrum of the average downstream amplitudes. At the excited frequencies, the estimated refractive indices and normalized wave numbers exceed those of a parallel whistler by factors of 2 to 4. Recall that the $B/En_{||}$ ratios, which were computed from the 128-second average wave amplitudes [Figure 11]), and the peak of the histogram distributions, which utilized the instantaneous wave amplitudes (Figure 12), both showed that the estimated refractive index was typically smaller than that expected for a parallel whistler. Although the evidence is not definitive, the strikingly different spectral shape and $B/En_{||}$ ratios certainly suggest that the wave bursts represent the local excitation of the downstream high-frequency magnetic waves. If this hypothesis is correct, we conclude from the observed $B/En_{||} > 1$ ratios that the downstream emissions are generated as whistler waves.

The interpretation of the large $B/En_{\parallel} \sim 2$ to 4 ratios during the burst is less certain. An obliquely propagating whistler has a refractive index which scales approximately as $n/n_{\parallel} \simeq (\cos\theta - \omega/\Omega)^{-\frac{1}{2}}$. Hence, even for $\omega/\Omega << 1$, $n/n_{\parallel}$ can significantly exceed unity if the whistlers propagate at large angles to the magnetic field. For $B/En_{\parallel} \sim 2$ to 4 and $\omega/\Omega \sim 1/20$ to 1/10, we would have $70° \leq \theta \leq 85°$. Of course, the Doppler shift introduces considerable uncertainty in this conclusion, especially since the inferred values of $\overline{k}$ are large. Using equation (6) for $\overline{k}$, the Doppler shift $\Delta\omega = \omega - \omega' = \underline{k}\cdot\underline{v}$ produces a frequency bandwidth $\Delta f/f \sim 1 - 2$ for $\cos\phi \sim 1/2$. If the emission frequency in the plasma rest frame satisfies $\omega' > \omega$ ($\omega' < \omega$), the calculated $n_{\parallel}$ underestimates (overestimates) the rest frame refractive index $n'_{\parallel}$ by a factor of order $(\omega/\omega')^{\frac{1}{2}}$. Hence, the rest frame $B/En'_{\parallel}$ could be closer to unity, corresponding to smaller propagation angles.

The magnetic bursts are reminiscent of the magnetosheath lion roars emissions. Lion roars were first identified as whistlers by Smith et al. (1969) on the basis of the observed frequency $f \sim 80$-200 Hz ($\omega/\Omega \sim 0.1$-0.2) and generally circular or elliptical polarization. Smith and Tsurutani (1976) showed that the lion roars propagate essentially parallel to the magnetic field ($\theta \leq 20°$) and occur preferentially in regions of depressed magnetic field strength. Thorne and Tsurutani (1981) and Tsurutani et al. (1981) demonstrated that the field depressions were accompanied by plasma density enhancements and suggested that the anti-correlated field and density oscillations might be slow-mode hydromagnetic waves or be a consequence of the mirror instability, which is driven by a perpendicular pressure anisotropy in a high-β plasma. Thorne and Tsurutani (1981) argued that, at the B-field minima, the whistler characteristic energy $B^2/8\pi N$ was reduced from its average magnetosheath value, thus permitting lower-energy electrons with small or modest thermal anisotropies to destabilize whistlers at relatively low frequencies ($\omega/\Omega \sim 0.1$-0.2); the higher density of the low-energy electrons would lead to an enhanced whistler growth rate.

The question naturally arises as to whether the magnetic wave bursts and/or the generally enhanced $f > f_{ci}$ waves behind interplanetary shocks are related to the lion roars phenomena observed downstream of the bow shock. At first glance, the large wave normal angle inferred from the high index of refraction ($B/En_{||} \sim 2$-4) suggests that the magnetic bursts are distinct from the nearly parallel propagating lion roars whistlers. However, suppose the magnetic bursts also occurred in magnetic field depressions with density enhancements. Then, the calculated index of refraction $n_{||}$, which normalized the measured B/E ratios, would be smaller than the actual local whistler index since $n_{||}$ scales approximately as $(N/B)^{\frac{1}{2}}$; recall that $n_{||}$ was calculated from the average values of density and magnetic field strength. For magnetosheath lion roars, the change in the ratio N/B is variable, but increases by a factor 2 to 8 are possible (Smith and Tsurutani, 1976; Tsurutani et al., 1981); hence, the local $n_{||}$ in the field minima is a factor $\sim$ 2 to 4 larger than the average magnetosheath value. If a similar increase in the local $n_{||}$ occurred during the magnetic bursts behind interplanetary shocks, the measured B/E ratios would be consistent with parallel whistler propagation.

We have examined high-resolution (0.16 second per field vector) magnetic field data during the two magnetic bursts at 1941 UT and 2222 UT. In both cases, the magnetic field strength was constant to within $\pm$ 1 gamma. High-time resolution measurements of the plasma density are unavailable on ISEE-3. However, for a constant field strength, the density would have to increase by 4 to 16 on a few-minute time scale in order to raise the local $n_{||}$

by a factor 2 to 4, and thereby reduce $B/En_{\parallel}$ to unity. Such large-density fluctuations are unlikely, especially with no corresponding magnetic field decrease as would be expected in the $\beta \sim 1$ downstream flow. Hence, we conclude that the inferred refractive indices of $B/En_{\parallel} \sim 2$ to 4 indicate oblique whistler propagation at least locally at the spacecraft. If the spacecraft is, indeed, within the generation region, the large wave-normal angles imply that the magnetic bursts are distinct from lion roars and may have a different free-energy source. Of course, we cannot eliminate the possibility that the magnetic bursts were generated as parallel whistlers at a distant source and that the wave normal refracted to large angles in propagating from the excitation region to the spacecraft, in this case, the magnetic bursts might be interpretable as lion roars.

6. SUMMARY AND DISCUSSION

Electromagnetic waves between the ion and electron cyclotron frequencies are nearly always present in the solar wind, at least at low-amplitude levels. When the background level detected by Helios near the sun is extrapolated tc 1 AU, it lies near the sensitivity threshold of the ISEE-3 plasma wave instrument. This background is apparently often detected by ISEE-3. This broadband electromagnetic noise is enhanced in at least the following circumstances. Its amplitude increases by typically two orders of magnitude at interplanetary shocks and remains well above threshold throughout the region of shock disturbance. It increases, though less than at shocks, in the high-density leading edges of fast streams and usually remains detectable throughout a fast-stream encounter. It increases in association with small-scale structures in the interplanetary field, such as tangential or rotational discontinuities, and reversible field magnitude dips. One statement that covers all of these cases is that it seems enhanced whenever the interplanetary field direction is variable.

Above a few Hz, the solar wind magnetic spectral density in one vector component normally has a falling power law frequency dependence. This spectrum joins the interplanetary field spectrum with a break in the spectral index in the range 1-10 Hz. The magnetosheath spectrum downstream of the terrestrial bow shock is qualitatively similar. Study of a limited number of events suggests that, even though the individual spectral indices vary from event to event, the high and low-frequency spectral indices tend towards a 2:1 ratio downstream of interplanetary shocks. Such a relationship was not apparent in the less intense fast-stream events. One observation suggests that the 2:1 ratio may be maintained in a kind of dynamical balance. Behind one shock, the interplanetary and broadband magnitudes temporarily decreased; the 2:1 spectral index relation, which prevailed prior to the amplitude minimum, was violated during the minimum, but re-established itself when the amplitude recovered. The observations discussed above, because they are so few in number, suggest mainly that the dynamic relation between the high and low-frequency magnetic spectra in the solar wind merits further study.

A statistical study of B/E ratios confirms that the electromagnetic waves have indices of refraction consistent with the whistler mode, as their $f_{ci} \leq f \leq f_{ce}$ frequency range suggests. Our statistical study did not settle whether the whistler waves propagate parallel to, or obliquely to, the interplanetary field.

Whistler waves have phase and group velocities comparable with, or exceeding, the solar wind speed. On the one hand, because their phase velocities can be comparable with the solar wind speed, their observed Doppler-shifted frequency spectrum cannot be related uniquely to the solar wind frame K-vector spectrum. On the other hand, to the extent that whistler mode energy does not simply convect with the solar wind, the waves observed at one point may be generated elsewhere, by plasma conditions unrelated to those detected locally, and propagate through a turbulent solar wind to the spacecraft. Because the interplanetary field direction is ordinarily variable when enhanced whistler noise is observed, the angle between the whistler propagation vector and the interplanetary field will change as the waves propagate and refract. For this reason, the spacecraft should detect a distribution of wave-normal angles that is broader than that at the source.

We studied short bursts, of a few-minutes duration, of whistler noise. In these cases, the normally falling spectrum has a distinct peak near the center frequency of one of the plasma wave instrument's spectral channels. These relatively narrowband bursts do not appear to be like magnetosheath lion roars (Smith _et al._, 1969; Smith and Tsurutani, 1976; Thorne and Tsurutani, 1981) because they do not occur in local minima of the interplanetary field magnitude. They are also unlike the bursts discussed by Kennel _et al._ (1980) because they are unaccompanied by strongly-enhanced plasma waves. The burst indices of refraction at the spectral peak, inferred from measured B/E ratios, are larger than those typically observed and consistently larger than the index of refraction calculated by inserting the measured solar wind number density and magnetic field into the cold plasma dispersion relation for whistlers propagating parallel to the magnetic field. Assuming that the whistler bursts occur when the spacecraft is in or near a generation region, this fact suggests that the whistlers are generated propagating at angles exceeding 70° to the magnetic field. Although theoretical studies of whistler propagation in the turbulent interplanetary medium are clearly called for, the fact that the index of refraction is normally smaller than that in local whistler bursts suggests that those waves which reach the spacecraft from remote sources are refracted towards the parallel direction as they propagate.

The energies of the particles resonant with the whistler waves observed by ISEE-3 cannot be precisely calculated without accounting for Doppler shifting, and this requires knowledge of the wave propagation vector. For the shock event of April 4-5, 1979, we estimated both electron cyclotron and Landau resonance energies assuming the observed whistlers propagated either parallel or anti-parallel to the magnetic field. Both resonant energies scale as the magnetic energy per particle, $B^2/8\pi N$, which varied dramatically during this highly-structured event. In particular, the estimated cyclotron energy varied by four orders of magnitude. Since the observed whistler amplitude remained relatively constant, it is difficult to argue either that the waves were propagating parallel to the magnetic field or that they were amplified by cyclotron resonance interactions. Although we could not calculate precisely the electron energies for resonance with oblique whistlers, the fact that the Landau energies calculated using the parallel phase velocity varied much less suggests the observed waves may have been oblique whistlers that drew their free energy from Landau electrons.

The fact that whistler waves are nearly always present in the solar wind suggests there may nearly always be free energy in the solar wind electron distribution that either amplifies them or allows them to propagate to the spacecraft without significant damping, or both. Solar wind electrons may be divided into a "core" component and a "halo" component, with energies of 10-20 eV and 50 eV - few keV, respectively (Feldman, 1979). Fundamental arguments (Scudder and Olbert, 1979) indicate that a halo should form whenever the solar wind core electrons have a temperature gradient parallel to the magnetic field. In effect, halo electrons acquire their observed energy in their last Coulomb collision with core electrons at a point where the core temperature is much higher. The higher the energy of the electron, the further it reaches back into the temperature gradient, because the Coulomb mean-free path depends inversely on energy. In this case, the halo electrons form a third-moment heat-flux distribution. By modeling the solar wind electrons by two Maxwellians that drift relative to one another along the magnetic field while maintaining zero electron current, Gary _et al_. (1975) have shown that cyclotron resonance interactions with halo electrons can destabilize parallel whistlers. However, these waves are heavily damped at small oblique angles of propagation. To our knowledge, there have been no calculations of the amplification of very oblique whistlers whose wavelengths are near the electron inertial length c/ω_p: the waves we have inferred to be present in the solar wind.

In the limit that halo electrons are collisionless, they respond to the global structure of the solar wind, because they are then influenced primarily by the magnetic mirror force and the electric potential (Schulz and Eviatar, 1972). By their nature, halo electrons are the ones sensitive to the distant structures in the solar wind. Consider the relatively simple case of a flare-driven shock. Electrons behind the shock piston are in contact with an unusually hot solar corona; the halo distribution between the piston and shock is composed of electrons propagating large distances in a turbulent interplanetary medium, some of which communicate directly with the piston shock, and beyond. Given the observed variety of solar wind disturbances, we might expect the halo distribution to have a variety of forms, not all of which can be described by simple drifting Maxwellians. For example, highly unidirectional fluxes of > 60 eV electrons are known to flow along field lines away from the sun within the high-speed regions of most fast streams (Rosenbauer et al., 1976, 1977; Pilipp et al., 1977). Local heating perpendicular to the magnetic field could produce "conic" electron distributions, similar to the ion "conics" observed on auroral field lines, if the electrons are accelerated out of the heating region by the magnetic mirror force. In fact, the halo distribution does exhibit quite a few different structures at disturbed times (W.C. Feldman, private communication, 1981).

It is possible that no uniquely characteristic free-energy source may be responsible for the whistlers enhanced in the disturbed solar wind.

However, by adjusting their wave-normal angle, whistler waves have considerable flexibility to adjust their Landau and cyclotron energies in order to find a given free-energy source in velocity space. Many detailed instability calculations are required to decide whether the oblique whistler instability is flexible enough to tap many different free-energy sources, as proved to be the case for odd half-harmonic electrostatic waves in the magnetosphere (Kennel and Ashour-Abdalla, 1982). In any case, halo electrons are both ubiquitous and responsive to a variety of disturbances, features also characteristic of the whistler waves observed in the solar wind.

ACKNOWLEDGMENTS

We are pleased to acknowledge useful discussions with W. C. Feldman, A. M. A. Frandsen, C. Hetlinger, and B. T. Tsurutani. The research at TRW was supported by NASA under Contract NAS5-20682. The work at JPL represents one aspect of research carried out by JPL for NASA under Contract NAS7-100.

REFERENCES

Anderson, R. R., C. C. Harvey, M. M. Hoppe, B. T. Tsurutani, T. E. Eastman, and J. Etcheto, Plasma Waves Near the Magnetopause, J. Geophys. Res., 87, ____, 1982.

Beinroth, H. J., and F. M. Neubauer, Properties of Whistler Mode Waves Between 0.3 and 1.0 AU from Helios Observations, J. Geophys. Res., 86, 7755, 1981.

Burlaga, L., R. Lepping, R. Weber, T. Armstrong, C. Goodrich, J. Sullivan, D. Gurnett, P. Kellogg, E. Keppler, F. Mariani, F. Neubauer, H. Rosenbauer, and R. Schwenn, Interplanetary Particles and Fields, November 22 to December 6, 1977: Helios, Voyager, and Imp Observations Between 0.6 and 1.6 AU, J. Geophys. Res., 85, 2227, 1980.

Feldman, W. C., Kinetic Processes in the Solar Wind, in Solar System Plasma Physics, Vol. I (C. F. Kennel, L. J. Lanzerotti, and E. N. Parker, eds.), p. 321, North-Holland, Amsterdam, New York, Oxford, 1979.

Feldman, W. C., J. R. Asbridge, S. J. Bame, J. T. Gosling, and D. S. Lemons, Characteristic Electron Variations Across Simple High Speed Solar Wind Streams, J. Geophys. Res., 83, 5285, 1978.

Gary, S. P., W. C. Feldman, D. W. Forslund, and M. D. Montgomery, Heat Flux Instabilities in the Solar Wind, J. Geophys. Res., 80, 4197, 1975.

Gosling, J. T., J. R. Asbridge, S. J. Bame, and W. C. Feldman, Solar Wind Stream Interfaces, J. Geophys. Res., 83, 1401, 1978.

Gurnett, D. A., and R. R. Anderson, Plasma Wave Electric Fields in the Solar Wind: Initial Results from Helios-1, J. Geophys. Res., 82, 632, 1977.

Gurnett, D. A., Plasma Waves in the Solar Wind: A Review of Observations, in Solar Wind 4 (H. Rosenbauer, ed.), to be published, Springer-Verlag, Berlin.

Gurnett, D. A., and L. A. Frank, Ion Acoustic Waves in the Solar Wind, J. Geophys. Res., 83, 58, 1978.

Gurnett, D. A., F. M. Neubauer, and R. Schwenn, Plasma Wave Turbulence Associated with Interplanetary Shocks, J. Geophys. Res., 84, 541, 1979.

Hoang, S., J.-L. Steinberg, G. Epstein, P. Tilloles, J. Fainberg, and R. G. Stone, The Low-Frequency Continuum as Observed in the Solar Wind from ISEE-3: Thermal Electrostatic Noise, J. Geophys. Res., 85, 3419, 1980.

Kennel, C. F., Low Frequency Whistler Mode, Phys. Fluids, 9, 2190, 1966.

Kennel, C. F., and H. E. Petschek, Limit on Stably Trapped Particle Fluxes, J. Geophys. Res., 71, 1, 1966.

Kennel, C. F., and F. L. Scarf, Electromagnetic Pitch Angle Instabilities in Space, in Plasma Waves in Space and in the Laboratory (J. O. Thomas and B. J. Landmark, eds.), p. 451, Edinburgh Univ. Press, Edinburgh, 1969.

Kennel, C. F., F. L. Scarf, F. V. Coroniti, R. W. Fredricks, D. A. Gurnett, and E. J. Smith, Correlated Whistler and Electron Plasma Oscillation Bursts Detected on ISEE-3, Geophys. Res. Lett., 7, 129, 1980.

Kennel, C. F., F. L. Scarf, F. V. Coroniti, E. J. Smith, and D. A. Gurnett, Non-Local Plasma Turbulence Associated with Interplanetary Shocks, J. Geophys. Res., 87, ____, 1982.

Kennel, C. F., and M. Ashour-Abdalla, Strong Pitch-Angle Diffusion and Electrostatic Waves in the Magnetosphere, in Magnetospheric Plasma Physics (A. Nishida, ed.), Japan Publishing Co., Tokyo, 1982.

Neubauer, F. M., H. J. Beinroth, H. Barnstorf, and G. Dehmel, Initial Results from the Helios-1 Search Coil Magnetometer Experiment, J. Geophys. Res., 42, 599, 1977a.

Neubauer, F. M., G. Musmann, and G. Dehmel, Fast Magnetic Fluctuations in the Solar Wind: Helios 1, J. Geophys. Res., 82, 3201, 1977b.

Olson, J. V., R. E. Holzer, and E. J. Smith, High Frequency Magnetic Fluctuations Associated with the Earth's Bow Shock, J. Geophys. Res., 74, 4601, 1969.

Pilipp, W. G., R. Schwenn, E. Marsch, K.-H. Muhlhauser, and H. Rosenbauer, Electron Characteristics in the Solar Wind as Deduced from Helios Observations, in Solar Wind 4 (H. Rosenbauer, ed.), to be published, Springer-Verlag, Berlin.

Podgorny, I. M., Collisionless Shocks: Simulation and Laboratory Experiments, Il Nuovo Cimento, V. 2C, Serie 1, No. 6, 834, 1979.

Rosenbauer, H., H. Miggenrieder, M. Montgomery, and R. Schwenn, Preliminary Results of the Helios Plasma Measurements, in Physics of Solar Planetary Environments (D. J. Williams, ed.), p. 391, AGU, 1976.

Rosenbauer, H., R. Schwenn, E. Marsch, B. Meyer, H. Miggenrieder, M. D. Montgomery, K.-H. Muhlhauser, W. Pilipp. W. Voges, and S. M. Zink, A Survey of Initial Results of the Helios Plasma Experiment, J. Geophys. Res., 42, 561, 1977.

Schulz, M., and A. Eviatar, Electron Temperature Asymmetry and the Structure of the Solar Wind, Cosmic Electrodynamics, 2, 204, 1972.

Scudder, J. D., and S. Olbert, A Theory of Local and Global Processes Which Impact Solar Wind Electrons, I. The Origin of Typical 1 AU Velocity Distribution Functions-Steady State Theory, J. Geophys. Res., 84, 2755, 1979.

Smith, E. J., R. E. Holzer, M. G. McLeod, and C. T. Russell, Magnetic Noise in the Magnetosheath in the Frequency Range 3-300 Hz, J. Geophys. Res., 72, 4803, 1967.

Smith, E. J., R. E. Holzer, and C. T. Russell, Magnetic Emissions in the Magnetosheath at Frequencies Near 100 Hz, J. Geophys. Res., 74, 3027, 1969.

Smith, E. J., and B. T. Tsurutani, Magnetosheath Lion Roars, J. Geophys. Res., 81, 2261, 1976.

Stix, T., The Theory of Plasma Waves, McGraw-Hill, New York, 1962.

Thorne, R. M., and B. T. Tsurutani, On the Generation Mechanism for Magnetosheath Lion Roars, Nature, 293, 384, 1981.

Tsurutani, B. T., E. J. Smith, R. R. Anderson, K. W. Ogilvie, J. D. Scudder, D. N. Baker, and E. W. Hones, Jr., Lion Roars and High-β Plasma Tubes in the Magnetosheath, to be submitted, J. Geophys. Res., 1981.

TABLE I

Date	Shock Time (UT)	Spectrum Time (UT)	Spectral Index	
			0.04 Hz $< f < 3$ Hz	$f > 8.8$ Hz
		SHOCK SPECTRA		
November 12, 1978	0028	0222	0.72	1.61
April 5, 1979	0120	0832	0.86	1.5
April 24, 1979	2327	2335	0.81	1.65
June 6, 1979	1840	2200	1.02	2.0
		FAST-STREAM SPECTRA		
January 2, 1979		1850	1.1	2.66
May 22, 1979		1200	1.07	2.52

FIGURE CAPTIONS

Figure 1 - A 24-hour summary of the shock and downstream flow on April 4-5, 1979. The top panel shows the electric field amplitudes from 0.311 to 3.1 kHz, and the fourth panel shows the wave magnetic field amplitudes from 17 to 178 Hz; the solid tone represents the 128-second average, and the dots indicate the peak wave signal detected during the averaging interval. The central panels display the three components of the magnetic field, and the bottom panel shows the magnetic field strength, both taken from the common pool tape. The $f > f_{ci}$ magnetic wave noise is strongly enhanced at the shock (0120 UT) and persists downstream until about 1800 UT. Accompanying the $f > f_{ci}$ waves is the large-scale disorder of the interplanetary magnetic field.

Figure 2 - A 24-hour summary of the shock and the upstream and downstream flows on June 6-7, 1979. The top panel displays selected electric field channels from 31 Hz to 100 kHz. The second panel shows the magnetic field strength and B_z-component; note the large-scale disorder in B_z which starts at the shock (1840 UT) and persists until about 0600 UT on June 7. The bottom panel displays the wave magnetic field amplitudes from 3.2 Hz to 178 Hz. The $f > f_{ci}$ noise is strongly enhanced at the shock and persists as long as the disorder in the magnetic field.

Figure 3 - A 24-hour summary of the solar wind fast stream on January 2-3, 1979. The top panel shows the 1.78 kHz electric field amplitude

which peaks at the leading edge of the fast stream. The second and third panels display the B_y-component and the total strength of the magnetic field. Panels 4 and 5 show the solar wind velocity and plasma density, respectively. The bottom panel displays the 17.8 Hz magnetic wave amplitude. The $f > f_{ci}$ waves commence as the B_y-component becomes disordered, and the waves persist until after 2400 UT when the interplanetary field becomes more ordered.

Figure 4 - A 24-hour summary of the solar wind fast stream on May 22-23, 1979. The format is the same as Figure 3 except that the B_z-component of the magnetic field is plotted rather than B_y. Again, the $f > f_{ci}$ magnetic wave noise is strongest during the interval when the interplanetary magnetic field is highly disordered (0600 to 2400 UT).

Figure 5 - A 24-hour summary of the solar wind discontinuity on February 5-6, 1979, in the same format as Figure 3. The magnetic field rotation at 2155 UT may also be a weak shock since the flow velocity and magnetic field strength have a small jump. The $f > f_{ci}$ magnetic waves are enhanced when B_y is strongly disordered.

Figure 6 - Magnetic amplitude spectra in gamma/$(Hz)^{\frac{1}{2}}$ in the frequency range 0.04 Hz $< f < 10^3$ Hz which were obtained from the JPL magnetometer ($f < 3$ Hz) and the TRW search coil ($f > 3.2$ Hz). On the right-hand side are spectra (A, B, C, and D) which were taken in the downstream flow of four interplanetary shocks. "Eyeball fit" straight lines

have been drawn through the data points. The spectral index ($f^{-\alpha}$) at high frequencies ($f > 17$ Hz) is about twice the value of the low-frequency ($f < 3$ Hz) index. On the left, the spectra labeled α and β were measured in two fast-stream encounters. Above 56 Hz, the amplitude is at the detector threshold. The high-frequency stream spectra are steeper than the post-shock spectra.

Figure 7 - Low-frequency ($f < 3$ Hz) vs high-frequency ($f > 17$ Hz) spectral index obtained from the straight-line fits to the amplitude spectra. The solid circles are from individual spectra which were obtained behind the four shocks in Figure 6. These are four separate spectra for each shock, and the spectra are separated by more than one hour. The average value of the high and low-frequency spectral index is shown as the point A, which is enclosed by the one standard deviation "error" box. The post-shock points cluster about the average ratio of 2:1. Six spectral indices from the three non-shock events (two spectra each) are shown by the stars. For the non-shock flows, the high-frequency spectral index is larger, and the low-frequency index is more variable than for the post-shock flows.

Figure 8 - Three magnetic amplitude spectra taken downstream of the June 6, 1979, shock. The 2010 UT and 2200 UT spectra show the 2 to 1 ratio of high to low-frequency spectral indices. At 2100 UT, the IMF spectrum has a lower amplitude and spectral index, indicating a period of magnetic quiescence. The $f > f_{ci}$ spectrum is steeper, and the 2 to 1 ratio is not observed.

Figure 9 - Detailed plasma, magnetic field, and wave measurements from 0700 to 1000 UT on April 5, 1979. The top panel shows the solar wind velocity. The second panel shows the one-minute average of the magnetic field strength (solid line) and the five-minute average of the plasma density (dashed line). The magnetic field decrease and density increase between 0800 and 0900 UT result in a reduction of the whistler characteristic energy from 60 eV to 2 eV. The third panel shows the 128-second average of the 17.8 Hz spectral amplitude. The bottom panels show the minimum election energy for cyclotron resonance and Landau resonance with a 17.8 Hz parallel whistler. For each panel, two curves are plotted which give the energy range corresponding to the Doppler broadening of the plasma rest frame wave number spectrum. The dramatic decrease in the cyclotron resonant energy after 0830 UT implies that a parallel whistler should have a strong damping or growth interaction with thermal solar wind electrons. The resonant energies for oblique whistlers are higher than for parallel modes.

Figure 10 - High-frequency magnetic amplitude spectra taken at various times during the 0700-1000 UT post-shock flow on April 5, 1979. The bottom curve represents the 128-second average amplitude, and the top curve represents the peak amplitude during the averaging interval. Although the whistler cyclotron and Landau energies changed significantly between 0750 UT and 0950 UT, the spectral shape and amplitude varied only slightly.

Figure 11 - An expanded display of the downstream flow of the June 6, 1979,

shock. The top panel shows the solar wind proton density and flow velocity, and the second panel shows the magnetic field strength, both from the common data pool tape. The bottom two panels display the 56 Hz wave electric and magnetic field spectral amplitudes. Note the substantial reduction in the 56 Hz electric field interference level behind the shock at 1840 UT. The central panel shows the estimated wave index of refraction B/E, based on 128-second averages, normalized to the calculated refractive index for parallel propagating whistlers $n_{||}$. The ratio $B/En_{||}$ is typically between 0.5 and 1.0, except around 2100 UT where a deep minimum in the magnetic amplitude occurs in conjunction with a density depression; here, $B/En_{||}$ approaches 0.1, suggesting the presence of predominantly electrostatic emissions.

Figure 12 - A histogram display of the number of times a given refractive index ratio $B/En_{||}$ occurred in the 10-minute interval 2010-2030 UT, June 6, 1979, vs $B/En_{||}$ calculated from the simultaneous measured values of B and E. At each of the four frequencies, there are 292 B/E measurements. The histograms peak at $B/En_{||} < 1$, with the two lower frequencies having a substantial number of events with $B/En_{||} > 1$; the two higher frequencies are more strongly concentrated at $B/En_{||} < 1$.

Figure 13 - The top two panels display the wave electric and magnetic field amplitude spectra at four times during a magnetic wave burst from 1941:28 to 1944:30 UT. The lower curve is the 16-second average, and the upper curve is the peak spectral amplitude in each frequency

channel during the averaging interval. The bottom panel shows the estimated refractive index $B/En_{\parallel}$ (solid dots) and the normalized wave vector $\bar{k} = kc/\omega_p$ (circled dots). In the first and fourth columns, the magnetic spectrum has the typical post-shock power law shape, and $B/En_{\parallel}$ is near or below unity. During the magnetic burst, the magnetic spectrum develops a plateau or peak at 31.6 and 56 Hz; at 56 Hz $B/En_{\parallel}$ is between 2 and 3.

Figure 14a - The strong magnetic wave burst from 2222:46 to 2226:21 UT is displayed in the same format as Figure 13. As the burst develops, the magnetic spectrum develops a broad plateau or peak between 17.8 and 100 Hz; the electric field spectrum has a significant peak at 100 Hz. The refractive index ratio $B/En_{\parallel}$ is above 2 for frequencies between 31.6 and 178 Hz, and peaks at 4.6 and 100 Hz.

Figure 14b - Continuation of Figure 14a. The $B/En_{\parallel}$ ratio remains significantly above one until the burst decays at 2226:21 UT. The large $B/En_{\parallel}$ ratios suggest that the magnetic bursts are whistlers which are generated with large wave normal angles.

ORIGINAL PAGE IS OF POOR QUALITY

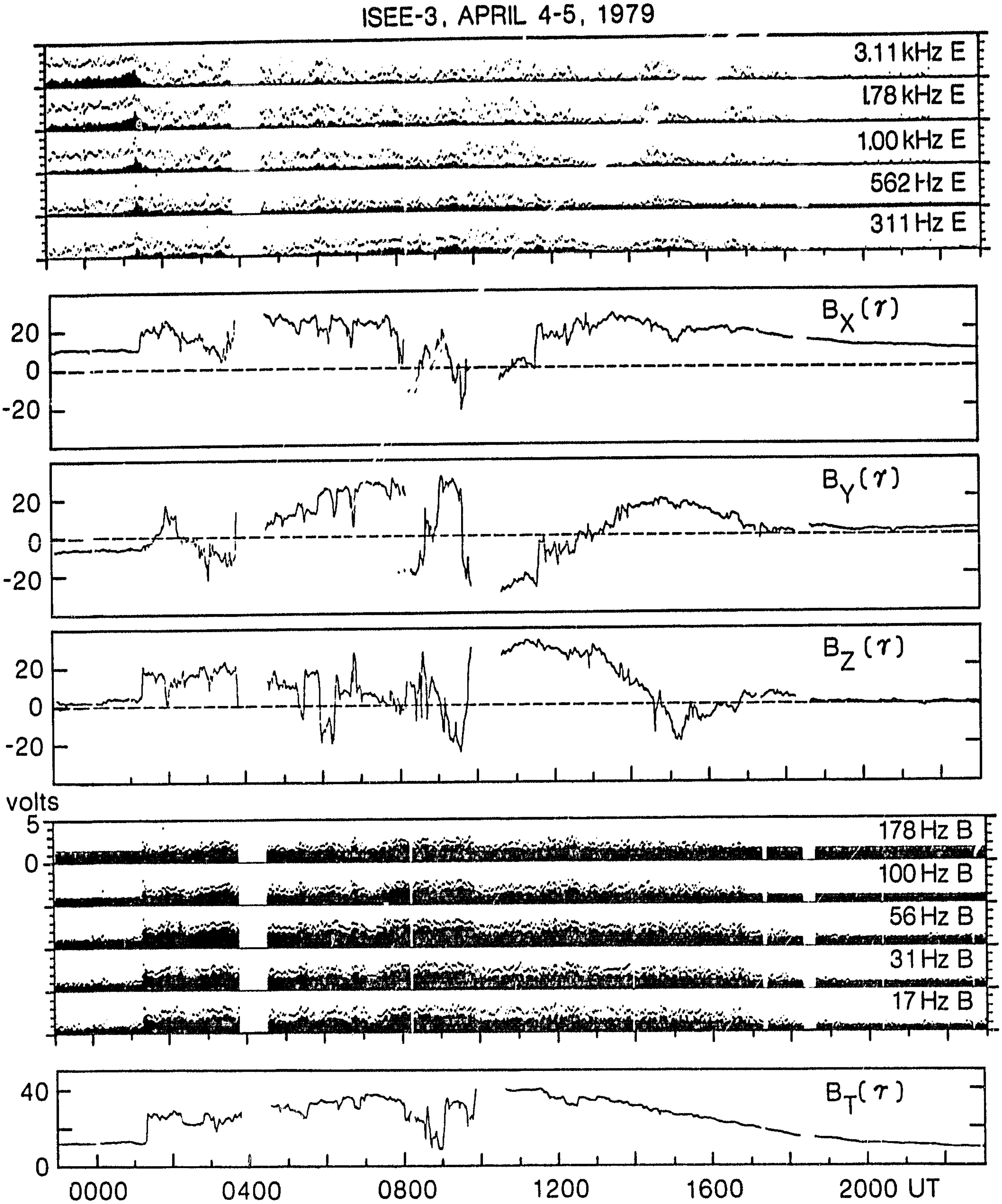

Figure 1

ORIGINAL PAGE
OF POOR QUALITY

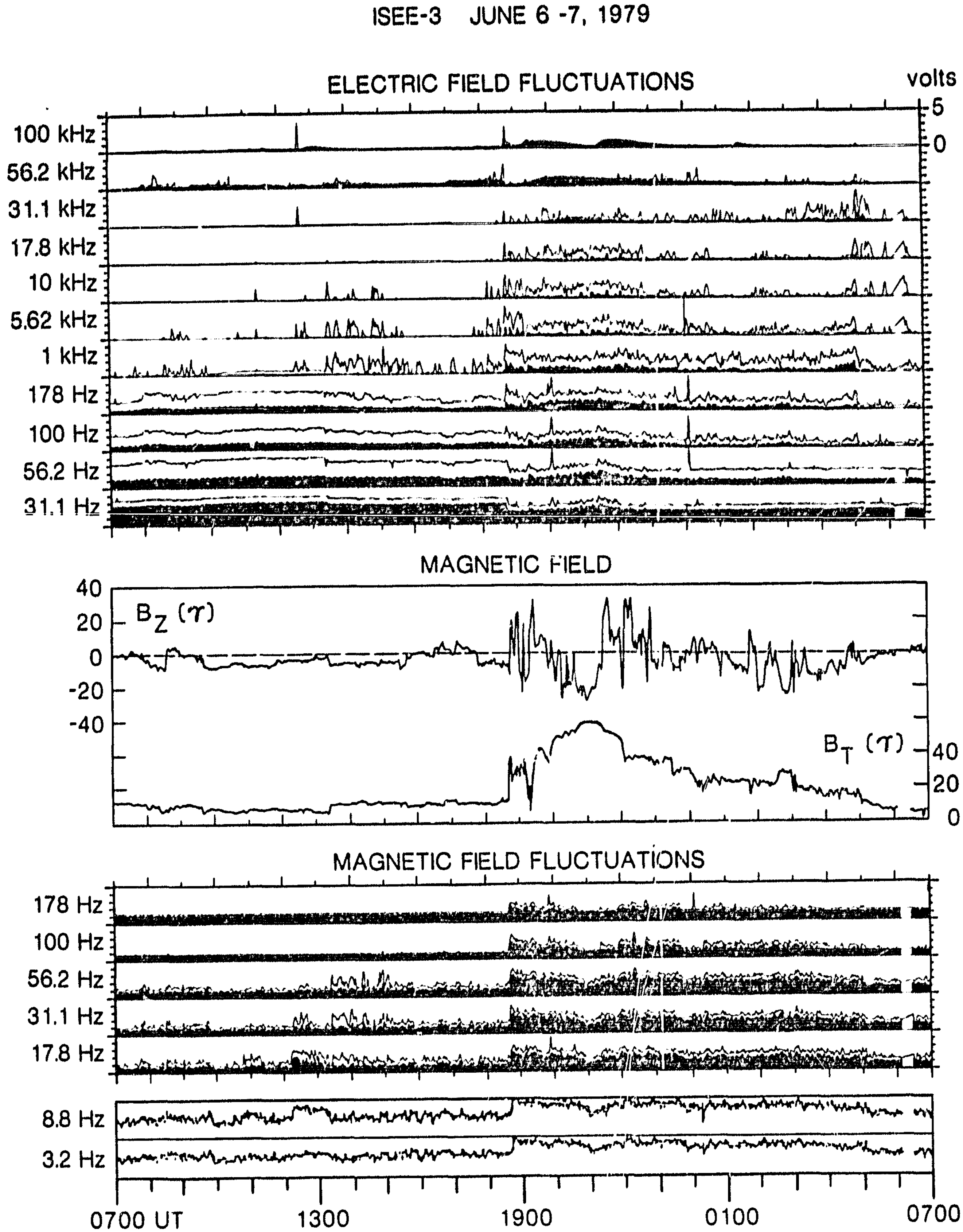

Figure 2

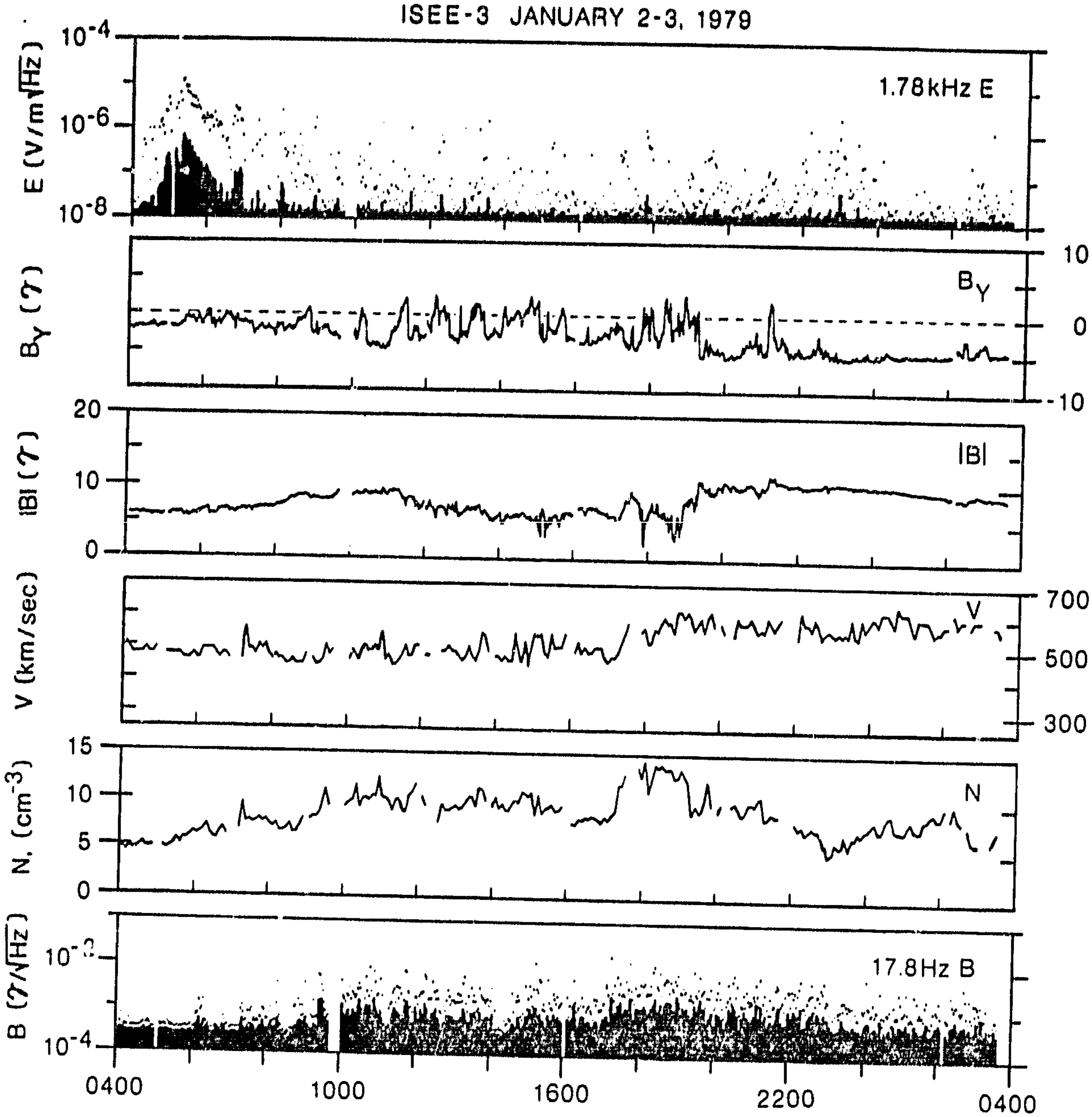
ISEE-3 JANUARY 2-3, 1979
E (V/m√Hz)
10^-4
10^-6
10^-8
1.78kHz E
B_Y (γ)
B_Y
10
0
-10
|B| (γ)
|B|
20
10
0
V (km/sec)
V
700
500
300
N, (cm^-3)
N
15
10
5
0
B (γ/√Hz)
17.8Hz B
10^-4
0400
1000
1600
2200
0400

Figure 3

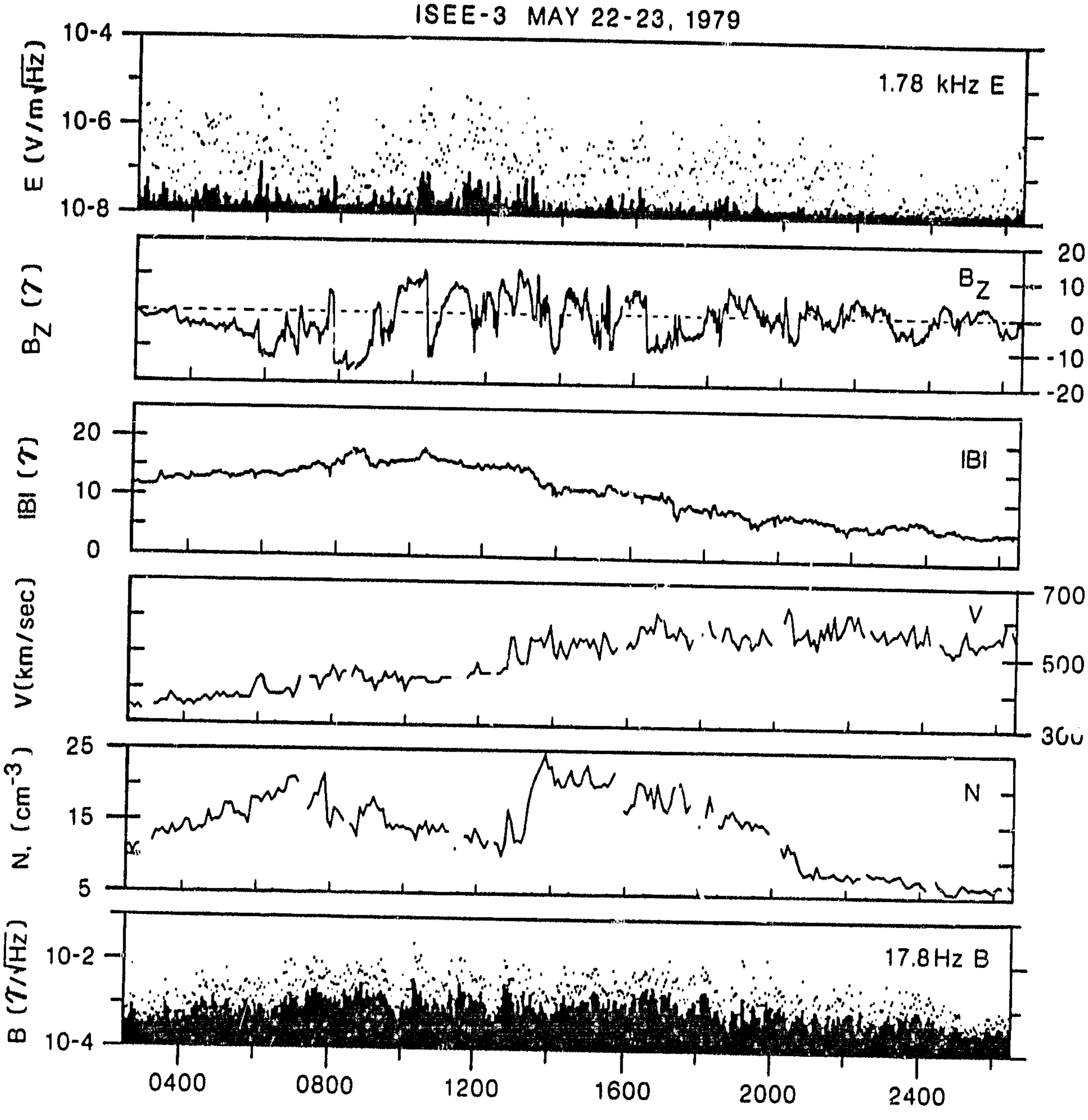
ISEE-3 MAY 22-23, 1979
10-4
10-6
10-8
E (V/m√Hz)
1.78 kHz E
B_Z (γ)
B_Z
20
10
0
-10
-20
|B| (γ)
|B|
V(km/sec)
V
700
500
300
N, (cm-3)
N
25
15
5
B (γ/√Hz)
17.8 Hz B
10-2
0400
0800
1200
1600
2000
2400

Figure 4

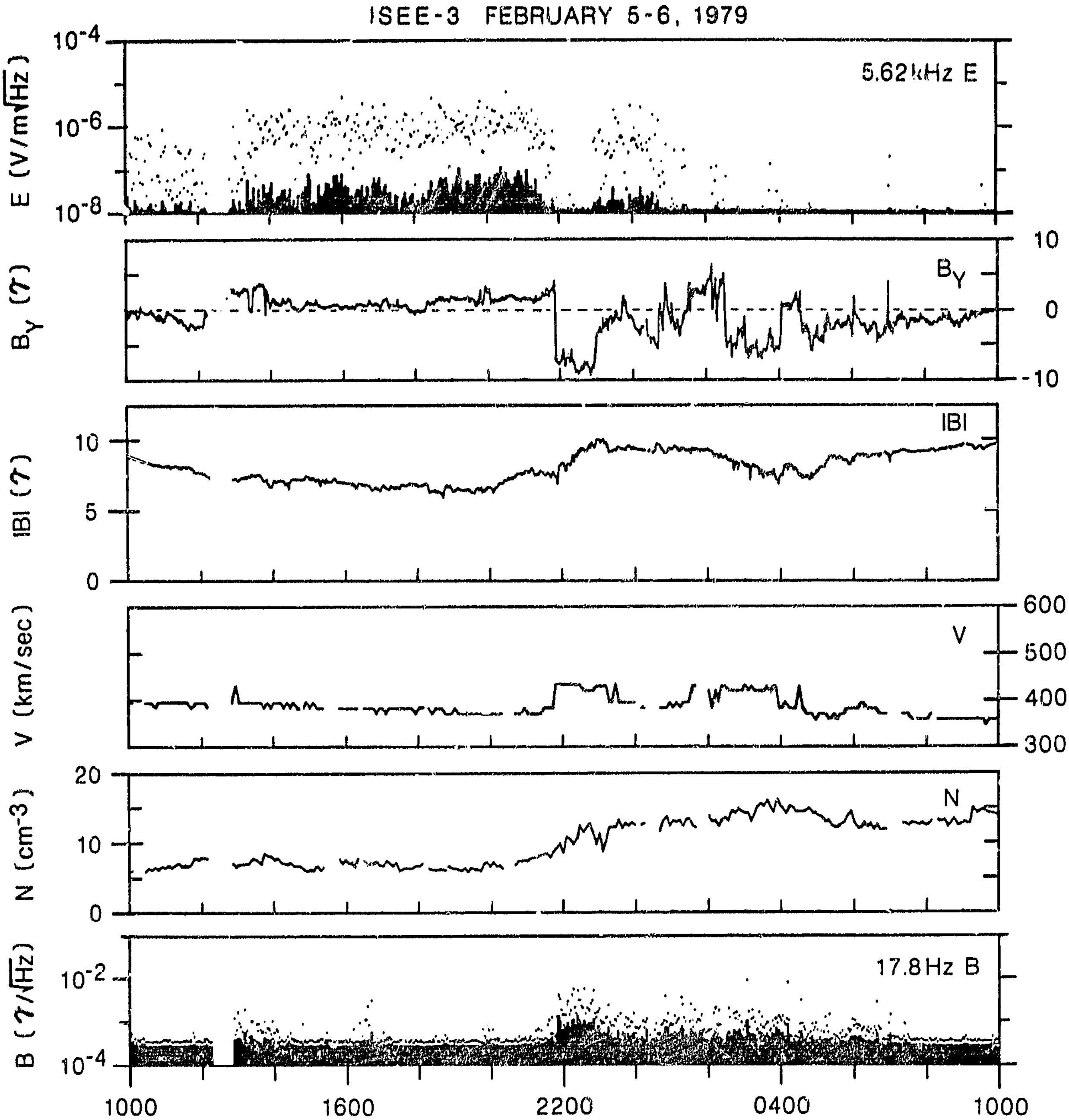
ISEE-3 FEBRUARY 5-6, 1979
5.62kHz E
E (V/m√Hz)
10-4
10-6
10-8
BY
BY (γ)
10
0
-10
IBI
IBI (γ)
10
5
0
V
V (km/sec)
600
500
400
300
N
N (cm-3)
20
10
0
17.8Hz B
B (γ/√Hz)
10-2
10-4
1000
1600
2200
0400
1000

Figure 5

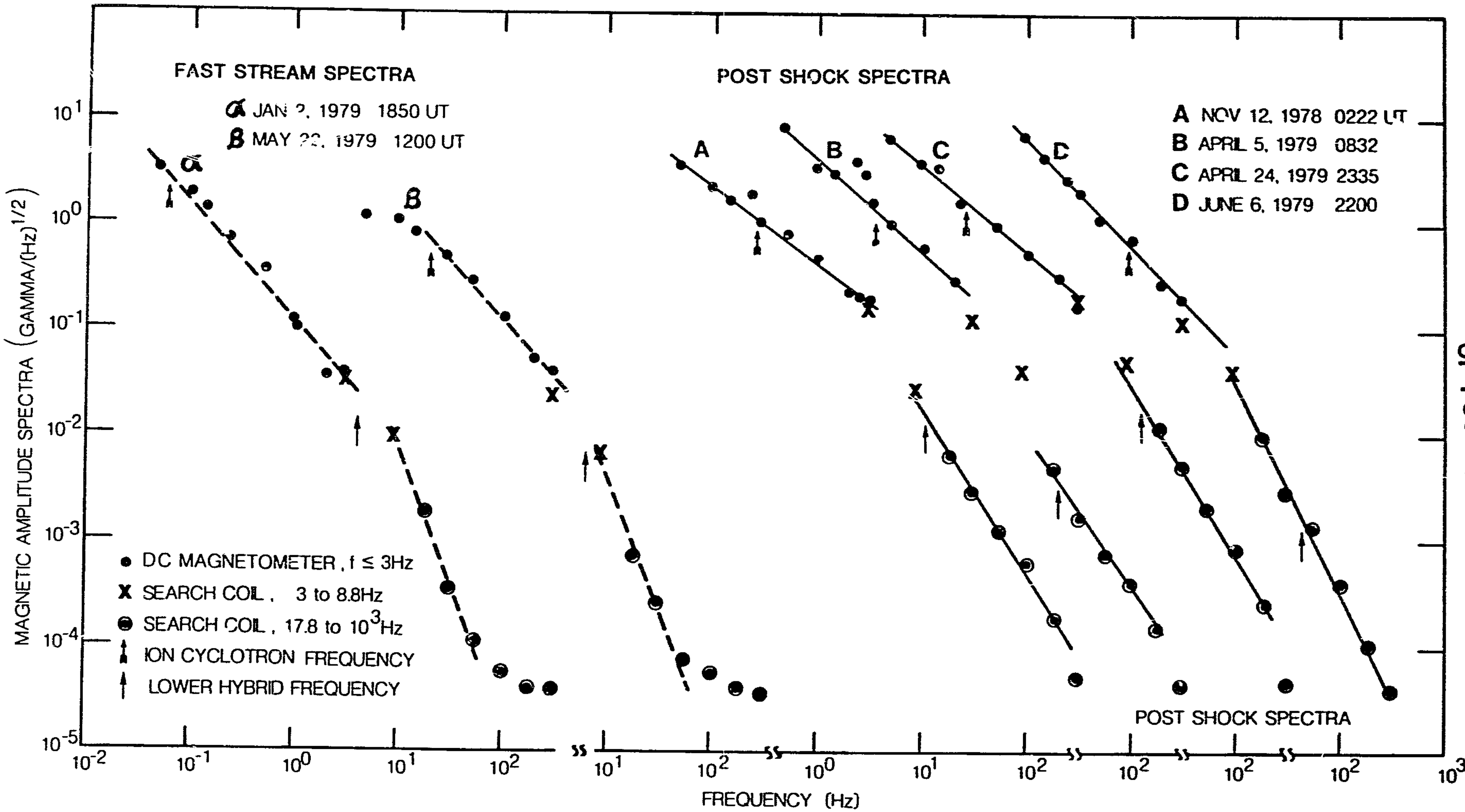
FAST STREAM SPECTRA
α JAN 2, 1979 1850 UT
β MAY 22, 1979 1200 UT
POST SHOCK SPECTRA
A NOV 12, 1978 0222 UT
B APRIL 5, 1979 0832
C APRIL 24, 1979 2335
D JUNE 6, 1979 2200
POST SHOCK SPECTRA
DC MAGNETOMETER, f ≤ 3Hz
SEARCH COIL, 3 to 8.8Hz
SEARCH COIL, 17.8 to 10³Hz
ION CYCLOTRON FREQUENCY
LOWER HYBRID FREQUENCY
MAGNETIC AMPLITUDE SPECTRA (GAMMA/(Hz)^1/2)
FREQUENCY (Hz)

Figure 6

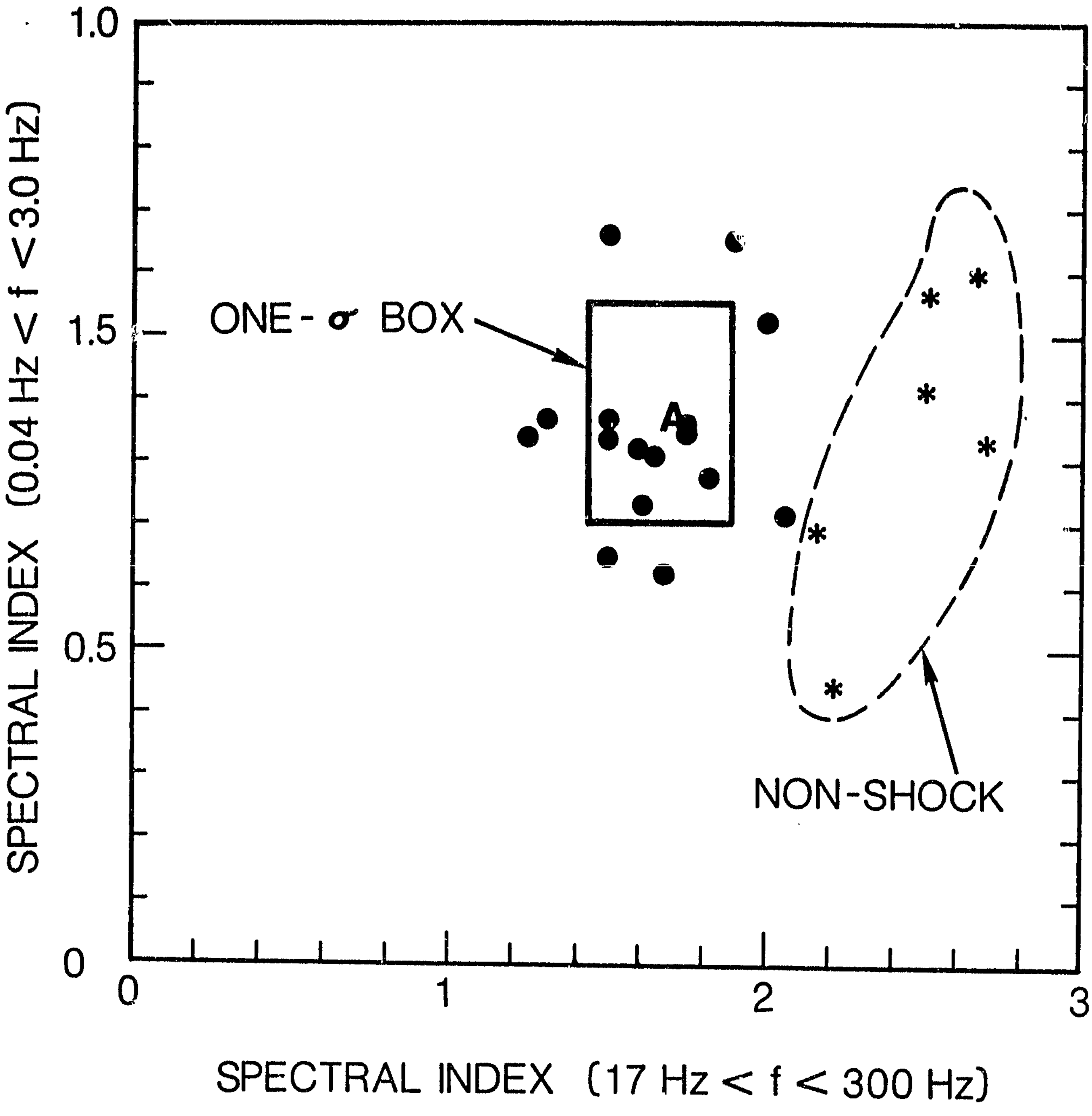
1.0
1.5
0.5
0
0
1
2
3
ONE - σ BOX
A
NON-SHOCK
SPECTRAL INDEX (0.04 Hz < f < 3.0 Hz)
SPECTRAL INDEX (17 Hz < f < 300 Hz)

Figure 7

ORIGINAL PAGE IS
OF POOR QUALITY

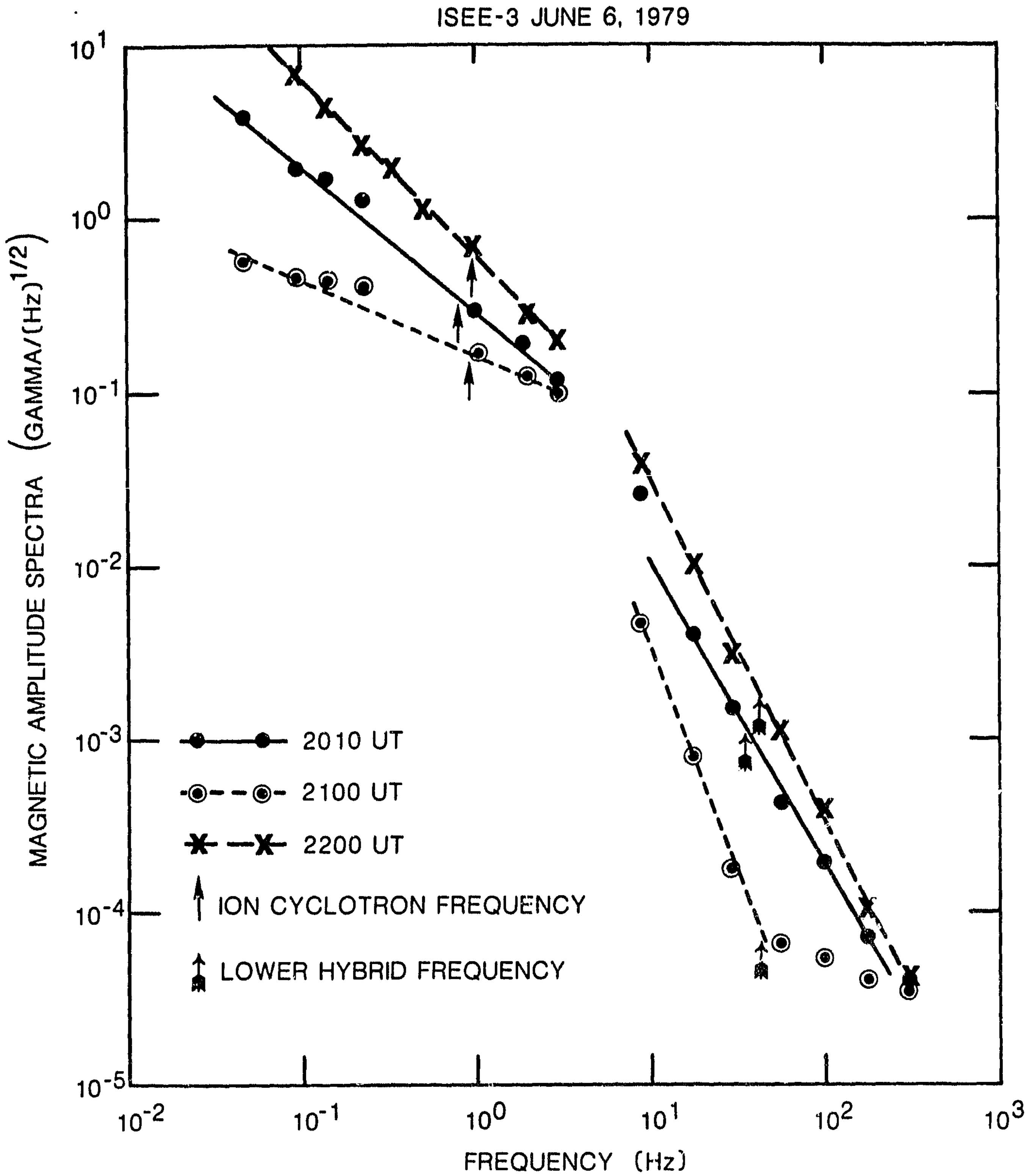

Figure 8

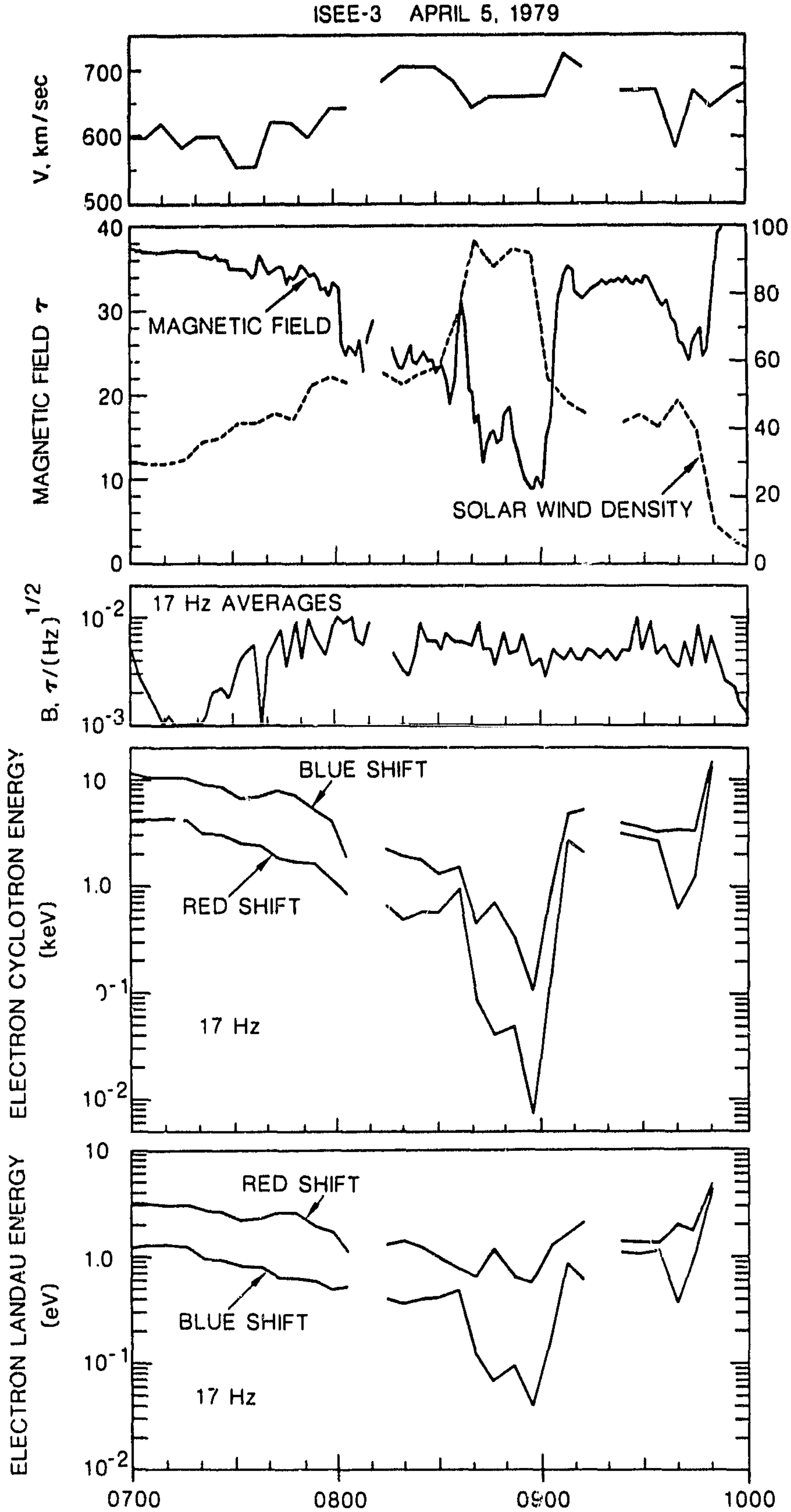
ISEE-3 APRIL 5, 1979
V, km/sec
700
600
500
MAGNETIC FIELD γ
40
30
20
10
0
MAGNETIC FIELD
SOLAR WIND DENSITY
DENSITY, cm^{-3}
100
80
60
40
20
0
B, γ/(Hz)$^{1/2}$
17 Hz AVERAGES
10^{-2}
10^{-3}
ELECTRON CYCLOTRON ENERGY (keV)
10
1.0
10^{-1}
10^{-2}
BLUE SHIFT
RED SHIFT
17 Hz
ELECTRON LANDAU ENERGY (eV)
10
1.0
10^{-1}
10^{-2}
RED SHIFT
BLUE SHIFT
17 Hz
0700
0800
0900
1000

Figure 9

ORIGINAL PAGE IS
OF POOR QUALITY

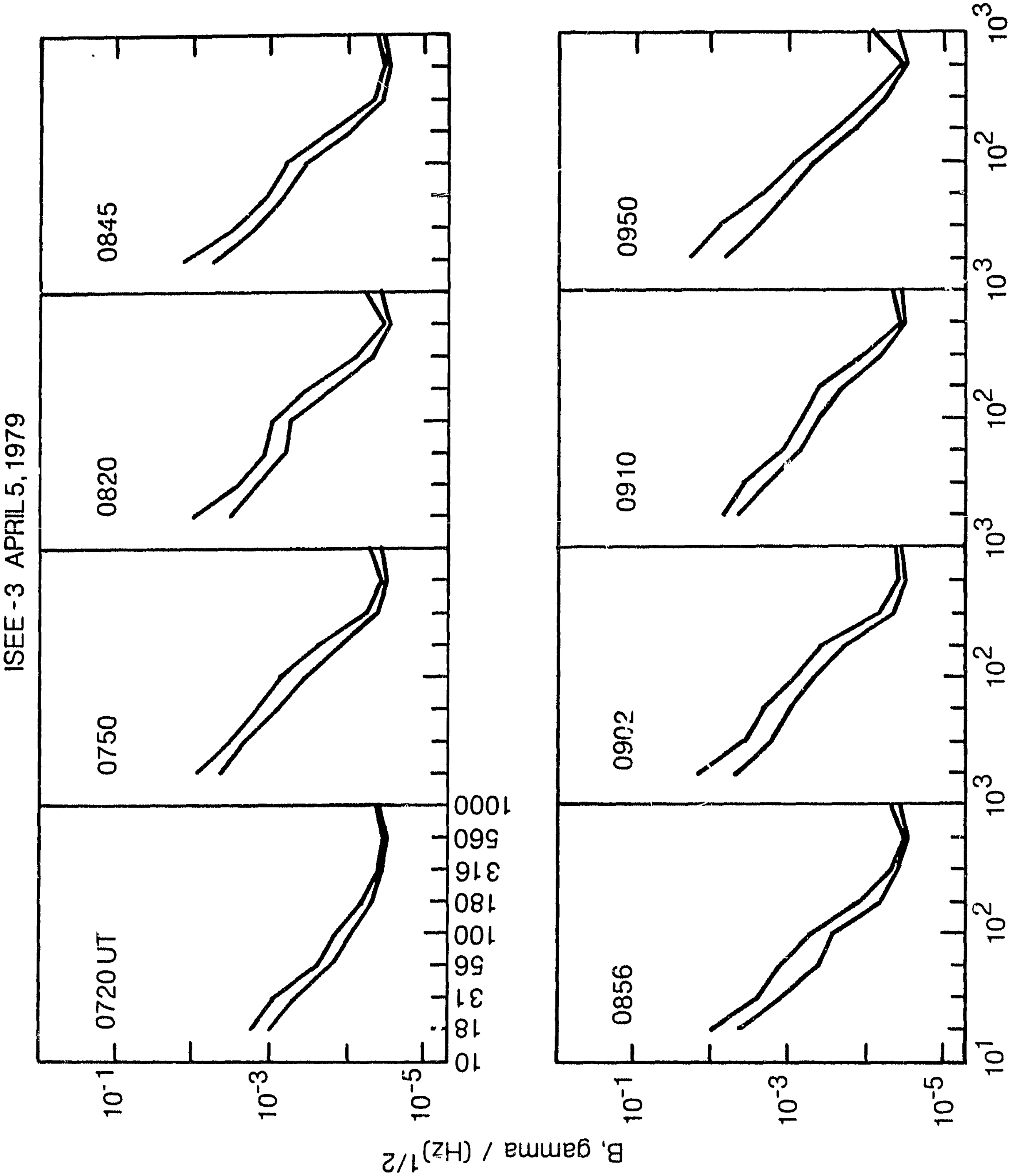

Figure 10

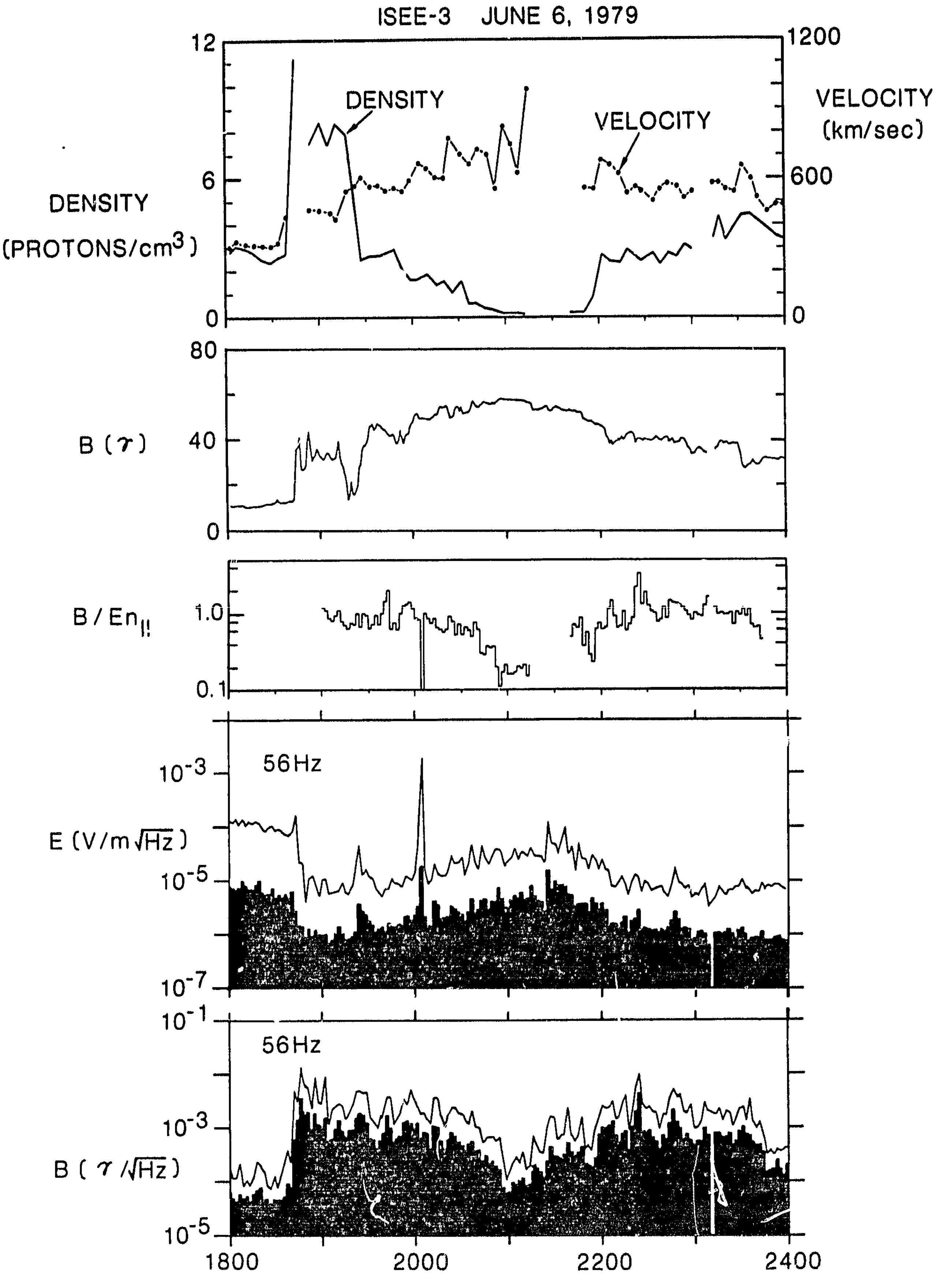
ISEE-3 JUNE 6, 1979
DENSITY
VELOCITY
DENSITY
(PROTONS/cm3)
VELOCITY
(km/sec)
12
6
0
1200
600
0
80
40
0
B (γ)
B / En||
1.0
0.1
56Hz
E (V/m√Hz)
10-3
10-5
10-7
10-1
56Hz
B (γ/√Hz)
10-3
10-5
1800
2000
2200
2400

Figure 11

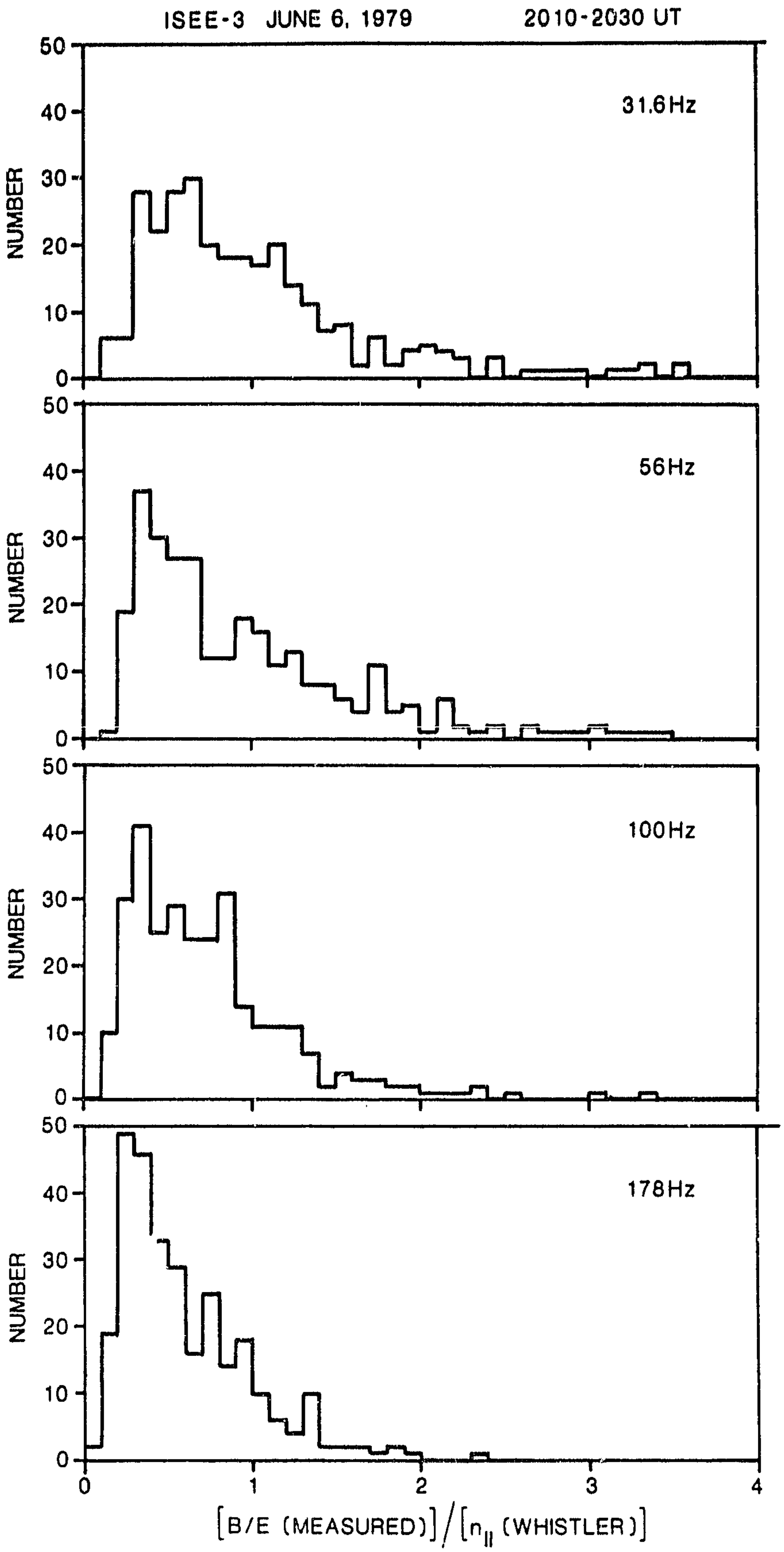
ISEE-3 JUNE 6, 1979 2010-2030 UT
31.6Hz
56Hz
100Hz
178Hz
NUMBER
0
10
20
30
40
50
0
1
2
3
4
[B/E (MEASURED)]/[$n_{\parallel}$ (WHISTLER)]

Figure 12

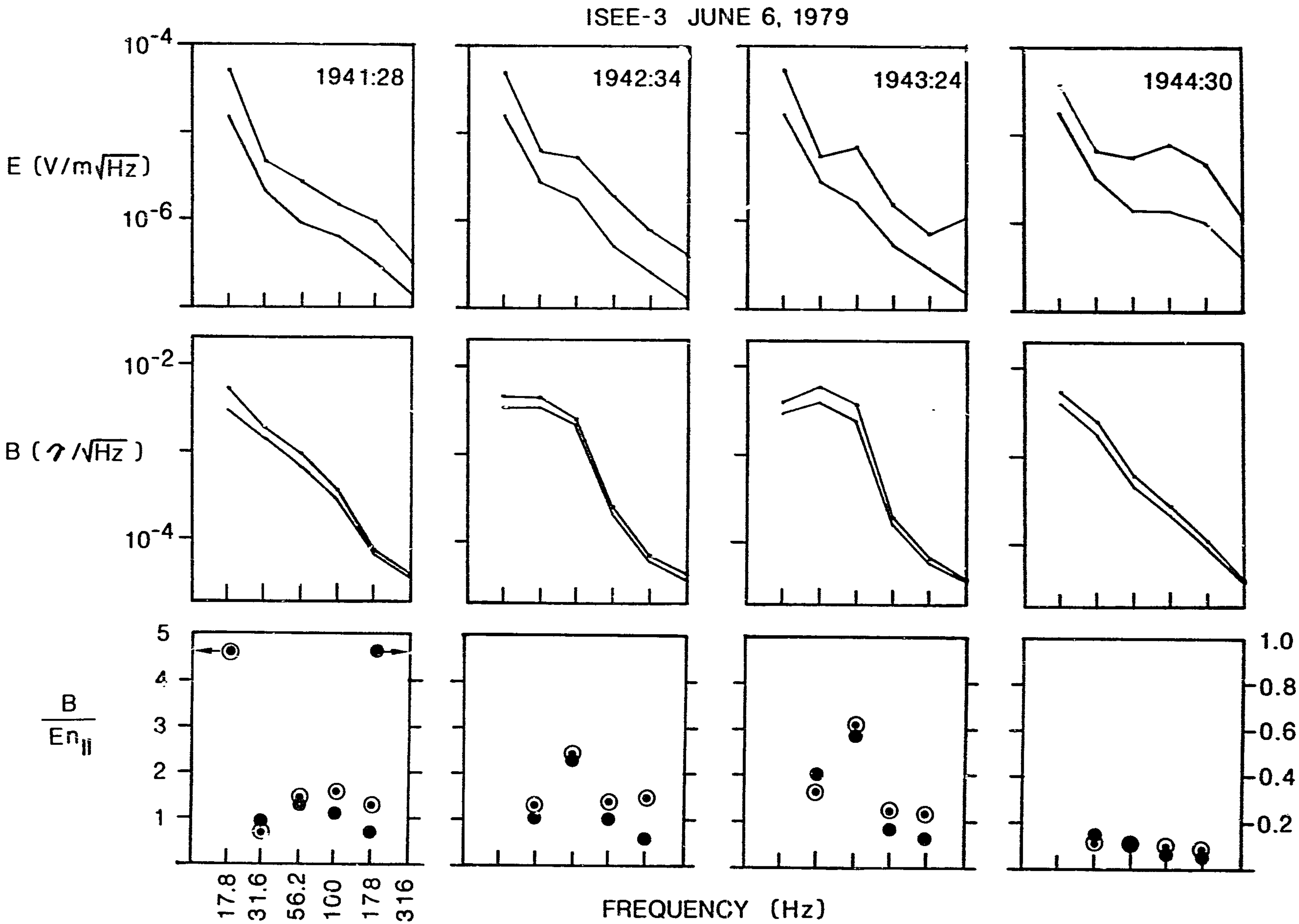
ISEE-3 JUNE 6, 1979
1941:28
1942:34
1943:24
1944:30
E (V/m√Hz)
10^{-4}
10^{-6}
B (γ/√Hz)
10^{-2}
10^{-4}
B/En∥
5
4
3
2
1
K̄
1.0
0.8
0.6
0.4
0.2
17.8
31.6
56.2
100
178
316
FREQUENCY (Hz)

Figure 13

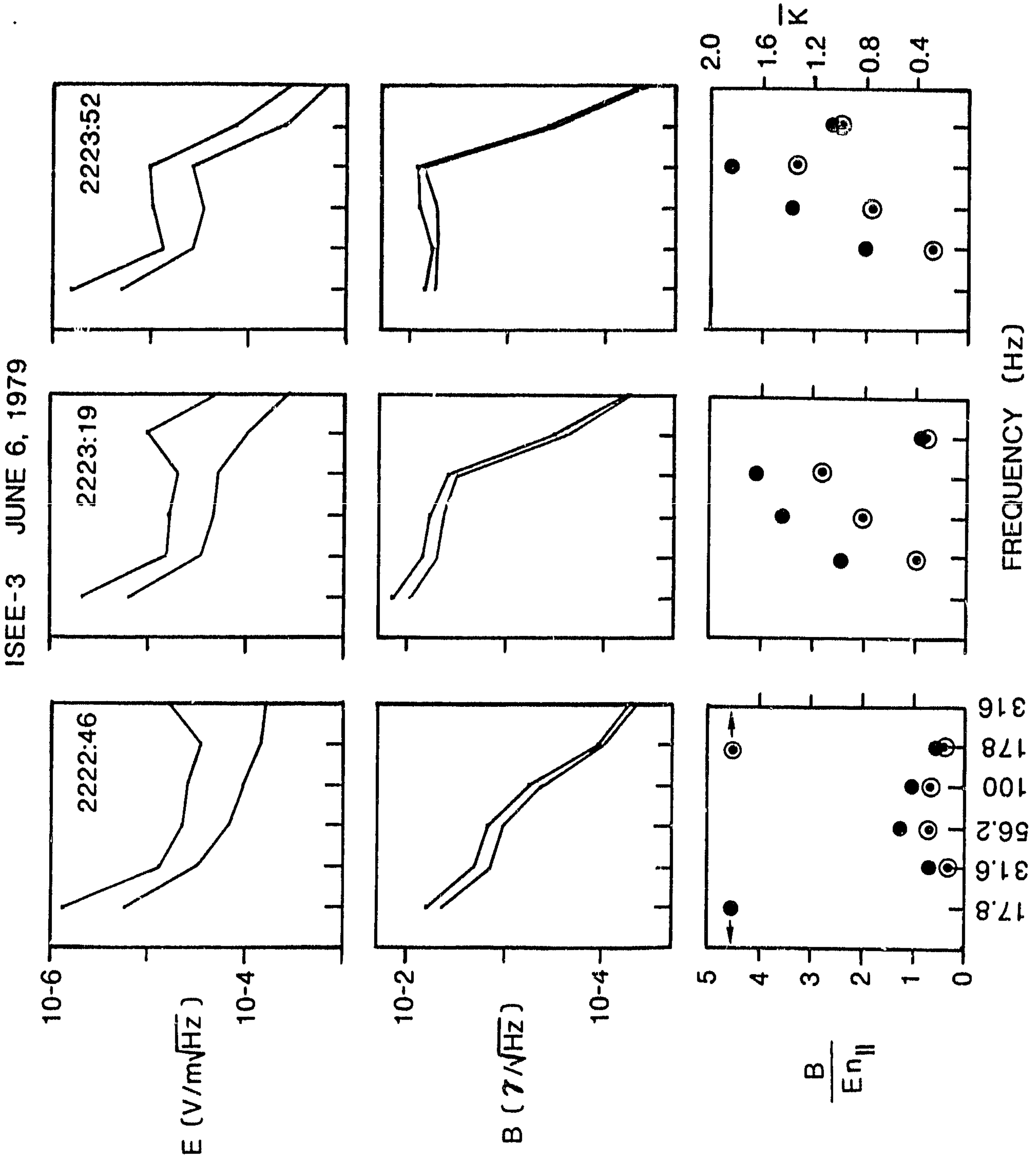
ISEE-3 JUNE 6, 1979
2222:46
2223:19
2223:52
E (V/m√Hz)
10-6
10-4
B (γ/√Hz)
10-2
10-4
B / En∥
5
4
3
2
1
0
K̄
2.0
1.6
1.2
0.8
0.4
17.8
31.6
56.2
100
178
316
FREQUENCY (Hz)

Figure 14a

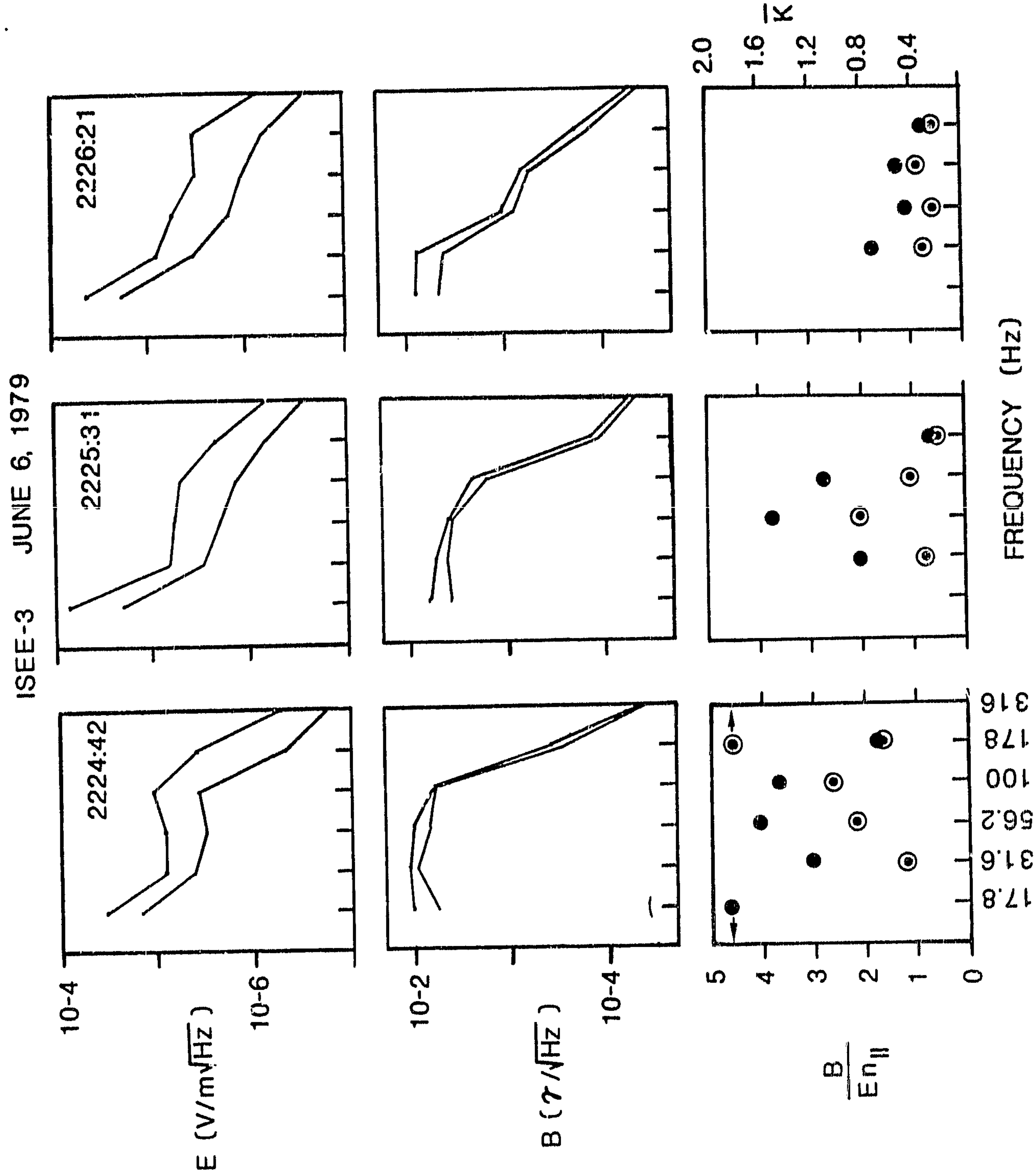
ISEE-3 JUNE 6, 1979
2224:42
2225:31
2226:21
E (V/m√Hz)
10-4
10-6
B (γ/√Hz)
10-2
10-4
B/En∥
0
1
2
3
4
5
17.8
31.6
56.2
100
178
316
FREQUENCY (Hz)
K
2.0
1.6
1.2
0.8
0.4

Figure 14b

DRAFT March 8, 1982

THE ISEE-3 MISSION

TO THE EARTH'S TAIL

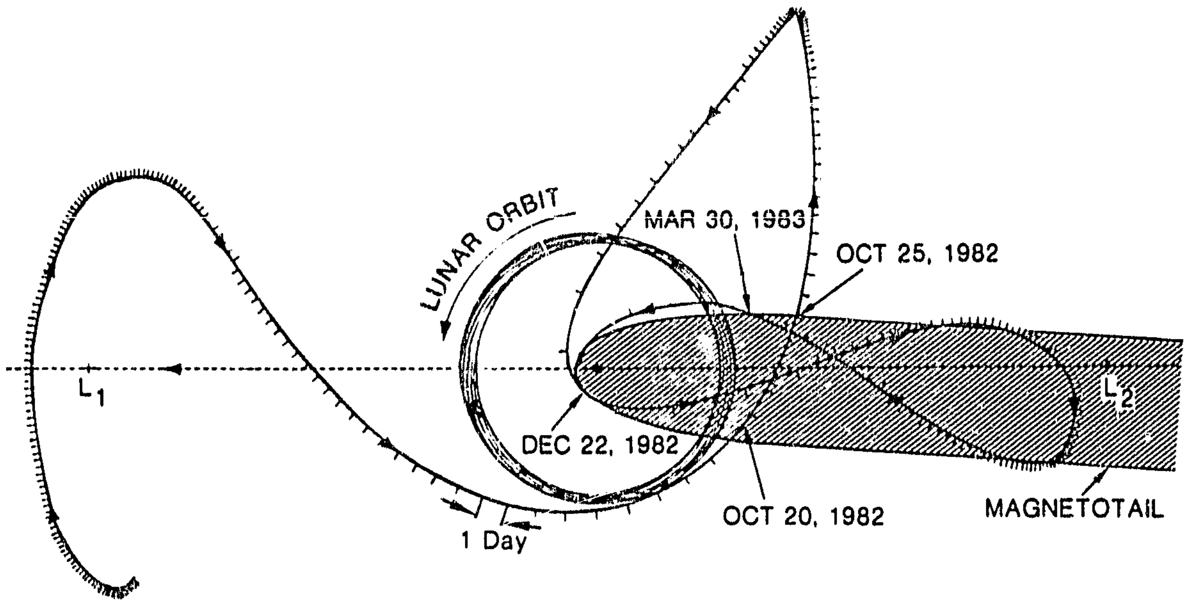

MARCH 1982

APPENDIX C

THE ISEE-3 TAIL MISSION WORKING GROUP

F. L. Scarf, TRW, Chairman (ISEE-3 plasma waves)

R. W. Farquhar, GSFC, Mission Analyst

T. von Rosenvinge, GSFC, ISEE-3 Project Scientist (ISEE-3 cosmic rays)

Contributors:

E. J. Smith, JPL (ISEE-3 magnetic fields)

K. Ogilvie, GSFC (ISEE-3 ion composition)

R. J. Hynds, Imperial College (ISEE-3 low-energy protons)

F. Ipavich, Univ. of Maryland (ISEE-3 ionic charge and nuclear mass)

J. Gosling, LASL (ISEE-3 solar wind plasma)

R. Lin, Univ. of Calif., Berkeley (ISEE-3 X-rays and electrons)

PREFACE

In the ISEE-3 prelaunch Press Kit (Release No: 78-118, August 4, 1978), it was stated that "...the halo orbit path is the most unusual ever proposed for a NASA space mission. The plan to place ISEE-3 in this orbit was devised by Dr. Robert W. Farquhar ...who originated the concept in his doctoral thesis." In fact, the prelaunch trajectory studies identified a number of other extremely exciting mission options for ISEE-3, and Figure 1 shows one way in which the spacecraft could be moved from the sunward libration point, L, to the corresponding L_2 point deep in the earth's magnetic tail. This drawing was prepared in 1974

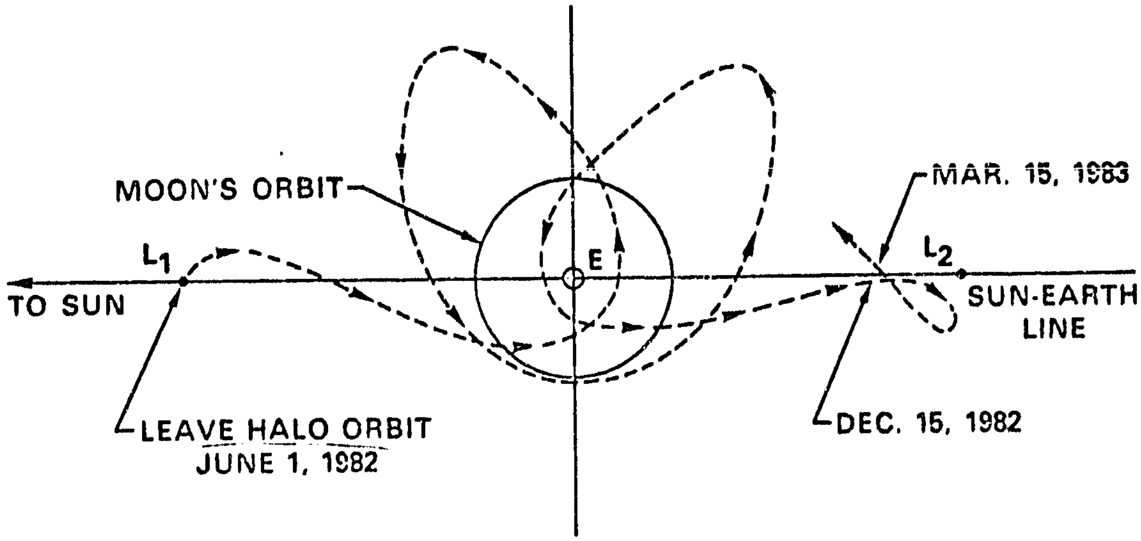

Figure 1

and circulated to the ISEE investigators in 1975. During the past few years, there have been many informal discussions about the advisability of moving ISEE-3 to the tail after completion of the prime mission phase (i.e., after August 12, 1981), and Figure 1 shows that this type of extended mission option could be implemented in the 1982-1983 time period.

At the Meudon meeting of the ISEE Science Working Team (July 27-28, 1981), there was a brief preliminary discussion of an ISEE-3 tail mission, and it was decided to proceed with a detailed mission analysis together with an evaluation of the science return. On December 21, 1981, the Director of the Astrophysics Division at NASA Headquarters formally requested that Goddard Space Flight Center study various options for ISEE-3, including a move to the geomagnetic tail, followed by a mission to Comet Giacobini-Zinner. At the recent GSFC meeting of the ISEE Science Working Team (February 8-9, 1982), Fred Scarf presented the science arguments for both mission options, and Robert Farquhar gave a progress report on the feasibility study. In the ensuing discussion, it became evident that there was general support for sending ISEE-3 to the geomagnetic tail and to Giacobini-Zinner, and it was requested that separate reports on these mission options be prepared by working groups under the leadership of Fred Scarf (tail) and Ed Smith (comet).

RATIONALE FOR AN ISEE-3 TAIL MISSION IN 1982-1983

- <u>TIMING</u>

  ALL THREE ISEE SPACECRAFT HAVE COMPLETED THEIR PRIMARY MISSIONS.

  IF ISEE-3 IS IN THE DISTANT TAIL IN 1982-1983, STADAN CAN STILL ACQUIRE DATA FROM ISEE-1,2 (APOGEE IN THE NEAR TAIL), AND DE 1,2 WILL STILL BE OPERATING.

  IMP-8 CAN PROVIDE SOLAR WIND INPUT DATA FOR A 3 TO 4 MONTH PERIOD IN EARLY 1983, WHEN ISEE-3 WILL BE OUT OF THE SOLAR WIND.

  ISEE-3 CAN COMPLETE ITS TAIL MISSION BEFORE BEING SENT TO INTERCEPT COMET GIACOBINI-ZINNER.

- <u>NEW SCIENCE</u>

  ISEE-3 WILL PROVIDE THE FIRST IN-SITU DATA ON THE TAIL CONFIGURATION AND DYNAMICS IN THE UNEXPLORED REGION FROM BEYOND LUNAR ORBIT ($\approx 80\ R_e$) TO THE L_2 LIBRATION POINT ($240\ R_e$).

  THE ISEE-3 PAYLOAD WILL YIELD FIRST ORDER INFORMATION ON THE DISTANT MAGNETOPAUSE, PLASMA SHEET, PLASMA MANTLE, B-FIELD DYNAMICS, WAVE-PARTICLE INTERACTIONS, AND ENERGETIC PARTICLES. THE SCIENCE RETURN WILL BE VAST IN COMPARISON WITH THE LIMITED KNOWLEDGE AVAILABLE FROM PIONEER 7,8.

- <u>RELATION WITH OPEN</u>

  THE ISEE-3 TAIL MISSION WILL PROVIDE PRECURSOR INFORMATION NEEDED FOR THE FINAL DESIGN OF GTL (DATA ON TRAJECTORY SELECTION, ORBITAL OPERATIONS, FUEL CONSUMPTION, INSTRUMENT SEQUENCING, ETC.).

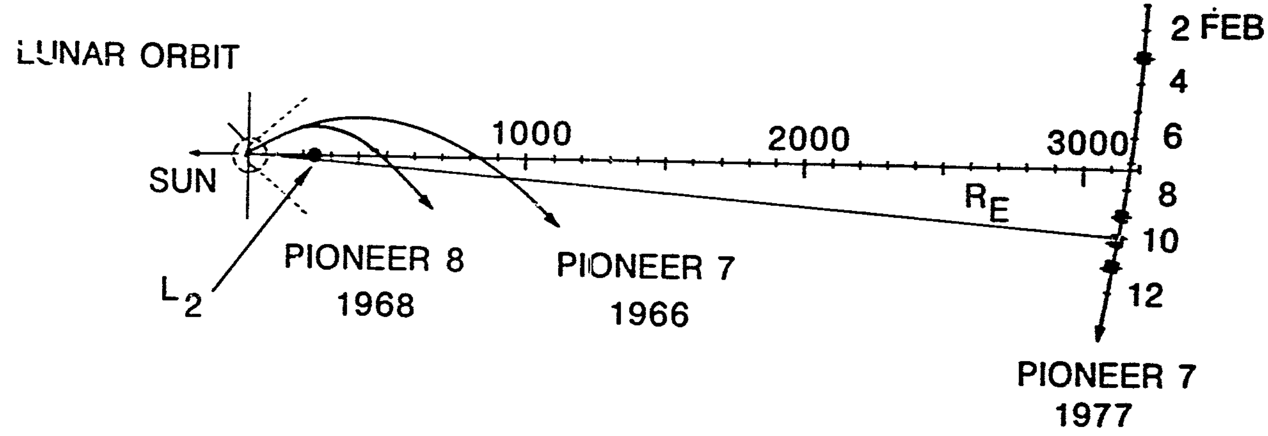

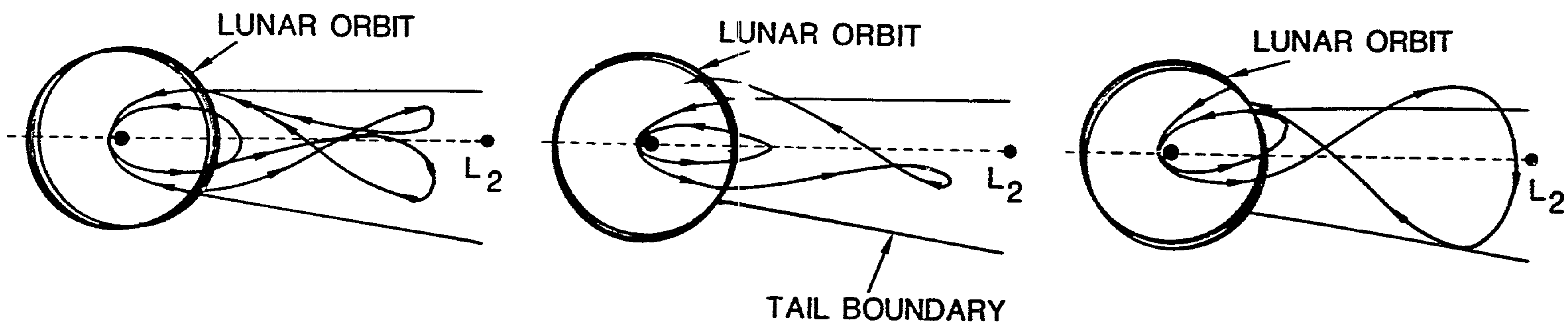

POSSIBLE GTL TRAJECTORIES

PIONEER 7 TAIL MEASUREMENTS AT 1000 R_J

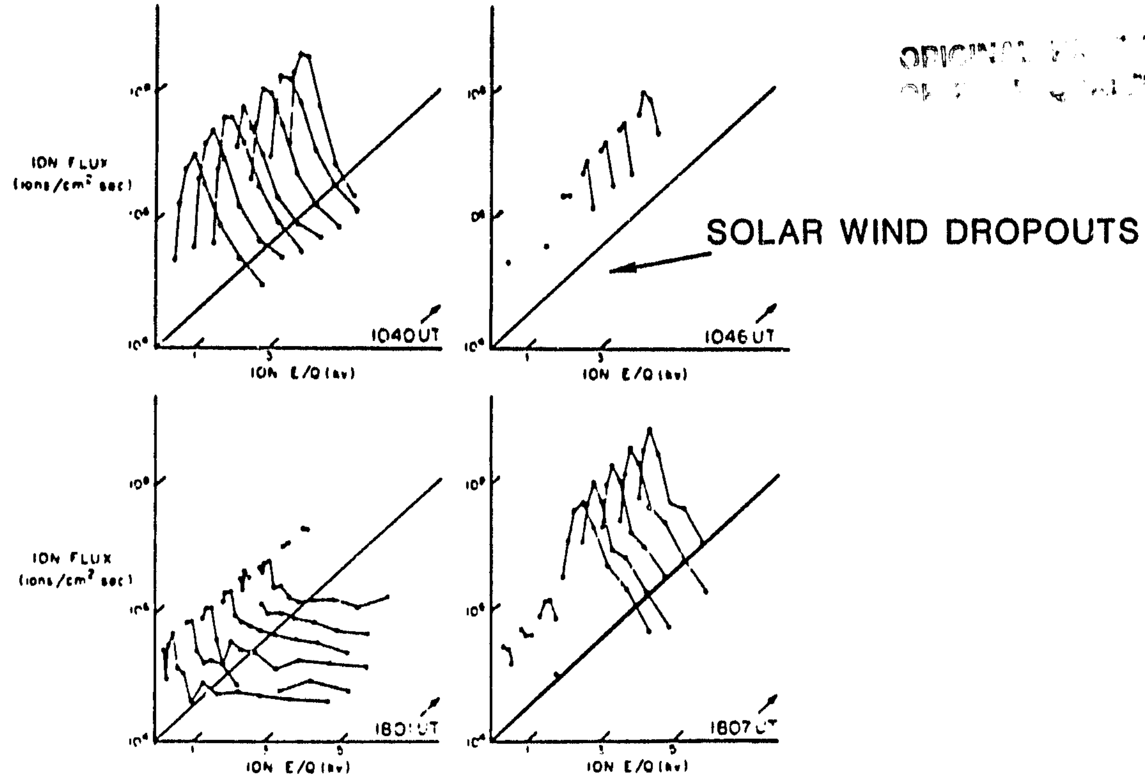

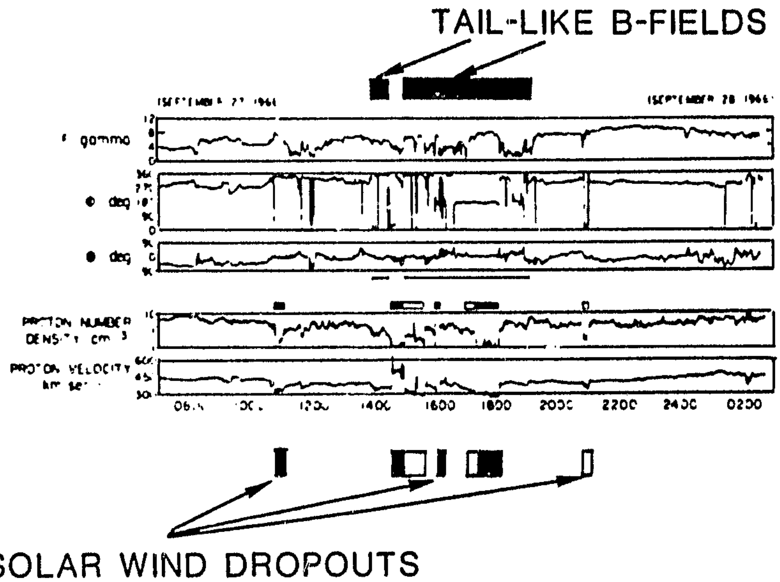

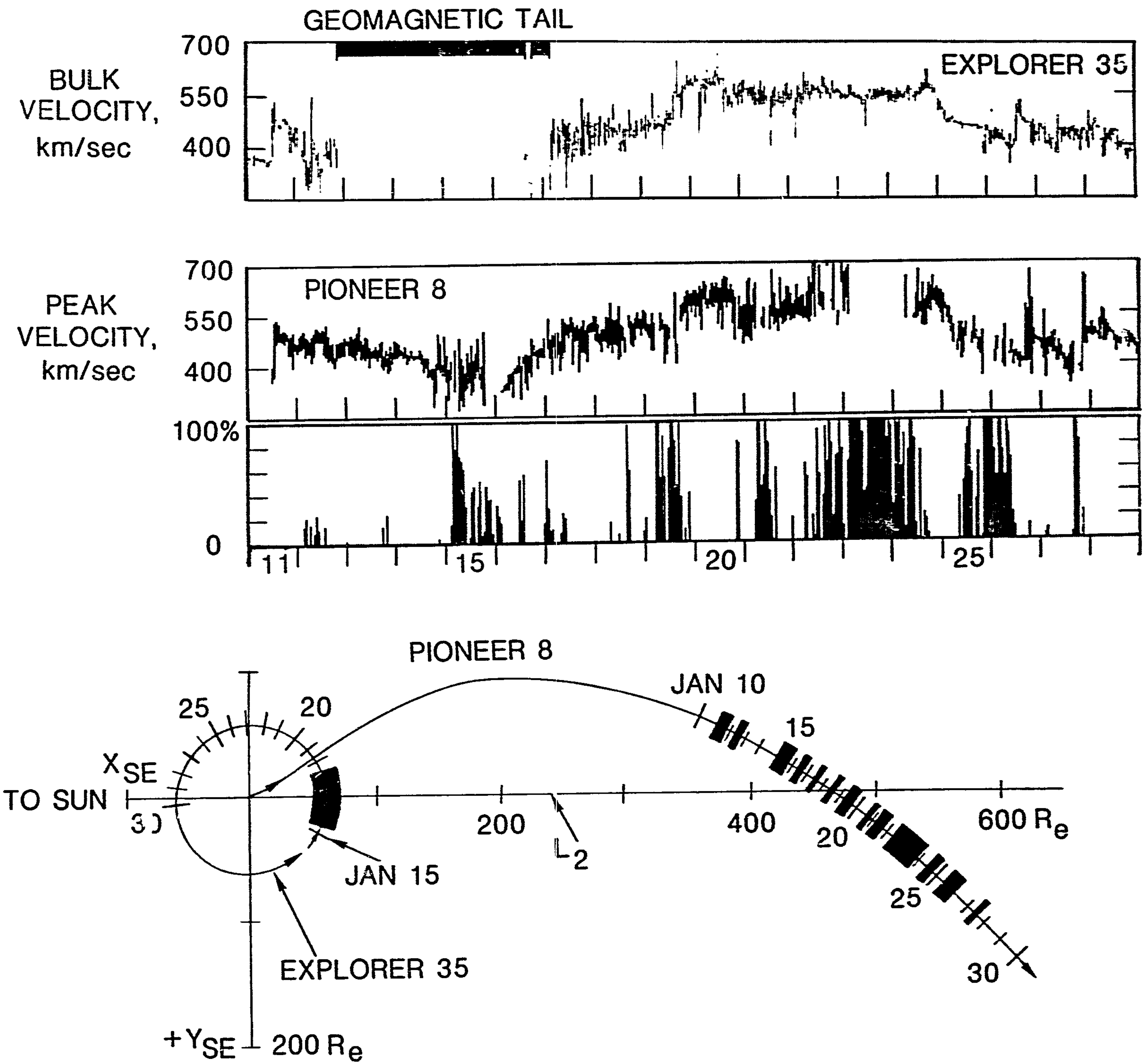
GEOMAGNETIC TAIL
BULK VELOCITY, km/sec
700
550
400
EXPLORER 35
PEAK VELOCITY, km/sec
700
550
400
PIONEER 8
100%
0
11
15
20
25
PIONEER 8
JAN 10
15
20
25
30
X_{SE}
TO SUN
200
L_2
400
600 R_e
JAN 15
EXPLORER 35
$+Y_{SE}$
200 R_e

ORIGINAL PAGE IS
OF POOR QUALITY

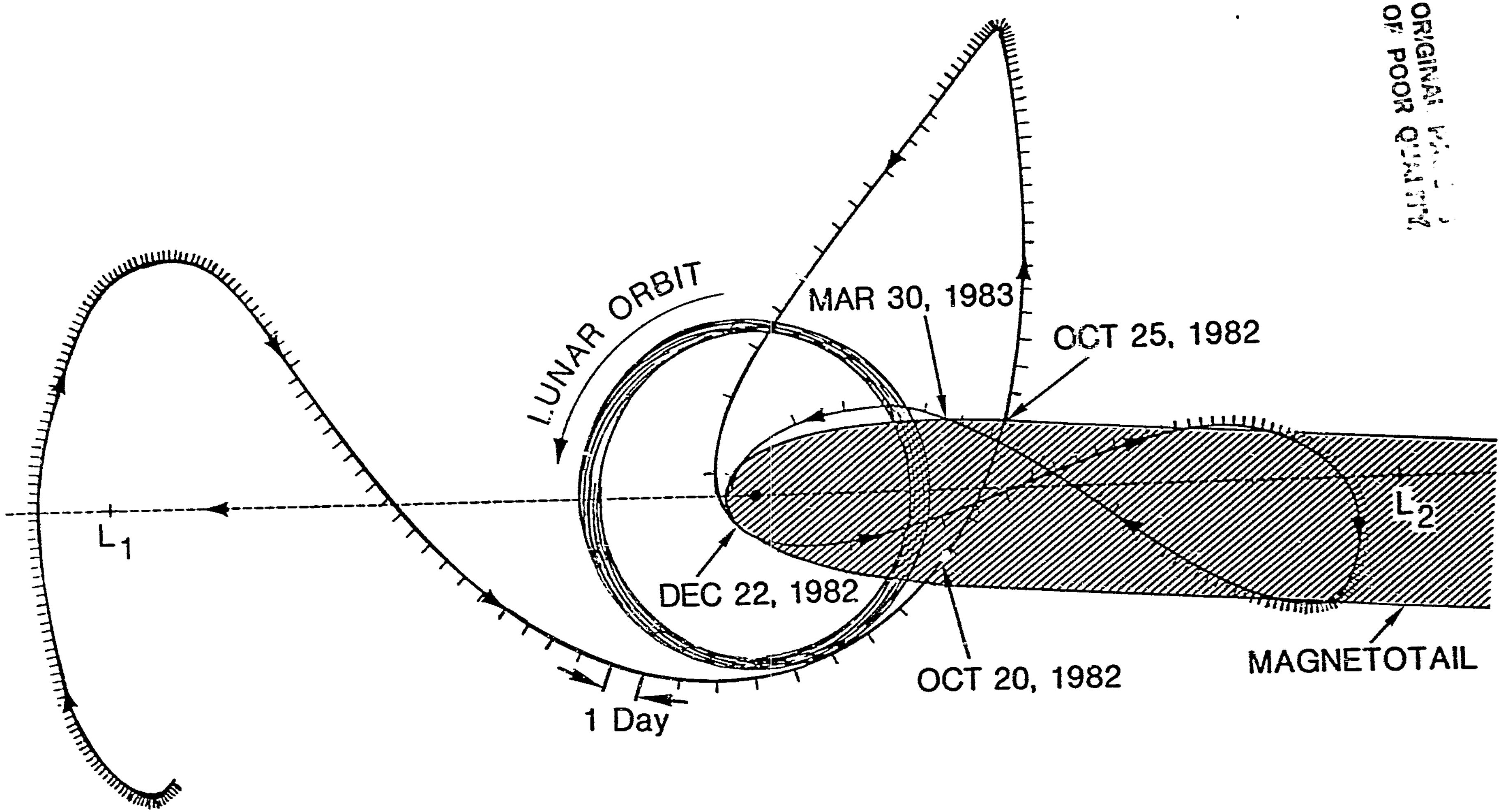

The ISEE-C Experiments

Instrument Title	Principal Investigator
X rays and electrons	K.A. Anderson
X rays: 8 to 72 keV, electrons: 2 to 1000 keV	
Solar wind plasma	S.J. Bame
Ions: 150 eV to 7 keV, 4.2% FWHM; electrons: 5 eV to 2.5 keV, 10% FWHM	
Three dimensional distribution function	
High energy cosmic rays	H.H. Heckman
Species H through Fe (resolution 0.15 atomic mass unit, $1 < Z < 26$)	
Low energy cosmic rays	D. Hovestadt
Particle composition, up to 20 MeV/nucleon	
Energetic protons	R.J. Hynds
Protons: 30 keV to 1.4 MeV; alpha-particles: 1.4 to 6 MeV	
Cosmic ray electrons and nuclei	P. Meyer
Electrons, 5 to 400 MeV (DES); protons, 36 to 13 000 MeV (DES), 13 GeV (IES)	
Elements separated, helium-sulphur, 60 to 13 000 MeV/nucleon (DES), >13 GeV/nucleon (IES)	
Plasma composition	K.W. Ogilvie
470 eV/Q to 10.5 keV/Q, M/Q 1.4 to 6.5, 3% FWHM resolution	
Plasma waves	F.L. Scarf
Magnetic field: 8 channels, 60-dB range, 20 Hz to 1 kHz	
Electric field: 16 channels, 80-dB range, 20 Hz to 100 kHz (continuous, no switching)	
Radio mapping	J.L. Steinberg
Three-dimensional tracing of paths of type III bursts in band from 20 kHz to 3 MHz	
Helium vector magnetometer	E.J. Smith
Eight ranges (±4, ±14, ±42, ±640, ±4000, ±22 000, and ±140 000 γ).	
Frequency response 0 to 3 Hz with three bands (0.1 to 1, 1 to 3, and 3 to 10 Hz) for measurements of fluctuations parallel to the spacecraft spin axis	
High energy cosmic rays	E.C. Stone
Ranges: $Z = 3$ to 28 (Li to Ni), $A = 6$ to 64 (^{6}Li to ^{64}Ni), energy = 2 to 200 MeV/nucleon	
Mass resolution: Li, 0.065 to 0.83 proton masses; Fe, 0.18 to 0.22 proton masses	
Medium energy cosmic rays	T. von Rosenvinge
Nuclei: $Z = 1$, 0.5 to 4 MeV/nucleon (SPA) and 4 to 500 MeV/nucleon (MPA), $2 \leq Z \leq 26$, 0.5 to 500 MeV/nucleon (MPA)	
Electrons: 0.7 to 0.2 and 0.3 to 12 MeV	
Isotopes: $Z = 1$ and 2, 4 to 80 MeV/nucleon; $3 \leq Z \leq 7$, 8 to 120 MeV/nucleon; $8 \leq Z \leq 16$, 10 to 200 MeV/nucleon	

ISEE-3 MAGNETIC FIELD INVESTIGATION

(SMITH)

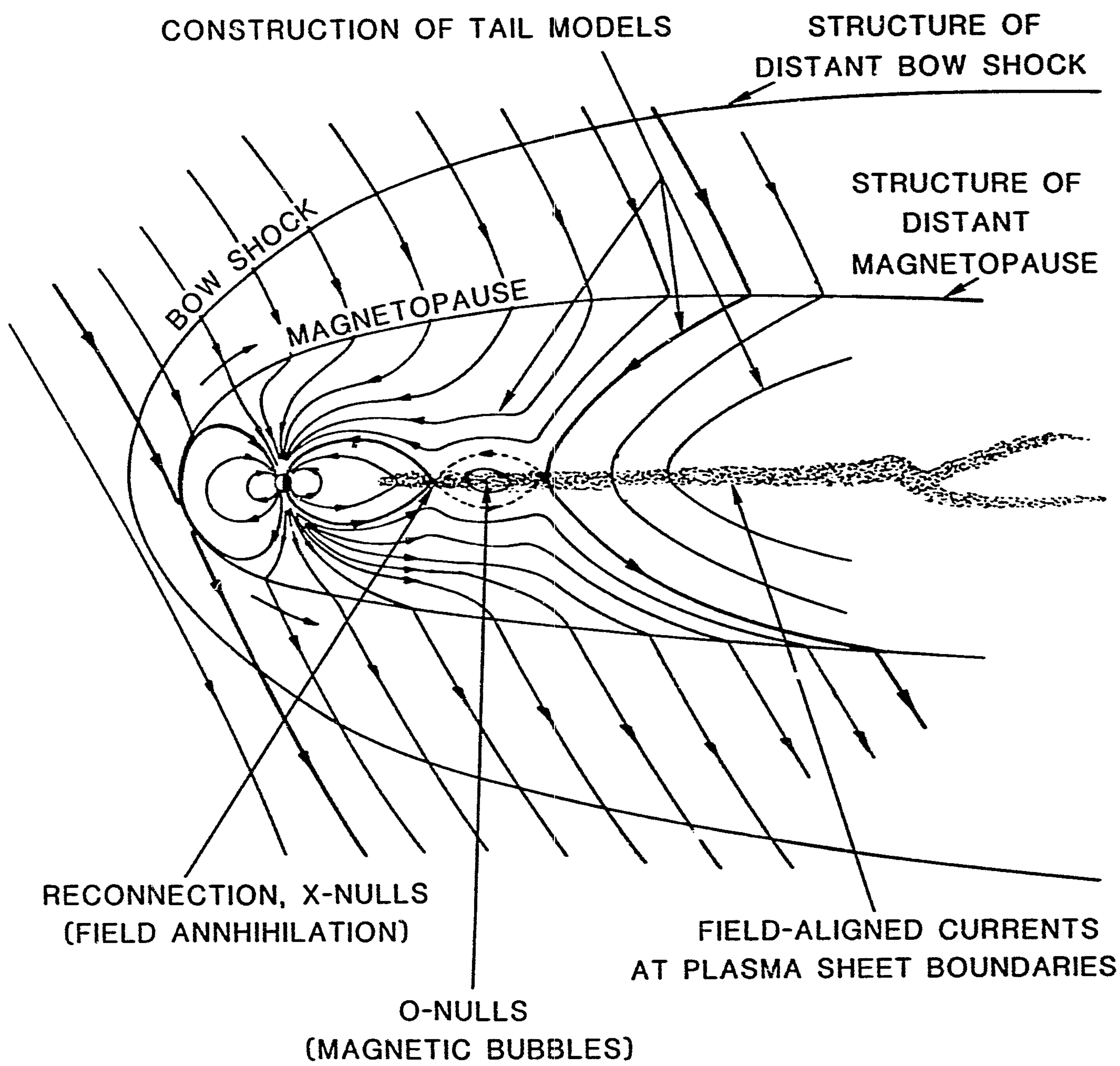

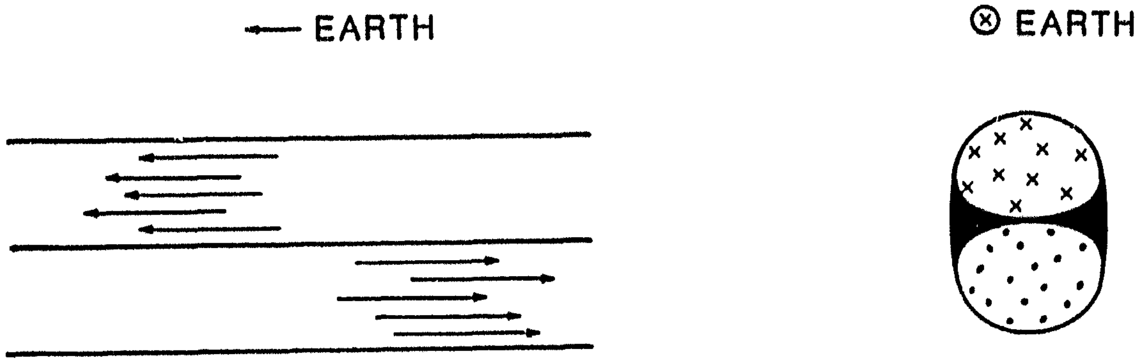

(a) ORDERED TAIL CONFIGURATION

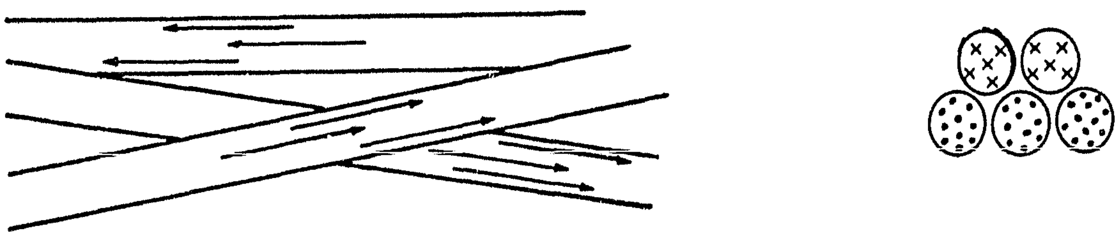

(b) DISORDERED TAIL

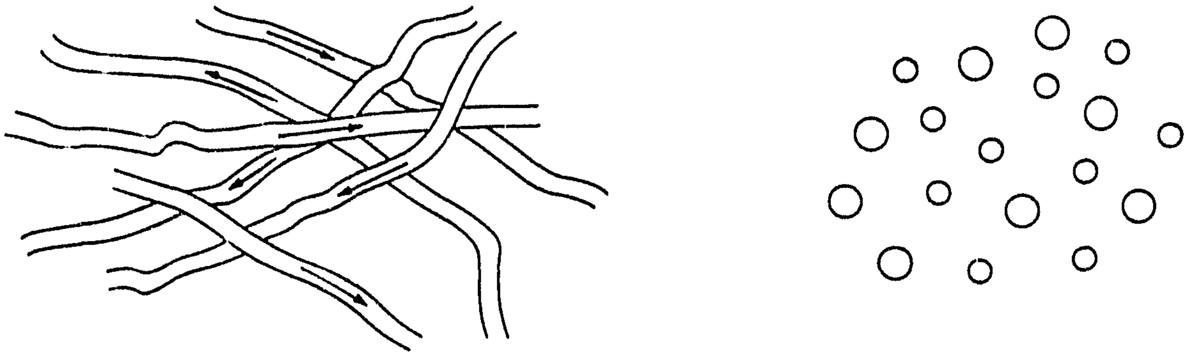

(c) TURBULENT TAIL

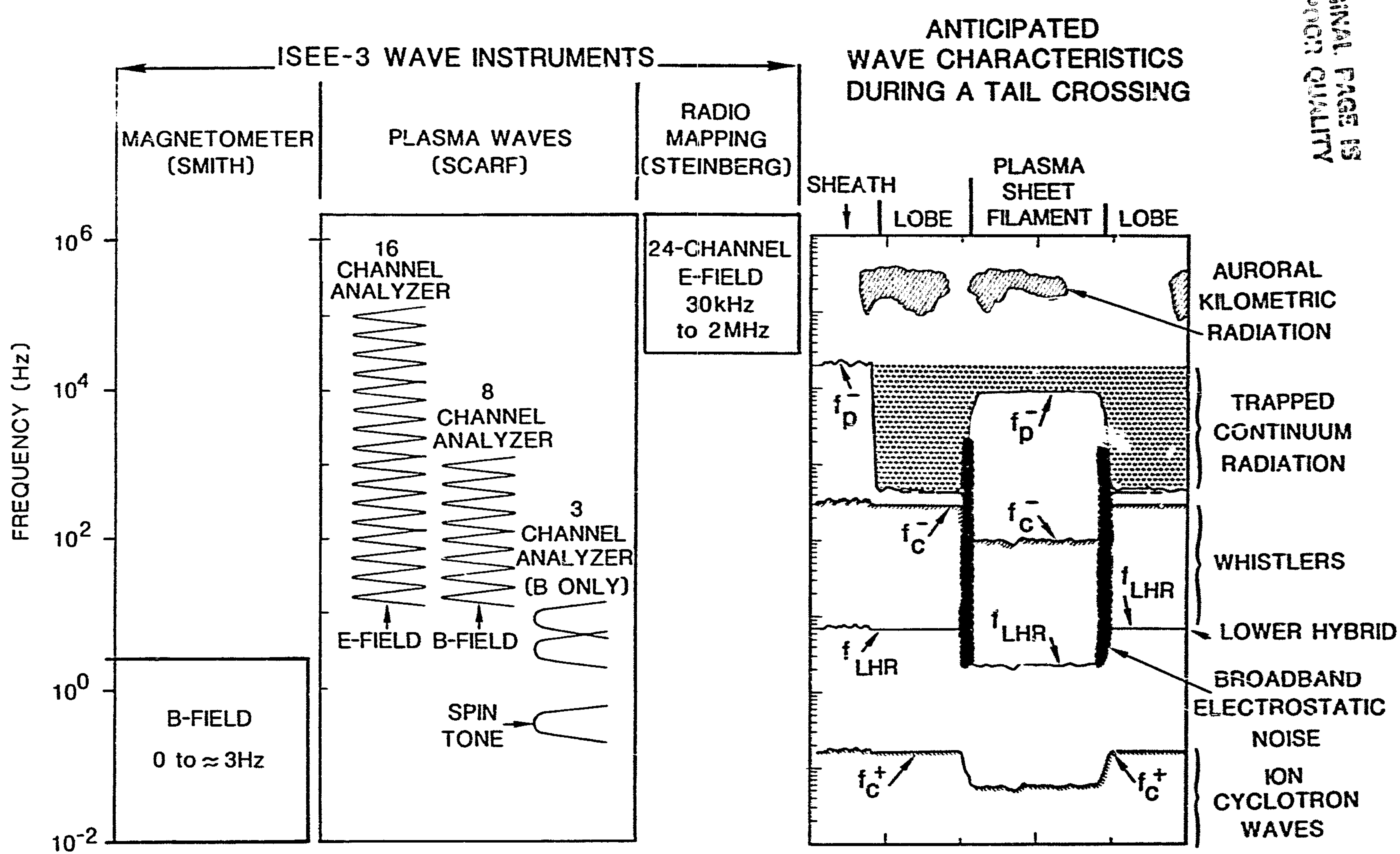
ISEE-3 WAVE INSTRUMENTS
MAGNETOMETER (SMITH)
PLASMA WAVES (SCARF)
RADIO MAPPING (STEINBERG)
ANTICIPATED WAVE CHARACTERISTICS DURING A TAIL CROSSING
FREQUENCY (Hz)
10^6
10^4
10^2
10^0
10^-2
B-FIELD
0 to ≈ 3Hz
16 CHANNEL ANALYZER
8 CHANNEL ANALYZER
3 CHANNEL ANALYZER (B ONLY)
E-FIELD
B-FIELD
SPIN TONE
24-CHANNEL E-FIELD 30kHz to 2MHz
SHEATH
LOBE
PLASMA SHEET FILAMENT
LOBE
AURORAL KILOMETRIC RADIATION
TRAPPED CONTINUUM RADIATION
WHISTLERS
LOWER HYBRID
BROADBAND ELECTROSTATIC NOISE
ION CYCLOTRON WAVES
f_p^-
f_c^-
f_LHR
f_c^+

STATUS OF ISEE-3 ION MEASUREMENTS

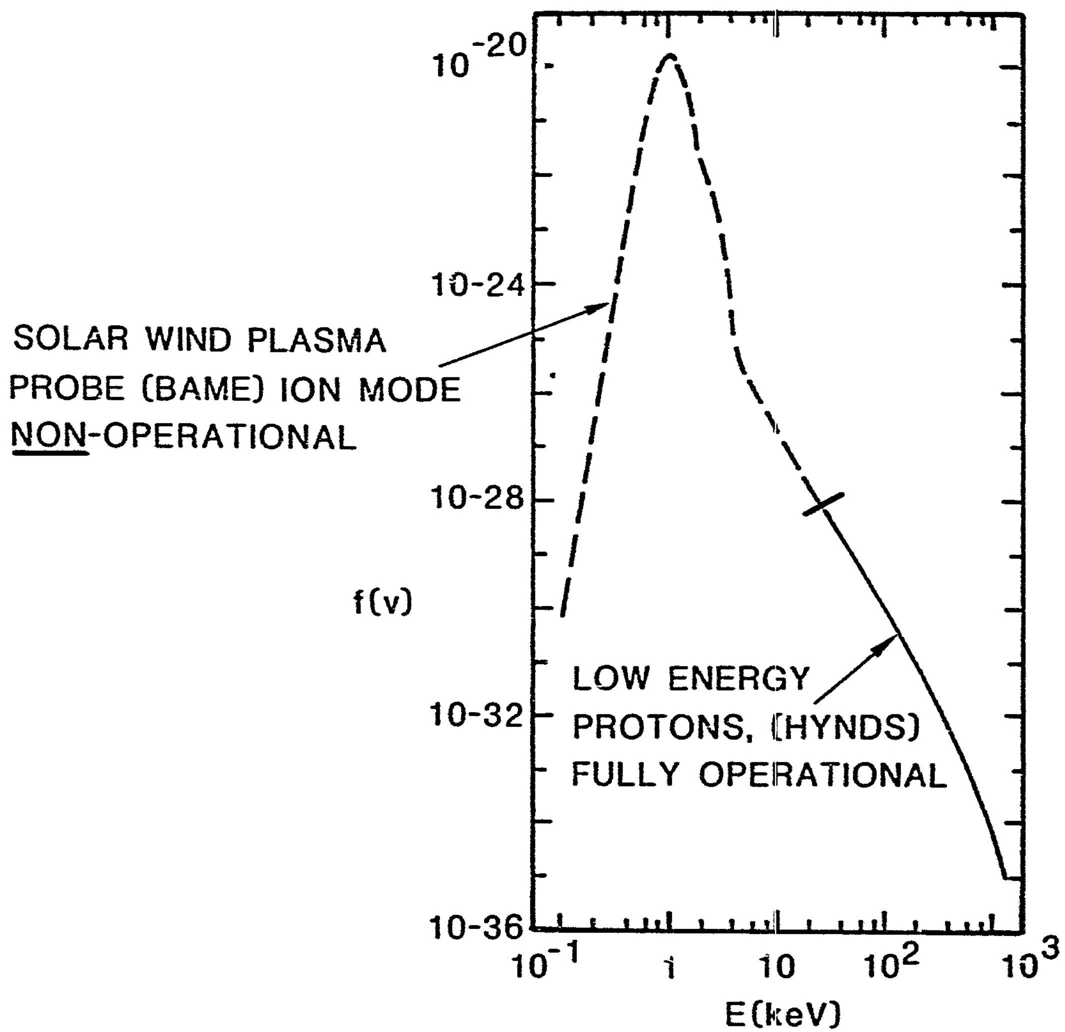

CHARACTERISTIC PARAMETERS DEDUCED FROM THE

ISEE-3 ELECTRON PLASMA PROBE OBSERVATIONS (BAME)

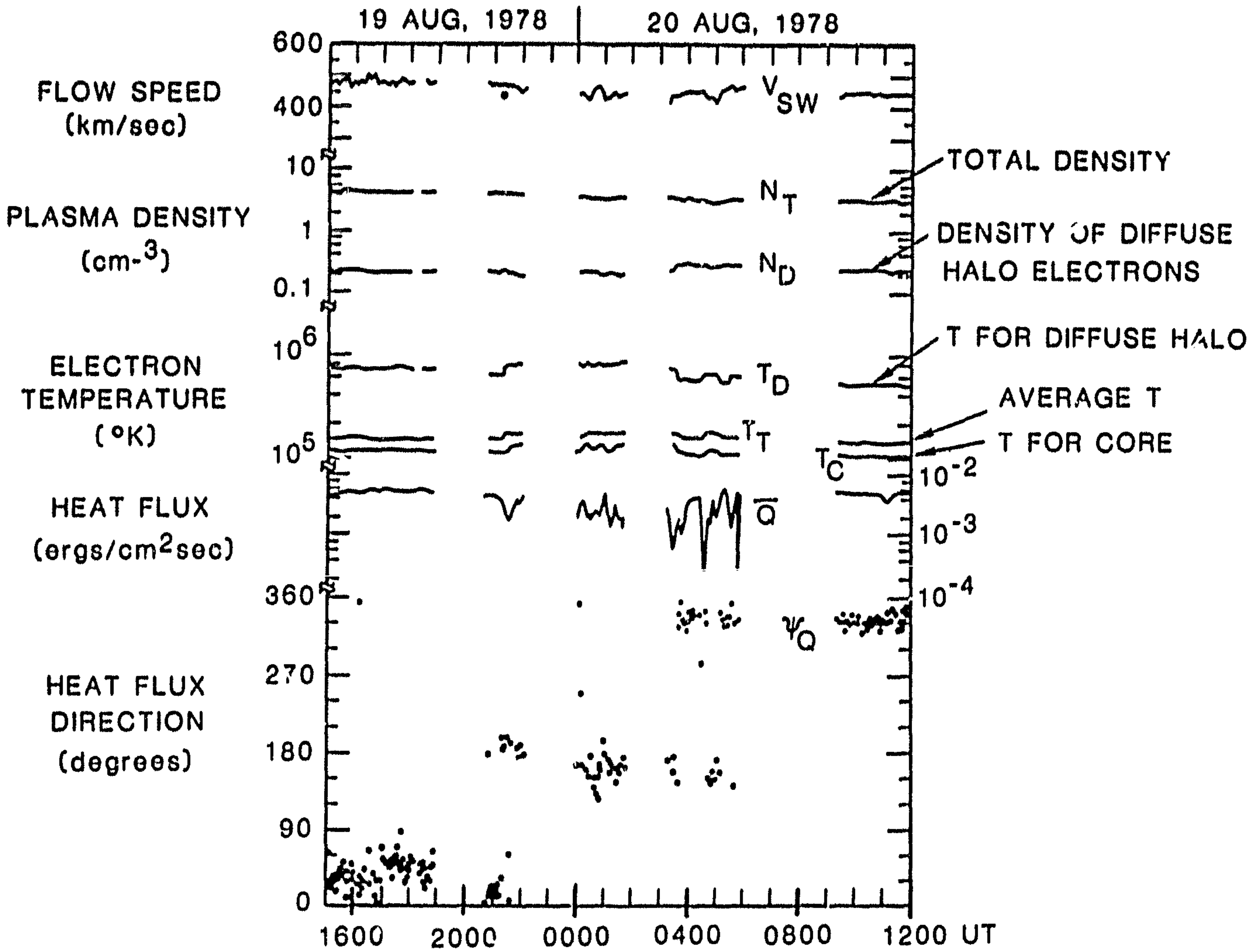

[THE MEASUREMENTS OF THE ELECTRON DISTRIBUTION FUNCTION ALSO PROVIDE DATA ON THE THERMAL ANISOTROPIES, THE HALO-CORE SPEED DIFFERENCES, ETC.]

ISEE-3 ION COMPOSITION INVESTIGATION

(OGILVIE)

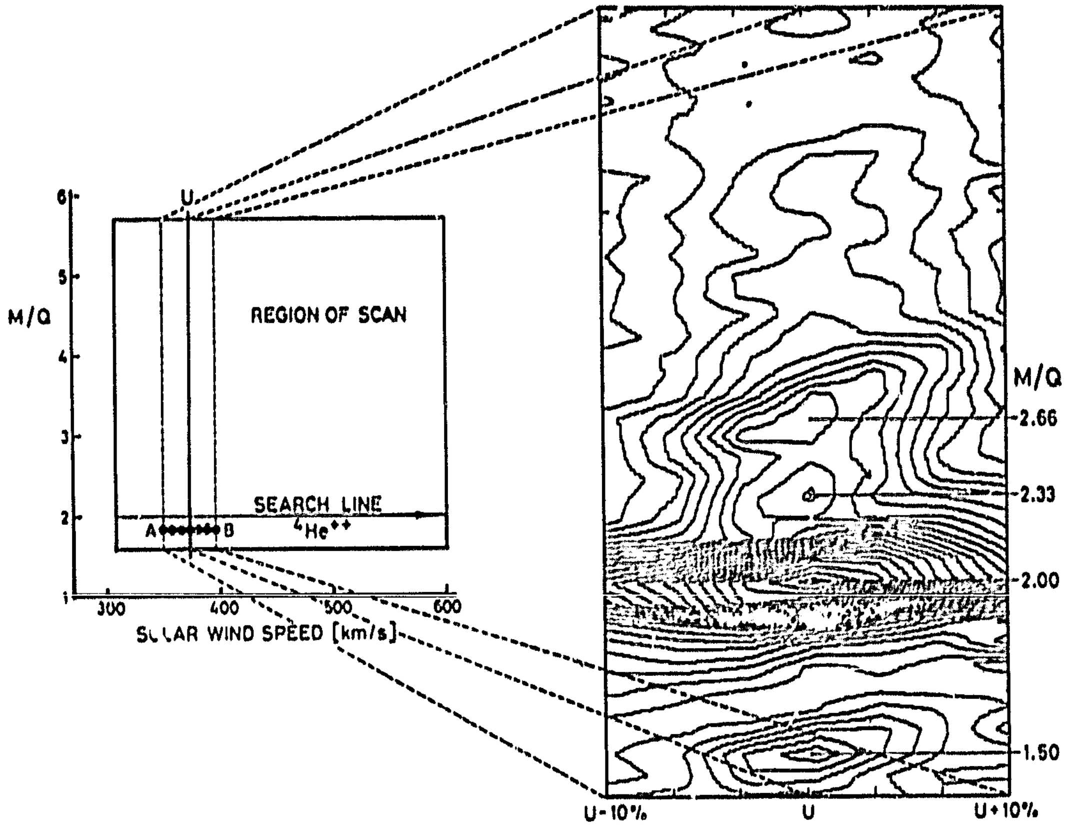

EXAMPLES OF OPERATION IN THE TAIL:

- THE INSTRUMENT CAN DETECT FLOWING O^+ IONS (IF U < 300 km/sec), CAN MEASURE THE SPEED, AND IDENTIFY THE SPECIES (PLASMA SHEET)
- THE INSTRUMENT CAN BE OPERATED IN A MODE SENSITIVE TO H^+, He^+ AND He^{++} IONS (WIND, MAGNETOSHEATH, AND MANTLE)

ANTICIPATED PLASMA SHEET MEASUREMENTS FROM THE ISEE-3 LOW ENERGY COSMIC RAY INSTRUMENT (D. HOVESTADT)

ISEE-1 APRIL 19, 1978
1515-1535 UT
$R \approx 12.5\ R_e$, NEAR MIDNIGHT

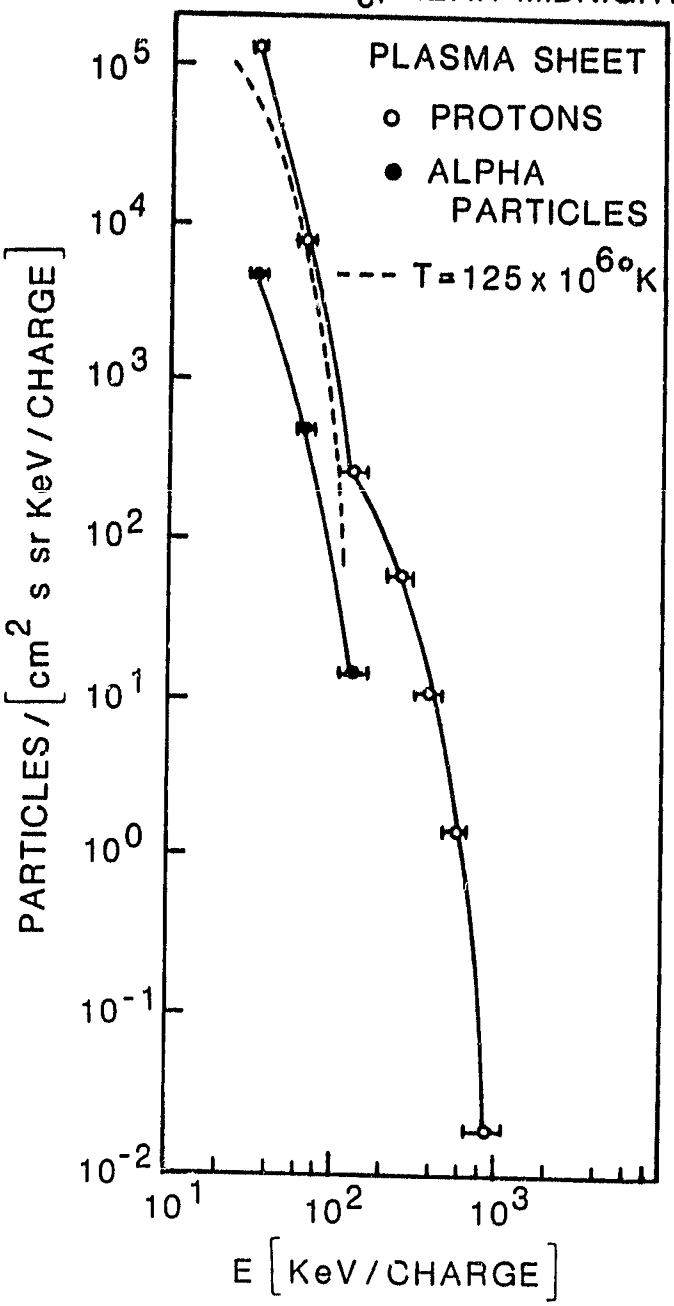

SUMMARY: SCIENCE RETURN FROM THE ISEE-3 TAIL MISSION

- FIRST OVERALL RECONNAISANCE OF THE TAIL BETWEEN THE LUNAR ORBIT AND L_2.
- FIRST DIRECT OBSERVATIONS OF THE TAIL MAGNETIC FIELD, THE LOW-ENERGY ELECTRON DISTRIBUTION FUNCTION, THE DISTANT PLASMA SHEET IONS, FLOWS OF ENERGETIC PARTICLES, AND WAVE-PARTICLE INTERACTIONS IN THE REGION OF EXPECTED TAIL BREAKUP INTO FILAMENTS OR DISCONNECTED JETS.
- FIRST SEARCH FOR TRAPPED CONTINUUM RADIATION IN THE DISTANT GEOMAGNETIC TAIL; ABSOLUTE EVALUATION OF PLASMA DENSITY IN THE SHEET FILAMENTS AND TAIL LOBES.

SIGNIFICANT POST-ISEE PROBLEM AREAS FOR OPEN/GTL

- ISEE-3 HAS NO OPERATING PLASMA PROBE FOR SOLAR WIND IONS (OPEN/GTL IS NEEDED TO PROVIDE COMPREHENSIVE DATA ON THE DISTANT BOW SHOCK, THE MAGNETOSHEATH, MAGNETOPAUSE, PLASMA MANTLE, AND WAKE REGION SURROUNDING TAIL FILAMENTS).
- ISEE-3 HAS HIGHLY INCOMPLETE COVERAGE FOR SUPRATHERMAL IONS AND ELECTRONS (RECONNECTION/FIREBALL PROBLEMS ARE NOT REALLY ADDRESSED, AND THE FULL OPEN PROGRAM IS REQUIRED FOR UNDERSTANDING OF PLASMA ENTRY/HEATING).
- ISEE-3 DOES NOT HAVE 4π COVERAGE FOR PLASMA AND ENERGETIC PARTICLES (ANALYSIS OF TAIL PHENOMENA ASSOCIATED WITH VORTICES, JETS, AND BEAMS REQUIRES OPEN/GTL).
- ISEE-3 HAS NO MEASUREMENTS OF DC ELECTRIC FIELDS (CONVECTION PATTERNS CANNOT BE IDENTIFIED).
- ISEE-3 DOES NOT HAVE COVERAGE FOR E-FIELD WAVES WITH $f < 10$ Hz (STUDY OF IMPORTANT ELECTROSTATIC ION CYCLOTRON AND HYBRID WAVE MODES ASSOCIATED WITH ION HEATING REQUIRES GTL CAPABILITY).